Revealing the spatio-temporal energy consumption of a mediterranean city : the case of beirut

Alaa Krayem

Université Fédérale
Toulouse Midi-Pyrénées

THÈSE

En vue de l'obtention du
DOCTORAT DE L'UNIVERSITÉ DE TOULOUSE

Délivré par l'Université Toulouse 3 - Paul Sabatier

Cotutelle internationale : Université libanaise

Présentée et soutenue par

Alaa KRAYEM

Le 17 septembre 2019

Révéler l'utilisation énergétique spatio-temporelle d'une ville côtière méditerranéenne: le cas de Beyrouth

---

Ecole doctorale : **SDU2E - Sciences de l'Univers, de l'Environnement et de l'Espace**

Spécialité : **Surfaces et interfaces continentales, Hydrologie**

Unité de recherche :
CESBIO - Centre d'Etudes Spatiales de la Biosphère

Thèse dirigée par
Jean philippe GASTELLU ETCHEGORRY et Haitham ZARAKET

Jury

M. Jean-Paul RUDANT, Rapporteur
Mme Nesreene GHADDAR, Rapporteure
Mme Chantal MAATOUK, Examinatrice
M. Jean-Louis ROUJJEAN, Examinateur
M. Haitham ZARAKET, Directeur de thèse
M. Jean-Philippe GASTELLU-ETCHEGORRY, Directeur de thèse
Mme Sara NAJEM, Co-directrice de thèse
M. Ahmad ALBITAR, Co-directeur de thèse

Revealing the spatio-temporal energy consumption of a Mediterranean city: the case of Beirut

Alaa Krayem

September 29, 2019

Abstract

To reduce greenhouse gas emissions and energy consumption in urban areas, understanding buildings energy performance and consumption patterns is essential for implanting effective energy management and efficiency strategies at a city scale. Such plans' implementation at large scale requires information on how the energy demands may change under specific interventions. Urban Building Energy Models (UBEM) are proposed tools to estimate current and future building's energy demand. These models rely on a bottom-up approach, combining both statistical techniques and physics-based methods.

This study aims at providing an enhanced modeling approach that simulates buildings' energy demand at high spatial and temporal resolution, which can help in evaluating energy management strategies and decision-making energy policies. The methodology is applied for the city of Beirut, representative of the Mediterranean region where the similarity of buildings technologies and climatic concerns among its cities is pronounced. The main objectives of the thesis are to develop, investigate and adjust a bottom-up energy modeling tool at urban scale; to provide evidence of the tool's suitability to support guidelines for future interventions; and finally to investigate the impact of the city's compactness on daylight availability and thus citizens' well-being.

In this case study based on two different districts within the city, a near-city-scale building energy model, BEirut Energy Model BEEM, is generated to estimate the building's stock electricity consumption. To reduce the modeling and computation time, an archetypal classification of the buildings based on their types and periods of construction is adopted. The additional information required to generate the 3D

model of the buildings are the number of floors, buildings' areas and a topographic map of the study areas. By coupling the models to the hourly weather conditions, the thermodynamic model of 3,630 buildings is simulated in EnergyPlus.

Adapting the model to Beirut's occupancy and users' behaviors is crucial to enhance the reliability of BEEM. The availability of metered electricity data allows the model calibration, which is based on buildings' clustering and finding the clusters' coefficients representative of specific energy patterns. After the training phase, the model's accuracy in predicting electricity consumption is improved. Comparing the actual consumption and the calibrated results, the averaged absolute percentage error of the electricity consumption was reduced from 310% to 41% in district A and from 326% to 39% in district B.

The calibrated model is combined with Geographic Information System (GIS) for a spatiotemporal distribution of energy demand patterns, which can help in assessing the most suitable intervention technologies. An analysis of the spatial distribution of electricity use demonstrates a spatial clustering that underlies urban energy demand which can be used for smart grid zoning.

The urban morphology affects the solar potential in an urban setting, which is a major driver in building's energy demand. Particularly, the daylight availability is examined by investigating its link with urban metrics such the buildings' orientation and heights. Revealing how sensitive such links are helps in optimizing urban design and structure, and informs retrofitting intervention strategies.

Keywords— Urban energy modeling, energy model calibration, decision support system, building energy performance, archetype classification, daylight accessibility

Résumé

Pour réduire les émissions de gaz à effet de serre et la consommation d'énergie dans les zones urbaines, il est essentiel de comprendre les performances énergétiques et les modes de consommation des bâtiments pour pouvoir mettre en œuvre des stratégies efficaces de gestion de l'énergie et d'efficacité énergétique à l'échelle de la ville. La mise en œuvre à grande échelle de tels plans nécessite des informations sur la manière dont les demandes en énergie peuvent changer dans le cadre d'interventions spécifiques. Les modèles énergétiques de bâtiments à l'échelle urbaine (UBEM) sont des outils proposés pour estimer la demande énergétique actuelle et future des bâtiments. Ces modèles reposent sur une approche ascendante (bottom-up approach) combinant à la fois des techniques statistiques et des méthodes basées sur la physique thermodynamique.

Cette étude vise à fournir une approche de modélisation améliorée simulant la demande énergétique des bâtiments à haute résolution spatiale et temporelle, ce qui peut aider à évaluer les stratégies de gestion de l'énergie et les politiques énergétiques décisionnelles. La méthodologie est appliquée pour la ville de Beyrouth, représentative de la région méditerranéenne, où la similarité des technologies de construction et des préoccupations climatiques de ses villes est prononcée. Les objectifs principaux de la thèse sont de développer, étudier et calibrer un outil de modélisation énergétique ascendante à l'échelle urbaine ; fournir des preuves de la pertinence de l'outil pour soutenir les directives pour les interventions futures ; et enfin, étudier l'impact de la compacité de la ville sur la disponibilité de la lumière du jour et donc sur le bien-être des citoyens.

Dans cette étude de cas basée sur deux quartiers différents de la ville, un modèle énergétique de bâtiment à échelle urbaine approximativement, applé BEirut Energy Model BEEM, est généré pour estimer la consommation d'électricité du stock de bâtiment. Afin de réduire le temps de modélisation et de calcul, une classification archétypale des bâtiments

basée sur leurs types et leurs périodes de construction est adoptée. Les informations supplémentaires requises pour générer le modÌle 3D des bâtiments sont le nombre d'étages, la superficie des bâtiments et une carte topographique des zones d'étude. En couplant les modèles aux conditions météorologiques horaires, le modèle thermodynamique de 3,630 bâtiments est simulé dans EnergyPlus.

L'adaptation du modèle à l'occupation de Beyrouth et aux comportements des utilisateurs est cruciale pour renforcer la fiabilité de BEEM. La disponibilité des données d'électricité actuelles permet la calibration du modèle, qui repose sur le regroupement des bâtiments et la recherche des coefficients des regroupements représentatifs de modèles d'énergie spécifiques. Après la phase de formation, la précision du modèle en matière de prévision de la consommation d'électricité est améliorée. En comparant la consommation réelle et les résultats calibrés, le pourcentage de l'erreur absolue moyenne de la consommation d'électricité a été réduite de 310% à 41% dans le quartier A et de 326% à 39% dans le quartier B.

Le modèle calibré est combiné au système d'information géographique (GIS) pour une distribution spatio-temporelle des modèles de demande d'énergie, ce qui peut aider à évaluer les technologies d'intervention les plus appropriées. Une analyse de la distribution spatiale de la consommation d'électricité met en évidence un regroupement spatial qui sous-tend la demande énergétique urbaine et qui peut être utilisé pour le zonage d'un réseau intelligent.

La morphologie urbaine influence le potentiel solaire en milieu urbain, qui est un facteur majeur de la demande énergétique du bâtiment. En particulier, la disponibilité de la lumière du jour est examinée en étudiant son lien avec des métriques urbaines telles que l'orientation et les élévations des bâtiments. Révéler à quel point ces liens sont sensibles permet d'optimiser la conception et la structure urbaines et de renseigner des stratégies de rénovation.

Mots Clefs— Modélisation énergétique urbaine, calibration de modèle d'énergie, système d'aide à la décision, performance énergétique de bâtiment, classification d'archétype, accessibilité à la lumière du jour

Acknowledgement

First of all, I would like to express my gratitude and appreciation for my thesis supervisor Dr. Sara Najem for her effective coaching and advice that were essential to the success of this work. I am extremely grateful for our friendly chats and your personal support in my academic and personal endeavours.

I thank Dr. Ahmad Al Bitar for his guidance and help and Pr. Haitham Zaraket for his dedicated support and patience. Furthermore, the success of my thesis would not have been possible without the support and nurturing of Dr. Ghaleb Faour.

My sincere thanks also go to Prof. Nesreen Ghaddar, Prof. Jean-Paul Roujean and Dr. Chantal Maatouk for doing me the honour of judging this work.

I am also grateful to Dr. Aram Yaretzian for his help especially in the archetypal classification and all the productive discussions we had, Dr. Ali Ahmad for his guidance and helpful contribution in the policy study, Dr. Issam Lakkis for his valuable discussions, Dr. Jocelyne Gerard for data sharing and Dr. Jawad Khalife for data acquisition.

All third floor team members at CNRS : Samah, Mariam, Mohamad, Hussein and Hussein. You really saved me with that "stupid" software ! It truly has been very good time in the lab. I would also like to extend my gratitude to Mahdi, for rescuing me in all IT matters, and to Wissam and Mohammad for answering my questions.

Thanks also to Eric and Nicolas for helping me during my stay in France. Special thanks to Cesar, for all the cool times we had while learning Arabic.

A big thank you to my friends Iman, Rouba, Sahar, Safaa and Wafaa for being around.

Special thanks to Ali, for all his love and support.

I am deeply indebted to my family for their unlimited and unconditional support.

Last but not least, a big thanks to my sister, Nour, for being there to change my mood whenever I am depressed, worried or tense.

Contents

List of Figures

List of Tables

List of Abbreviations

AC	Actual Consumption
ANN	Artificial Neural Network
ASHRAE	American Society of Heating, Refrigerating and Air-Conditioning Engineers
AUF	American University of Beirut
BA	Bottom Atmosphere
BAU	Business As Usual
BEEM	BEirut Energy Model
BEM	Building Energy Model
BOA	Bottom Of the Atmosphere
CAD	Computer-aided drafting
CIE	Commssion International de l'Eclairage
CDA	Conditional Demand Analysis
CNRS	Centre national de la recherche scientifique
CTF	Conduction Transfer Function module
DART	Discrete Anisotropic Radiative Transfer
DBSCAN	Density-Based Spatial Clustering of Applications with Noise
DEM	Digital Elevation Model
DHW	Domestic Hot Water
DSM	Digital Surface Model
DTM	Digital Terrain Model
ECCABS	Energy, Carbon and Cost Assessment for Building Stocks
EDL	Electricité du Liban

EM	Engineering Model
ECM	Energy Conservation Measures
EMPD	Effective Moisture Penetration Depth module
ESM	Energy Saving Measures
EUI	Energy Use Intensity
GDP	Gross Domestic Product
GHG	Green House Gas
GIS	Geographic Information System
GOV	Governmental building
HA	Higher Atmosphere
HAMT	Combined Heat and Moisture Transfer module
HOS	Hospital building
IFI	Issam Fares Institute
Illudiff	Diffuse Illumination
Illudir	Direct Illumination
LoD	Level of Detail
MAPE	Mean Absolute Percentage Error
MdAPE	Median Absolute Percentage Error
MA	Mid Atmosphere
MLP	Multi Layer Perceptron
MLRA	Multi-Linear Regression Analysis
NOAA	National Oceanic and Atmospheric Administration
OFF	Office building
RB	Radiative Budget
RES	Residential building
RPV	Rahman-Pinty-Verstraete
SCH	School building
SVF	Sky View Factor
TABULA	Typology Approach for Building Stock Energy Assessment

TOA	Top Of the Atmosphere
UBEM	Urban Building Energy Model
UHI	Uban Heat Island
USJ	University of Saint-Joseph
VAV	Variable Air Volume
WWR	Window to Wall Ratio

List of Nomenclature

A	Area	m^2
C	Circuity	–
C_z	Air capacitance	KJ/m^3
C_p	Specific heat capacity of air	$KJ/Kg/K$
D	Pairwise Distance	m
D_e	Euclidean Distance	m
E	Irradiance	$W/m^2/\mu m$
h	Convective heat transfer coefficient	$W/m^2/K$
h	Enthalpy of the air	J/Kg
H	Height	m
$\bar{H_S}$	Mean height of surrounding buidlings	m
I	Irradiance	W/m^2
L	Radiance	$W/sr/m^2$
$\dot{m}$	Flow rate	m^3/s
N	Number of bins	–
$\bar{O_S}$	Mean orientation of surrounding buidlings	$^\circ$
p	Probability	–
q''	Heat flux	W/m^2
R_f	Roughness coefficient	–
T	Temperature	$^\circ C, ^\circ K$
$\dot{Q}$	Heat load	J
X	Building x coordinate	m

Y	Building y coordinate	m
α	Extinction coefficient	–
Δ	Sky brightness factor	–
ε	Longwave emissivity of the surface	–
ε	Sky clearness factor	–
λ	Wavelength	nm
ϕ	Tilt angle of the surface	$^\circ$ or radians
ϕ_V	Luminous flux	W
$\phi_{e,\lambda}$	Spectral radiant flux	W/nm
$\bar{y}(\lambda)$	Luminosity function	–
Ω_i	Angular direction	sr
μ	Mean	[–]
ρ	Reflectance	–
σ	Stephan-Boltzmann constant	–
σ_{H_S}	Standard deviation of surrounding buildings' heights	m
σ_{O_S}	Standard deviation of surrounding buildings' orientations	$^\circ$
θ_s	Sun zenith angle	$^\circ$
Θ	Neural Network parameters	–
ζ, η and μ	Cosine angles	–

1. Introduction

1.1 General context

In 2016, 54.5% of world's population lived in urban areas. By 2030, cities are projected to house 60% of the global population [2]. Urban area are encountering unprecedented growth because of rural exodus due to socioeconomic factors such as seeking better job opportunities or higher education levels. Additionally, the development of the economy along with the concentrated industrialization in some areas at the expense of others, together with migration from poor countries suffering from economic problems, or asylum of citizens escaping from wars and political crisis zones are all contributing factors to the increase in urban population. Urbanization has the potential to make cities more prosperous and countries more developed, by creating wealth, generating employment and driving human progress. However, many cities around the world are suffering from persisting issues: increased residency in slums and informal settlements, challenges in providing urban services, climate change, exclusion and rising inequality, insecurity upsurge in international migration [3]. Among the climate challenges in urban environments is the urban warming measured in numerous cities across the world in addition to the Green House Gas (GHG) emissions [4]. One factor of the increased urban temperatures is the dominance of the artificial character of the cities at the expense of the natural green fractions. Another aspect of the urbanization is the economical structural change of the country. The concentration of the economic activities in the cities drives the labor force to shift from the agriculture sector to the industrial or services sectors in the city, phenomenon well-known as tertiarization. This transfer that accompanies the rural-urban migration, contributes indirectly in the increase in the energy consumption. First, due to lack in labor force, agriculture products have to be mechanized and transported from areas of production

to cities. Secondly, the needed transport services increase, leading to an increase in fossil fuels demand and hence, in its impacts on the urban climate. Last but not least, the economic growth in cities affects the behaviors and lifestyles of residents who tend to purchase commercial products and services, for example electrical appliances and accessories, increasing the energy consumption [5]. The city being a major energy consumer and GHG emissions contributor, a relevant understanding of its metabolism is pivotal in developing energy efficient strategies [6]. In order to ensure the optimization and the prioritizing of the energy conservation measures (ECM) to be applied, programmatic decision making or energy management is required. It consists of planning, implementing and monitoring energy supply, distribution and use in effective and efficient manners to reduce its waste and consumption. Furthermore, it studies the alternative and environment friendly resources, technical organization, cost effectiveness, and behavioral shifting to improve energy quality, availability and impacts on environment and nature [7]. However, understanding how a city's energy system changes over space and time under these interventions is crucial to support the decision making process. The building sector has been identified as responsible of 30%-70% of primary energy consumption in cities [8] and 30% of the gas emissions [9]. Therefore, developing Building Energy Models (BEM) at city scale are essential for energy supply management. These models have been developed and served as design enabler tools at individual building level [10]. They are typically used at the early design stage and throughout the design process to evaluate various design options and optimize the overall performance of building systems. Extending the energy modeling scope to the urban scale allows the assessment of building to building interactions (shading, heat exchange,etc.), and of building to other urban components interactions such as the urban heat island and traffic. City scale energy balance models [11, 12, 13] based on top-down approaches are used for climatic modeling but they do not provide the needed details to test innovative scenarios at building scale. On the other hand, bottom-up physical simulation models were introduced as effective simulation tools to model the impact of the urban context on buildings energy demand [14, 15, 16, 17]. In this context, Reinhart and Davila [18] introduced the Urban Building Energy Models (UBEM), bottom-up physical simulation models as effective simulation tools to simulate the impact of urban context on buildings energy demand.

BEM and UBEM need to be reliable and adaptable in that they should provide accurate

estimates of the buildings energy performance. However, discrepancies often occur between the predicted model and the actual metered building energy use, mainly due to inputs' inaccuracy/uncertainty in model parametrisation and structure [19]. Hence, the calibration of energy models is critical to achieve a confidence level in model predictions and encourage their adoption. They range from deterministic manual iterative tuning [19, 20] to automatic calibration process using optimization techniques, machine learning algorithms or Bayesian calibration [21]. Once calibrated, UBEM can be useful to estimate impacts of new technologies and policies where no measured data is available and to reveal unknown occupant patterns.

Among the sources of energy consumption in buildings, solar irradiance and illuminance are considered renewable resources to increase buildings' energy efficiency through active and passive techniques and use of daylighting. The latter, combined with artificial lighting, has been investigated in numerous studies as part of a sustainable development strategy to insure the visual comfort, energy optimization and architecture aspect of the buildings [22, 23, 24]. Daylight and outdoor comfort are indicators for resident comfort and well-being [25]. The amount of solar energy and daylight reaching an urban environment is highly linked to the urban compactness, among its indicators the geometry of the urban canyon and the urban blocks, the streets and buildings' orientation. Evaluating the effects of these indicators on solar energy potential and daylight provide guidelines for urban form optimization in relation to retrofitting interventions on building envelopes and solar-energy applications in dense urban areas [26].

Of particular interest in this study is Beirut administrative district of Greater Beirut, Lebanon's capital. The city witnessed a horizontal and vertical expansion over the years (figure 1.1). This densification brought enormous challenges related mainly to the provision of urban services such as energy and to alleviating the impacts of climate change. The city held 50.7% of the urban population of the country and 44.6% of the total population in 2016 [2], and consumes 12% of the total national energy produced while it only covers 0.2% of the country's total area. Its tertiary sector (commercial sector, public offices, hotels and hospitals) and residential sector account for 73% and 26% of its electricity consumption respectively. These represent 39% and 14% of the electrification GHG emissions respectively [27]. While the energy demand is inflating, Lebanon has been suffering since many years, from a crisis in the energy sector. The country relies on oil products

importation to meet its energy needs, putting the country in a state of high vulnerability. Figure 1.2 shows the development of the Total Primary Energy Supply in Lebanon between 1971 and 2014. The net imports increased from 5.45 million of toe (tons of oil equivalent) in 2008 to 7.61 million of toe in 2014, of which 43% were used for electricity generation in 2014 [1]. The available capacity for electricity generation is 2670 MW [28], of which only 1500 MW to a maximum of 2000 MW are insured by EDL (Electricity of Lebanon) [29], the only public institution responsible of the generation, transmission, and distribution of electrical energy in Lebanon [30]. In other words, a maximum of 65% of the power generated is issued by the State and the rest by back-up private generators. Even though Beirut is subjected to the least rationing period (only 3 hours while it is up to 12 hours in some parts of the country), reducing its energy demand can alleviate the daily blackouts in the other regions. This situation challenges Lebanon's pledge to reduce its GHG by 30% by 2030 with 2015 being the base year. The country is then facing a significant challenge to manage its energy sector and integrate renewable energy. Therefore, developing an urban scale energy model is essential to Beirut's resources and energy supply management. The model serves as a decision support system by estimating energy consumption patterns and identifying grid peak demands with a spatiotemporal distribution. The latter, integrated with the potential solar production findings [31], helps in estimating the savings and recommending targeted energy-use policies to alleviate peaks and ensure an efficient resources distribution. Another feature of the energy model for Beirut is its capability to project the energy consumption under normal conditions. Currently, estimates of demands do not account for the suppressed amount of electricity, since during outages, occupants modify their behaviors and alter their energy consumption patterns and preferences.

[1]Lebanese army, Elbeyrouthy [CC BY-SA 4.0 (https://creativecommons.org/licenses/by-sa/4.0)]

Figure 1.1: Aerial photos of Beirut in different years from multiple sources.

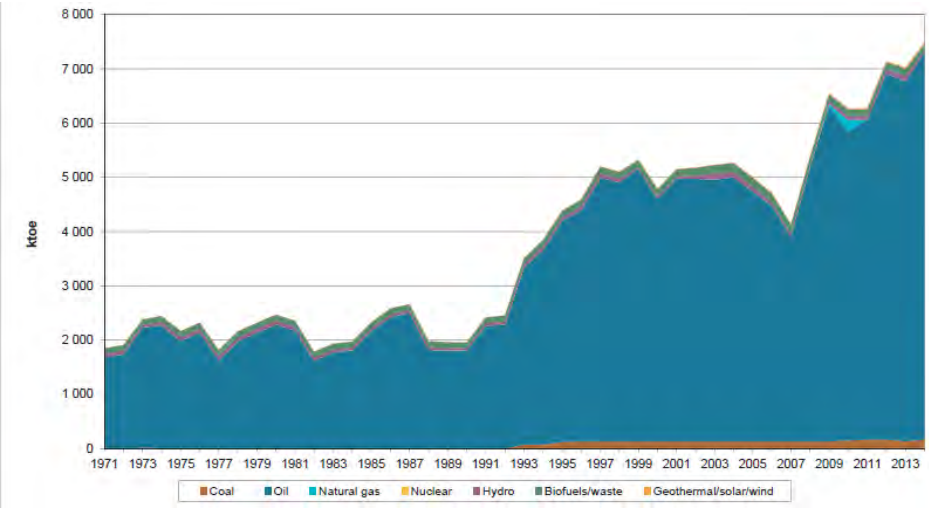

Figure 1.2: Total Primary Energy Supply evolution between 1971 and 2014 [1].

1.2 Thesis Outline

The thesis starts with an overview of the scope of this study and its motivation. Chapter 2 introduces the traditional and recent urban building energy modeling approaches and identifies their limitations and strengths.

Chapter 3 discusses the data requirements, sources and quality. Methods for data

management and preprocessing such as remote sensing and machine learning techniques are described. The archetype approach for urban massing models is applied and the algorithm that automatically creates the building multi-zone 3D model is introduced.

Chapter 4 presents the urban daylight potential and its relation to urban morphology. The selected simulation engine DART and its characteristics are presented. DART is used to approximate results of radiative budget in a more efficient manner. Further, results are processed so they represent the daylight potential within the city. Urban metrics are computed and their impact on the daylight access is studied.

Chapter 5 represents the energy implementation of the model. The theoretical background of the energy simulation engine EnergyPlus is included. The calibration methodology is discussed and results of the simulation are reported at high temporal and spatial resolution. The policy implications of the study are presented and were published as an energy policy brief available in the appendix B.

Chapter 6 summarizes the results of this dissertation and discusses the possible future work.

2. State of the art

2.1 Overview of urban building energy models

The building sector is responsible of a great part of the global energy consumption. Hence, it has a great potential in reducing GHG emissions and improving energy efficiency, by the mean of retrofitting and the use of high-efficient energy technologies in the demand side [32]. Moreover, it can contribute in the energy supply management by the integration of renewable energy production in buildings such as solar PVs. Hence, building energy modeling at city scale plays an important role as decision-making tools to plan strategies for the both demand and supply management of the energy sector. The main purposes of building energy models can be summarized as follows [33, 34]:

- predict present and future energy consumption, disaggregated by the factor of interest (e.g., building type, income, etc.) by quantifying the energy use as function of different input parameters.
- predict the technical and economic effects of different policy measures and energy consumption reduction strategies.

However, urban energy modeling is facing challenges among which the rarely accessible high level of detail (LoD) data, the systematic uncertainties, the heavy required computational resources, its sensitivity to urban microclimate and human behaviors [35]. The review section below starts with a brief introduction of urban building energy modeling approaches, then dive into the subcategories of each one to end with the chosen technique for this research, its benefits and challenges.

2.2 Modeling approaches: Top-down and Bottom-up models

Based on the literature review, there is no unique classification of the urban energy models. Even though, many approaches can be considered the same with different terminologies. For example, the forward approach proposed by 2009 ASHRAE Handbook relies on detailed physical description of the buildings and their systems as the engineering method discussed by Swan et al. [36] and the physical models suggested by Foucquier et al. [37] . In the following, a summary classification is discussed. Two main approaches have been used to model energy use patterns in urban context: *top-down* and *bottom-up* models [33].

2.2.1 Top-down models

Top-down models are mainly applied to explore the inter-relations between the energy sector and the socio-economic factors [33]. The main stream of top-down models is going from national or regional sector to individual buildings sector. They simply use the total energy consumption estimate and disaggregate it by attributing the energy consumption to buildings components without technical details. This workflow is easy since the required data (aggregated energy consumption data) is widely available. By using historical data, top-down models extrapolate from the status quo to predict near future energy patterns. However, if paradigm shifts in the energy sector are encountered, top-down models fail, which make them unsuitable for interventions and technological studies. Moreover, the identification of possible improvements such retrofitting or demolition is inhibited due to lack of details. The top-down models can be divided into two categories: econometric and technological. Econometric models study the energy consumption as function of economic variables such as gross domestic product (GDP), income, energy price and may include climatic conditions. As they rely on the past energy-economy interactions to predict current and future consumption, they lack technical details and are not suitable for climatic change impact evaluation as the latter may dramatically affect the pillars of a sustainable development: society, environment and economy. On the other hand, the technological models include other factors that affect the energy use such saturation effects, technological progress, structural change and so on [33]. An example of top-down models was developed

for the residential stock in Jordan [38]. A multivariate regression model with a time series analysis was adopted to predict future energy consumption and potential energy savings by correlating macroeconomic indicators such as income level, electricity and fuel unit prices, social indicators such as population and the weather conditions. Authors claimed that their approach might not be accurate but can inform about the future.

2.2.2 Bottom-up models

The first intuition of bottom-up models was to identify future energy efficiency measures capable to reclaim wasted energy resources. The impacts of these measures implementation, costs and doubts can be evaluated by developing different scenarios making bottom-up analysis a more realistic approach to specify energy reduction potentials and thereby GHG emissions [39]. Bottom-up models estimate individual end-uses, aggregate results according to their impacts on energy use, then extrapolate to regional or national level. This detailed approach allows for improvements and technological studies. By relating end-use energy consumption to macro-economic indicators, bottom-up models can gain some of top-down models strengths. Behavioral factors such as occupancy behavior, heating and cooling systems uses and energy gains may be incorporated in energy assumption increasing the accuracy of the model. However, due to the complexity of these occupant dependent variables, they are often assumed. This assumption level is a major drawback of some bottom-up models. In addition, large amount of data is required to efficiently describe each component contribution, which is limited in many countries. In addition, the sensitivity of input parameters is inappropriately described. Calculation and simulation techniques are in many cases time consuming, high costly and seek high level of expertise. According to Harish et al. [40], bottom-up models are based on two approaches:

- Forward approach: it involves the input of detailed parameters of the buildings to predict the outputs. Models based on this approach are highly accurate as thermodynamics and heat transfer equations are applied. In addition, building energy simulation software tools are widely developed incorporating complex equations for better prediction.
- Data driven approach: the inputs and the outputs of the model are known or have been measured. The data can be intrusive in case the experiments to gather

information are performed under normal system operation. When controlled experiments are limited by the building operation, nonintrusive data is collected. The energy consumption is estimated using regression analysis relating it to various parameters. Artificial algorithms such as Neural Networks and Support Vector Machines are applied when long-term energy estimation is requested to reduce the amount of performance data to be collected and the number of parameters to be identified when repeated operations such occupancy and set points schedules are encountered.

A more sophisticated and branched classification is proposed by Swan et al. [36], where the bottom-up models are classified into statistical and engineering models. Though, as the use of statistical learning algorithms is spreading widely, Zhao et al. [41] presented them in a separate group named Artificial Intelligence methods. Each of the aforementioned groups can be further sub-divided as studies and modeling techniques are in the process of development and growth.

Statistical models

Statistical models, also called inverse models [42], are primary used to identify building parameters by using existing data such as billing data and surveys information. They are particularly adopted to:

- Detect energy consumption abnormalities or malfunctioned systems
- Analyze impacts of retrofitting measures

Statistical models embed the strengths of top-down models as they use macroeconomic and socioeconomic variables such as energy price and income. They incorporate occupant behavior by attributing energy consumption to end-uses. In general, they are easy to develop and use. Regression and conditional demand analysis (CDA) are well-documented techniques and widely used [36]. As examples, linear regression models have been used to assess the electricity and fuel consumption of New York City [43] and correlate the energy performance for heating with the Surface area to Voume ratio S/V in the city of Carugate, Italy [44]. However, as they dont provide a detailed description of energy end-uses, they lack of flexibility and are limited when assessing new energy measures [33]. Large amount of data is required to correlate energy consumption with end-uses and to achieve an

acceptable accuracy level. In addition, when based on annual metered data, they are unable to predict energy use in monthly or hourly time steps or to simulate the combined impact of several energy efficiency measures in buildings [14].

Engineering models

Engineering models (EM) complex equations are widely incorporated in building energy simulation programs to overcome their complexity [40, 45], like EnergyPlus [46] and TRNSYS [47]. However, a detailed physical description of building properties and systems and precise weather characteristics are essential for these programs [48].

By applying engineering models, end-uses energy consumption are determined based on their physical functions and thermodynamics relations. Accordingly, a detailed description of their impacts on the aggregated energy consumption is provided. The model does not rely on previous data so it is more suitable to test new technologies and effectively estimate the low-cost energy efficiency opportunities and their appropriate combinations. Although EM are considered high accurate, occupant behavior and preferences are difficult to be included and are rather assumed. In consequence, the socio-economic factors are excluded [49]. In addition, large amount of inputs and high level of expertise are required to develop the models and solve the equations. To reduce EM complexity, some modelers proposed some alternatives to simplify the analytical approach, either by applying steady-state methods such as degree-day method and its optimization techniques [50], or by simplifying the building characteristics inputs by applying easy equations or using average values from statistical data. Filogamo et al. [51] assigned to their buildings average geometrical properties obtained from statistical data such as number of floors, number of inhabitants, floor dimensions (width, height and depth), shape ratio S/V, glazing surfaces, even Domestic Hot Water (DHW) and cooking energy intensities. Heating demands were assumed by classical calculation methods due to well-known behavior. Mata et al. [52] created an engineering bottom-up model called Energy, Carbon and Cost Assessment for Building Stocks (ECCABS). It is based on a physical approach by applying thermodynamic and transfer heat equations to estimate the net energy demand, assess energy savings measures ESM and CO2 emissions reductionsin residential building stocks in Sweden. In addition, the model is capable to calculate the costs savings from applying the ESM. The model applies its equations on representative buildings from

the studied stocks, then multiply the results by weighting coefficients, each one representing the fraction of buildings in the entire stock that belong to each building category. However, simplified models integrate a wide range of assumptions to the calculation procedures, hence, increase model uncertainty.

Dynamic simulation

Dynamic simulation consists of using energy performance software tools, like EnergyPlus [46] and TRNSYS [47], to overcome the complexity of EM. It is suitable for large buildings with complex systems simulation and are capable to involve control strategies [42]. Energy simulation programs are often based on two modeling techniques [45]: the analytical method and the numerical method. The first one solves linear differential equations with time independent parameters, while the second one uses a nodal network representation of the building and applies for each node a system of nonlinear and time dependent equations. The nodal network is then simulated simultaneously (e+). As the numerical method handles more complexity in the nodes interactions, it is more preferred. In general, a detailed physical description of building properties and systems and precise weather characteristics are essential for the software. Additionally, simulation relies on simplified inputs and assumed values related to behavioral parameters reducing the accuracy of the model [48]. In addition, it is still expensive in terms of expertise, time and costs. Harish et al. [40] provided a recuperative overview of energy simulation programs, their applications and limitations.

Archetypes

The classification of "reference building"is a commonly used concept to represent certain categories within a stock identified based on specified criteria. Then, the energy consumption of each category is calculated using EM methods. Results are aggregated to estimate the regional or national housing stock energy consumption. Three approaches are proposed to define building typologies:

- Real example building approach that selects, by experts, a real building as the most representative of specific parameters when statistical data is not available;
- Real average building approach that finds a real building which characteristics are

similar to the mean features of a statistical sample;

- Synthetical average building or Archetype approach that defines a virtual building attributed the mean features statistically detected from a sample.

These approaches were applied in the TABULA project (Typology Approach for Building Stock Energy Assessment). The aim of this project is to create a harmonized structure for European Building Typologies by the identification of reference buildings, to assess the actual energy performance and to study the impact of retrofits applied to existent buildings in terms of energy savings and CO2 emissions reductions [53]. The reference building selection is performed based on a categorization process where a building sample is split into categories according to climatic area, age and geometry. Then buildings were selected as references with geometrical and thermal characteristics. In another study, this procedure is compared to a cluster analysis, a technique to partition a set of houses into clusters with similar profiles [54]. However, the generation of archetypes seems to be a more reliable and applied technique. According to Swan et al. [36], archetypes are classified as engineering models. Their generation is achieved through two steps [55]:

- Segmentation: Key parameters that will be used to distinguish the archetypes can be identified from previous work, surveys, statistical algorithms or measured data. For example, Famuyibo et al. [56] ranked nine key independent variables (wall, roof, floor and window U-values, air change rate, heating system efficiency, dwelling type, floor area, DHW tank insulation) depending on their influence on energy use based on international literature and the available data sample. Then, to identify the most important variables, multi-linear regression analysis (MLRA) followed by clustering were performed. Attia et al. [57] determine parameters average values through surveys and literature review. A walk-through survey was conducted to identify schedules and users patterns. The archetypal data-tree is another approach to identify the representativeness of a parameter [58]. Each tier of detail represents the level of disaggregation of the selected parameter and each node represents the corresponding archetype. When comparing the results at each level, urban modelers can quantify the impact of the parameter and hence proceed to further subdivision or not. In general, it was found that building use (e.g., residence, office, etc.), age of construction, floor area and shape are the most used parameters for segmentation.

- Characterization: Each archetype is identified by its non-geometrical properties such as construction materials, occupancy rate, DHW, cooling and heating set points. Deterministic parameters can be assigned to archetypes gathered from buildings audits or existing database. Parekh [59] generated 56 archetypes based on age and location for the house stock in Canada. The archetypes representation included geometric configurations, thermal characteristics and operating parameter. With information gathered from surveys and previous data, the author defined average values that were used as default values for simulation program inputs. The main objective of the archetype libraries is to provide guidance to the house evaluator who must check values before any energy analysis. In a similar study, Heiple et al. [60] generated 30 archetypes for residential and commercial stocks in Houston city based on surveys and previous data. Building prototypes were then simulated using eQuest and results were visualized in GIS and spatially distributed for a better analysis of energy consumption spatial and temporal variation. Still, with the finer parameters, the model is not able to address the variety in energy consumption among the buildings of the same archetype. Furthermore, the available information determines the degree of confidence of the parameters. Among the high-uncertainty parameters are the occupant dependent variables, infiltration rates, thermal losses from distribution systems [61]. However, many approaches have been developed for a more realistic and robust representation of the occupant behavior.

Grey models or Hybrid models

Grey models are defined as models used when the information about a system are not very well known. For example, if the variables influencing a system are known but how exactly they affect the system is not clear, the system is considered a grey system [7, 41]. According to Fumo [62], they are hybrid models that first physically determine the building characteristics and systems contributing in the energy consumption, then involve a statistical analysis to identify the key parameters for a satisfactory energy prediction. Fonseca et al. [63] combined statistical data (archetypes databases) with analytical methods to develop a model that provides detailed qualitative and quantitative description of the energy supply. The model generates a spatiotemporal energy distribution for scenarios investigations and visualizes results via GIS platform. Potential wasted energy resources and building retrofits as well as

urban zoning analysis and distributed schemes integration were all examined and studied.

2.3 Urban building energy models

Urban Building Energy Model is a new bottom-up engineering model introduced by Reinhart and Cerezo [18], to combining the capabilities of statistical and engineering models to provide hourly energy assumptions, estimate the impacts of new technologies interventions, and incorporate occupant behaviors [14]. Another feature of UBEMs is the possibility to combine them with GIS platform. The resulting energy maps are then used for results analysis and comparison with measured data or surveys to help designers and policy makers.

UBEM apply heat transfer equations in and around the buildings that are represented each one as an individual 3D dynamic thermal model. UBEM are hence able to support complex scenario development. Furthermore, they can be combined with energy simulation programs. The energy modeling workflow of an UBEM requires high effort and time resources given the massive amount of data for potentially thousands of buildings. Assembling, managing, and automating the workflow is essential. For this purpose, the building stock is divided into archetypes to reduce complexity and computation requirements [14].

An illustrative case of UBEM is the Boston model developed by the MIT Sustainable Lab [55].The model was accomplished using a set of tools comprising GIS [64] for buildings' footprints importation, Rhinoceros 3D [65] as the CAD environment, and EnergyPlus as the thermal simulation engine. The workflow consists of generating the archetypes based on the year of construction and buildings' types, extruding the building's footprint to create the three-dimensional form, dividing it into floors, generating windows and assigning the specific thermal properties based on the building's archetype. Shading surfaces were determined and each building was then represented by a thermal model and its energy performance was simulated in EnergyPlus. A following study, where the same workflow was applied for a neighborhood of Boston, explored different ECM that can be applied to reduce the energy consumption [15]. Another example is the CityBES in the US, an open interactive web-based platform to automatically generate UBEMs based on city GIS dataset [16]. It provides results of energy end-uses on annual, monthly and hourly timescales with a

3D visualization of the city and its urban modules.
3DStock is another 3D model for the British building stock, which breaks buildings to floors with different activities, and floors to zones with different sub-activities. Geometrical data, electricity and gas consumption are attached to each Self-Contained Unit. 3DStock is capable of making projections of future consumption, or testing the impact of possible abatement measures and new technologies [17].
In the previous paragraphs, we discussed the recent trends of cities, the urbanization issues and challenges, and the climate change threats. Urgent interventions and feasible actions are required. In this context, energy management for urban policies rises with a particular importance, to reduce the energy consumption, improve its quality, increase its availability and reduce the GHG emissions resulting from its production. Urban models have been introduced to assist these objectives. An overview of traditional and recent modeling techniques was presented to explore the limitations and the strengths of each technique.

When managing the integration of renewable energy or application of retrofit measures at city level, scaling down to hourly energy consumption patterns is crucial. This high resolution temporal energy demand is determined by occupant activities, lifestyles and economic status. Hence, UBEM calibration concentrates on integrating the significant weight of occupant behaviors into the urban model. To encompass these aspects, probabilistic approaches are applied. In this context, Cerezo et al. [66] proposed a Monte Carlo simulation with probabilistic distributions method to characterize uncertain parameters related to building occupancy. The method was then validated by comparing it to two others deterministic methods for a district in Kuwait City. The probabilistic method showed less error in terms of average Energy Use Intensity (EUI) and standard deviation. Richardson et al. [67] developed a Markov-Chain Monte Carlo technique for stochastic occupancy model generation based on a time-series data. The data set consisted of 24-hour diaries, completed at ten-minutes time step by thousands of participants. It was used to derive transition probabilities matrices to predict the probability of the current state (resident is active or not) to change in the next time step. The model showed similar profiles as the data set, revealing its accuracy. As the model is freely available, He et al. [68] applied it to generate heating patterns of English houses. In order to validate their findings, they coupled the stochastic model to EnergyPlus and compared the results to

another set of simulations with a deterministic occupancy model. It has been obvious that the hourly thermal demands with the stochastic model are more realistic and representative for the dwellings. UBEM approach is the most useful and reliable one to estimate hourly energy consumption at urban level, and then explore the impacts of ECM and/or renewable energy technologies, it will be used in this study. However, since we have selected Beirut, it is important to point out that there is substantial work done for modeling energy consumption of buildings in the city. For example, Annan et al. [69] simulated the impact of natural ventilation on energy use in buildings by simulating one typical residential building in Beirut. Ghaddar et al. [70] have simulated the impact of air conditioning use on UHI and energy use in buildings in Beirut by adopting a top-down model approach. The authors found that the temperature in urban areas could increase by $0.8°C$ during the day and $4.7°C$ during the night due to the extensive use of air conditioning systems. A bottom-up approach was used to assess Lebanon's energy budget from 2010 to 2015 [71]. For the building sector, the calculations were based on the constructed area per building type, the climatic zone, the occupancy rates and the energy demands per end-uses per building type defined by a previous study *A roadmap for developing energy indicators for buildings in Lebanon* [72]. The latter study results were obtained after simplified calculations conducted for a business as usual case (BAU) under coastal climate and with assumptions of the boundary conditions based on expertise. However, both studies did not account for the different properties of buildings envelope. All the above studies can be complemented by an archetypal classification of the buildings and more detailed BEM for more accuracy and applicability.

2.4 Conclusion

This chapter provides an overview of the urban energy modeling techniques applied for energy assessment at urban scale. Top-down models are easy to use models but lack the essential details for interventions and technological details. On the other hand, bottom-up models estimate energy consumption at individual buildings which makes them suitable for assessing feasibility of strategies and action plans. Advantages and drawbacks of statistical and engineering models are provided. To benefit from both models' advantages, UBEM are

introduced as a combination of a statistical approach (in archetypes generation) and an engineering approach (in the physical-based equations of the energy budget). Hence, it is decided to adopt the UBEModeling technique in this study, as it can help in achieving the thesis objectives.

3. Data management and 3D model generation

3.1 Introduction

Data preprocessing is an inevitable technique in data mining, especially if the available data is incomplete, inconsistent, noisy or contains out-of-range or unreliable values. When a large dataset needs to be cleaned, detecting anomalies becomes a difficult task. Instant interventions to adjust or modify it are time consuming in this case. Preprocessing algorithms are hence implemented and used. In this context, remote sensing and GIS are helpful in image processing to detect buildings, extract their information, and to create digital elevation profile of the city. Moreover, recent trends focus on integrating machine learning in remote sensing processes and in data management. The goal of this chapter is to provide an overview of the application of remote sensing and machine learning in urban environment. In the next sections, an archetypal classification of the buildings in Beirut is provided, followed by a detailed description of the 3D model generation steps.

3.2 Remote sensing for data preprocessing

Remote sensing techniques are widely used for many applications such as mapping crops practice [73], snow monitoring [74], determination of clouds and precipitation properties [75], and environmental policy support [76]. In urban environment, they can inform about the optical and thermal properties of the materials in the urban canopy [77]. In this study, remote sensing was applied in urban context for data preparation and cleaning, as will be discussed in the next sections.

Buildings detection and segmentation

Identifying the geometrical properties of buildings in the city is a crucial step to create the 3D model. Buildings in Beirut were digitized from a 2008 aerial photo of $15cm$ resolution. The resulting shapefile was checked using a 2016 Pleaides image of $1.5m$ resolution, to identify new and reconstructed buildings. This process led to identify 17,572 buildings in Beirut administrative area, with their latitude and longitude coordinates, as well as their areas and perimeters. The data was stored in a shapefile "Beirut buildings' shapefile". Information about 7,122 buildings in different areas within Beirut were surveyed by the University of Saint Joseph USJ. The dataset, associated to the GIS in the form of attribute tables, labels each building by its footprint and a certain number of entry fields summarized in table 3.1. However, when cross-checking these data with the Pleaides satellite image, the buildings' footprints did not reside over their actual positions. By joining buildings from USJ with those digitized from the aerial photo by their centroids, $1,289$ buildings were not identifiable and therefore were excluded. Further inspection of the data revealed that 5.44% of the buildings from USJ have incorrect information as follows:

- 8 buildings with incorrect number of floors and construction year
- 266 buildings with incorrect number of floors
- 62 buildings with incorrect construction year

Manual intervention was applied when possible by checking each building on Google earth to correct the number of floors, and by comparing different images of Beirut from Google Earth historical imagery [1]. For the urban energy model, information such as the type and year of construction of the buildings are indispensable. Therefore, buildings with incomplete information were excluded. This reduced the number of buildings from 7,122 to 3,630 distributed as follows (figure 3.1): 818 buildings in district A and 2,814 in district B. Bi-monthly electricity consumption from 2015 of a set of buildings was provided by EDL and added to the updated dataset. Buildings near the shore (up to $1Km$ inland) have in general their facades face west and/or north with large windows overlooking the sea. To take into consideration this feature, we labeled these buildings. Moreover, a comprehensive survey was used to label glazed buildings as "glazed". These buildings were represented by

[1] https://www.google.com/earth/

3D thermal models as will be discussed in chapter 5.

The previous intervention led to a discontinuity in the urban layout. However, for the daylight and solar access analysis, all buildings in the zones of interest were retained. Buildings with missing function were considered residential. When no year of construction was available, it was assumed that the buildings were built after 1991.

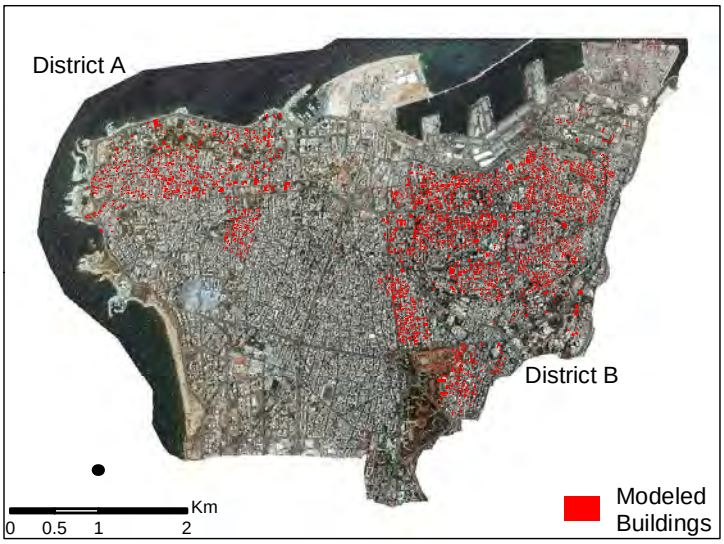

Figure 3.1: Buildings' distibution over Beirut.

Data Origin	Form	Type	Original field name	Designation
USJ survey	Shapefile	Polygon	Building footprint	-
			Enquete ID	Building ID
			Annee	Year of construction
			Fonction	Function
			NbreEtage	Number of floors
			area	Area of a floor
			perimeter	Perimeter of a floor
EDL	Shapefile	Numeric values	Mois 2	Electricity consumption in January and February
			Mois 4	Electricity consumption in March and April
			Mois 6	Electricity consumption in May and July
			Mois 8	Electricity consumption in June and August
			Mois 10	Electricity consumption in September and October
			Mois 12	Electricity consumption in November and December

Table 3.1: Original variables datasets and the selected variables for BEEM.

Construction of the DSM and buildings' heights identification

In 2018, the Lebanese Army identifies the buildings heights in Beirut by attributing each one an elevation point. The "Army heights" shapefile was joined to Beirut buildings shapefile. $17,632$ points were identified, with an increase of 60 buildings compared to Beirut buildings shapefile. The analysis of the data shows that this difference is due to the following:

- 2,920 polygons had no corresponding elevation points
- 13,270 polygons had one elevation point
- 1,380 polygons had more than one elevation point

Three reasons were identified responsible of buildings with no elevation points:

1. Beirut buildings shapefile account for all buildings constructed until 2016 while the Army field work was achieved in 2018. Many buildings were built between these two years. Note that in some cases. the elevation point resided outside the polygon, so manual intervention was applied to link each point to its nearest building. Otherwise, the buildings were not attributed any height.
2. Some buildings were attributed more than one elevation point, for example on the roof and the rooftop. In this case, the lowest point was kept. However, sometimes the multiple points were considered and the building was split into many buildings with the same properties. This assumption is accepted especially for the radiative budget study where the height is critical.
3. Some points had unreliable values, for example negative values, and were therefore excluded.

The army heights were compared to the Digital Surface Model (DSM) obtained from the processing of Tristereo Pleiades images (figure 3.2). Figure 3.3 shows a high accuracy concerning the (x,y) geolocation of the two images. A high correlation was revealed between the elevation points and the DSM pixels values, as shown in figure 3.4. It was found that 50% of the differences between the elevation points and the DSM fall within the range of $[0, 3m]$.
The buildings' heights were then obtained by subtracting the Digital Terrain Model (DTM) provided by the National Council for Scientific Research (CNRS) from the DSM.

Figure 3.2: Elevation points of buildings (left) and DSM profile (right)

(a) Aerial image

(b) DSM profile

(c) Matching aerial image and DSM

Figure 3.3: a) Digitizing buildings using aerial image. b) Generation of Beirut DSM using Pleiades images. c) Matching of the digitized buildings with the DSM shows high accuracy of the DSM results.

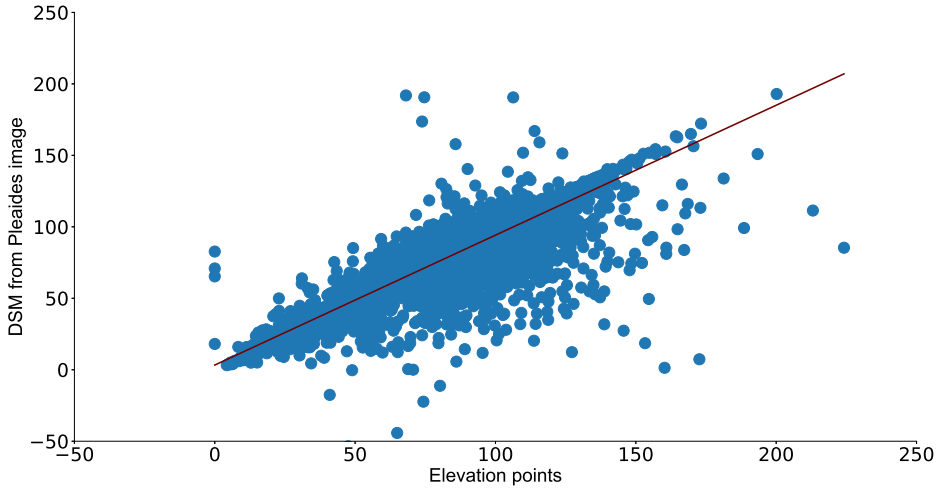

Figure 3.4: Correlation between elevation points from the Army field work and the DSM raster image obtained from processing Pleaides images. $R^2 = 0.866$

3.3 Machine learning for oultier detection

The problem of outliers is that they have the effect of misclassification of data and affect the outputs attributes [78]. An "outlier is an observation, which deviates so much from other observations as to arouse suspicions that it was generated by a different mechanism" [79]. Outlier detection is applied in many fields such as intrusion and fraud detection, medical diagnosis, sensor networks, image processing and many other domains. Outlier detection techniques can operate under supervised mode (when training data for both normal and outliers classes is available), semi-supervised mode (when training data is only available for normal or abnormal class instances), and unsupervised mode [80, 81]. Some prominent categories of outlier detection techniques in the unsupervised outlier detection setting are proximity-based methods [82], which treat outliers as points which are isolated from the remaining data [83]. They rely on notions of distance (how far the instance is from the majority of other instances in the dataset) or density (how similar is the density around the instance to the density around its neighbors). Density-Based Spatial Clustering of Applications with Noise DBSCAN is a fairly used unsupervised clustering method. It has the ability to find non-linear clusters based on density. The DBSCAN algorithm works by going through all data points, and find neighbors that are closer to each other than a certain parameter ϵ and therefore considered to be in a same cluster.

Autoencoders are another method used for outliers detection. They are unsupervised multi-layer neural networks, with symmetric architecture. The number of nodes in the input layer is the same as in the output, and the number of nodes in the middle layers is small. The objective of an autoencoder is to train the output to reconstruct the input as close as possible, with low dimension representation. This reduced representation of the data is a natural approach for discovering outliers, which are harder to be represented in this form, and therefore their error score will be large [82]. The use of DBSCAN and autoencoders before the calibration process will be discussed further in section 5.4.2.

3.4 Generation of the 3D model

3.4.1 Archetypes generation

To overcome the complexity of dealing with a large dataset of distinct buildings, archetypes were generated. An archetype is a set of geometrical and non-geometrical properties that characterize a building's thermal performance. Non-geometrical properties include the thermal resistance of the construction materials, occupancy schedules and appliances densities [15]. As previously mentioned, archetypes generation consists of two steps [14]: the *segmentation* of buildings with similar properties based on key parameters such as the type, age, shape [56, 84, 53, 61], and the *characterization* of the thermal properties for each archetype. This information was gathered from buildings audits [57], existing database [51, 59, 66] or local expertise and previous literature [56]. In this study, the buildings were grouped based on two parameters: the building's type and the year of construction based on a historical architectural analysis of the buildings. The building type helps in setting a building's occupancy patterns and determining its internal heat loads, while its year of construction informs about construction material and methods. For the specific case of Beirut, five distinguished construction periods were identified in the literature: 1900-1923, 1924-1940, 1941-1960, 1961-1990, and 1991 and on [85]. Regarding the type, the buildings were grouped in five classes: residential, mixed, hospitals, schools and governmental buildings. In total, $5 \times 5 = 25$ archetypes were generated. Thermal properties were acquired from the Technical Guide for the application of the Thermal Standard for Buildings in Lebanon [86], published in 2005. Missing information was obtained from ArchSim default library [87] and online libraries [88]. A priori, non-geometrical properties, including light and equipment loads intensities and usage schedules were set by referring to ASHRAE standards [89]. HVAC systems performance coefficients were obtained from reference [72]. Finally, ArchSim library was updated with the missing properties as inputs for the simulations. Figure 3.5 summarizes the adopted workflow.

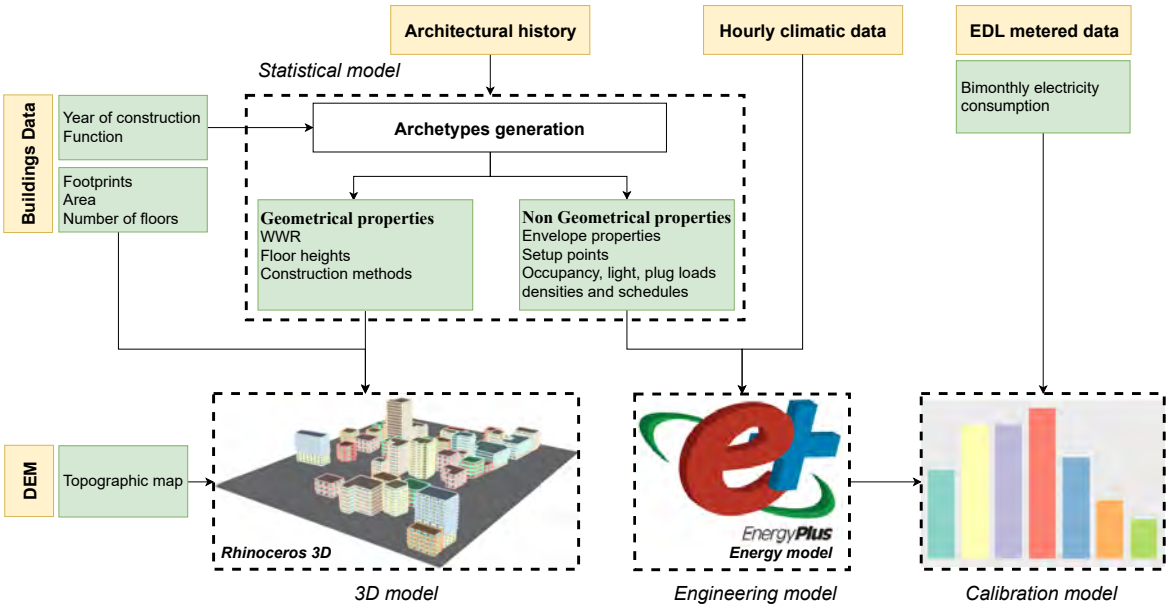

Figure 3.5: Beirut Energy Model BEEM methodology flowchart.

3.4.2 3D model

After preparing the data, buildings were divided into floors and each was assigned an archetype. The geometry modeling process is shown in figure 3.6. The buildings footprints and the topographic map contours were imported to Grasshopper, a free plugin of Rhinoceros 3D (which is not a free software tool but with a 3 months trial) [65]. After generating the Digital Terrain Model (DTM) using Delaunay triangulation, buildings footprints are projected on the DTM surface. The polygons were then extruded to the buildings heights. Then, using the ArchSim tool, each building was divided into its number of floors, each represented by a single thermal zone. No further zoning was applied in this study. Next, windows were generated on free facades, which resulted from excluding adjacent walls and those whose neighboring wall is less than $3m$ apart. To have a more realistic representation of the buildings, the number of windows per facade was restricted by its width and the Window to Wall Ratio WWR given by orientation and year of construction. In this respect, windows were generated with a spacing of $5m$ for residential buildings and $4m$ for non-residential buildings. The WWR was primarily identified according to the year of construction. Values ranged between 0.15 in 1900-1923 and up to 0.7 after the 1990s. However, if the building overlooks the sea, the WWR was increased to

0.7 to take into account the north and west highly glazed facades. In addition, fully glazed buildings and first floors of mixed buildings, considered as retail shops, were assigned a 0.95 and 0.8 WWR respectively. Another feature of BEEM is the possibility to include balconies, which are added to free walls of residential floors having an area greater than $15m^2$.

Potential shading surfaces from neighboring buildings were determined in the 3D model based on a two-step process. In general, a building will shade another one at a certain time of the day if the length of its shadow is greater than the distance between the two buildings at this time. However, the shadow length varies over the day in function of the sun angle. The longest shadow is provided with the smallest angle, but this will lead to a great number of shadows on one building. To overcome this issue, each building (of height H) that is $3.78H$ away from the target building within a radius of $300m$ is considered as a building that casts a shadow. The multiplicative coefficient 3.78 was calculated as in [8], based on a sun angle of 14.8°, corresponding to 80% of the time between 5:30 am to 8 pm in Beirut. We chose this interval to include all the time when the sun is shining, in winter and summer. To accomplish this task, we used the equations provided by the NOAA solar calculator [2]. To further reduce the number of shading surfaces, a ray tracing algorithm was used to detect only the neighborhood buildings' surfaces that obscure the solar radiation. Once the 3D model was completed, each thermal zone was assigned the simulation parameters from the buildings database.

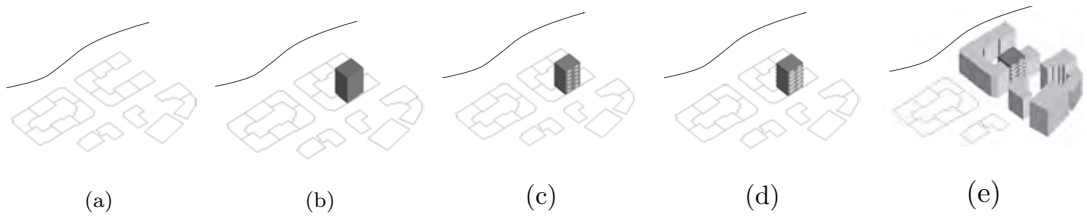

Figure 3.6: Fig. (a) shows the DTM creation, followed by a simple extrusion shown in Fig. (b), then windows and balconies generation in (c) and (d) respectively, and finally the adjacency and shading are shown in (e).

[2]https://www.esrl.noaa.gov/gmd/grad/solcalc/

3.5 Conclusion

This chapter shows how remote sensing is applied in urban environment for urban components detection, such as buildings. It also stresses its effectiveness for data preprocessing. However, combining it with machine learning algorithms would enhance its applicability and feasibility. In this context, machine learning application is becoming an inevitable requirement in data management and in results processing as will be shown in next chapters.

A statistical approach to create archetypes for buildings characterization is introduced. The results of these processes are fed to the automated generator of 3D massive models that will be used for the daylight assessment and energy modeling.

4. Urban daylight model

4.1 Introduction

The radiation budget is an important component of the energy budget of buildings. It contributes directly by the solar gains by exterior surfaces, and indirectly by the energy savings achieved by replacing artificial lighting with daylight. This chapter focuses on daylight accessibility in the urban context by simulating first the luminous energy in two different zones, using DART. Then, the importance of a high LoD 3D model in daylight assessment is investigated, as well as the variation of the daylight along the buildings' elevations. A neural-network approach linking urban morphology to daylight accessibility is presented.

4.2 Presentation of DART model

To estimate the intercepted solar radiation, we simulate the radiative budget of the different urban geometries (walls, roofs, glazed surfaces, ground) using DART. DART, a free software tool, is a 3D model that computes the radiation propagation through the earth-atmosphere system, over the entire optical domain, ranging from visible to thermal infrared wavelengths [90]. It works with any experimental and instrumental configuration (altitude and spatial/temporal/spectral sensor resolution, sun and view directions, atmosphere, ...). It provides two major types of products for natural and urban landscapes:

- **Satellite/plane/in-situ spectrometric and LiDAR acquisitions:** These are useful for sensitivity studies, for procedures that invert satellite images. Figures 4.5 and 4.2 represent exemples of these products results. Terms BOA (Bottom of the Atmosphere), Sensor and TOA (Top of the Atmosphere) indicate that the images are simulated for a sensor at the bottom, within and top of the atmosphere.

- **Radiative budget RB:** It corresponds to the budget of the incident, intercepted, absorbed, scattered and thermally emitted radiation. It can be computed per scene element and per type of scene element such as "roofs", "walls", "trees", etc. Vegetation fluorescent RB can be also simulated. The radiative budget is computed based on a ray tracing approach detailed in section 4.2.3. Different scattering orders are simulated:

    1. Direct illumination (Illudir): radiative budget of direct sun illumination. At this step, scattering and absorption are null.
    2. Direct and diffuse illumination (Illudif).
    3. Multiple iteration steps (Iter1, Iter2,...).
    4. Infinite extrapolation (IterX): corresponds to the actual observed radiative budget.

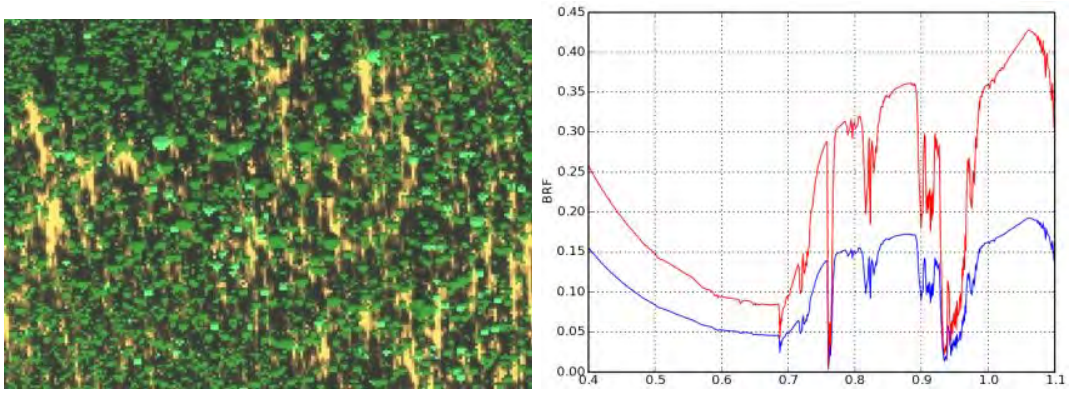

(a) (b)

Figure 4.1: DART simulation of Chris sensor. Howland forest, USA. a) Image. b) TOA VIS-NIR spectra.

DART is composed of four executable modules to parametrize the simulation:

- *Direction*: it calculates the directions of propagation of the radiation in the space 4π.
- *Phase* : it computes the optical properties of the surfaces (i.e. opaque surfaces and earth scene), the atmosphere and the vegetation.
- *Maket* : it simulates the 3D architecture of the scene.
- *Dart* : it simulates the radiative budget.

Figure 4.2: DART images of St. Sernin basilique (Toulouse). Radiometer: a) BOA, b) TOA, c) Airborne LIDAR (display with SpdLib software). Atmosphere: mid-latitude summer. Visibility = $23Km$.

4.2.1 Earth-Atmosphere scene

General introduction

The scene to model is contained in a rectangular parallelepiped divided into parallelepiped cells (voxels) (figure 4.3). The cells size, defined by the user and used to simulate the earth scene are in general smaller than those used to simulate the atmosphere. In DART, a scene element is either a volume or plane surface. The former is a 3D juxtaposition of cells filled with turbid material used to simulate fluids (air, water...) and vegetation. The latter is a juxtaposition of triangles or parallelograms used generally to simulate urban elements and topography [91]. In addition, DART scene can contain empty cells (i.e. without interaction with the radiation) or mixed cells (i.e. contains turbid matter and surface elements).

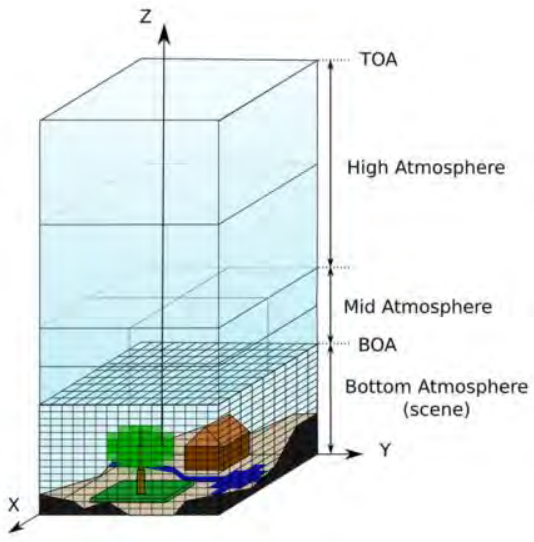

Figure 4.3: Earth-atmosphere representation

Boundary conditions

Even though the scene in DART is represented as a finite parallepiped, infinite landscapes can be also simulated as the juxtaposition of a given pattern.

- Isolated scene: a ray that exists the scene is eliminated.
- Repetitive scene: the scene and topography (DEM: Digital Elevation Model) are duplicated for simulating an infinite landscape. To get a spatially continuous scene and avoid that a ray is reintroduced under the ground, the DEM is regularized so that altitudes of the opposite faces of the scene are equal. A ray that exits the scene through a vertical scene side enters the scene through the symmetric vertical scene side, with the same direction and at the same altitude.
- Infinite slope: the scene is repeated by ensuring continuous slopes. For that, the altitudes of the edges of the scene are shifted by a constant value at each edge. a ray that exists the scene through a vertical scene side enters the scene through the symmetric vertical scene side, with the same direction and the constant vertical shift.

3D objects

Objects in DART can be generated having simple geometrical forms. In this study, the CAD environment of DART is used to create plots or quadrilaterals containing turbid matter to

simulate vegetation. It is also used to create schematic trees. Each tree specie is defined by many characteristics [77]:

1. The height of the trunk under and in the crown.
2. The diameter of the trunk under the crown.
3. The shape of the crown (trapezoid, truncated cone, compound cone, ellipsoid, compound ellipsoid), and associated parameters (e.g. diameter, height).
4. The azimuth rotation around the vertical axis of the tree.
5. The presence or absence of branches.
6. The crown levels, and for each defined level, the horizontal and vertical distributions of H, the diameter of the trunk, the optical properties of the leaves, trunk and branches.

The position and the size factors of the trees can be defined by three ways:

- Exact position and dimensions of the trees.
- Exact position and semi-random size of the trees.
- Semi-random positions and sized of the trees.

The trees trunks are represented by triangles while the crown can be represented by turbid cells or a cloud of triangles the density and distribution of which are defined by the user.
DART can also generate buildings of four walls and complex roof forms, roads and aquatic surfaces, and landforms derived from a terrain model imported as a raster image.
DART has also the possibility to import 3D objects generated by 3D CAD software tools such as Rhinoceros, Blender, etc. These objects are represented by triangles (or parallelograms), classified into groups based on their corresponding materials. Therefore, a building is composed of a minimum of three groups of triangles: "walls", "windows" and "roof". Each 3D object can be treated as a set of triangles or mixed or totally transformed into turbid cells. This can be used for the vegetation. The transformation from "triangles" to "turbid cells" reduces significantly the computational time. During this transformation, the properties of the turbid matter is either calculated by DART given the triangles properties, or set by the user himself.

Atmosphere

The atmosphere has a major role in the radiative budget, via the absorption, emission and diffusion of the radiation. Its impact depends on its state (pressure, temperature), spatial

distribution of its components (gases and aerosols) and the wavelength considered. DART simulates the effect of the atmosphere by meshing it into cells the size of which is inversely proportional to the density of the component particles of the atmosphere. The atmosphere is simulated as the superposition of three matrices of cells "air":

- Bottom atmosphere (BA): cells "air" at Earth landscape level, i.e. below landscape top altitude.
- Mid atmosphere (MA): from BA up to HA. It is made of cells that are usually larger than BA cells.
- Higher atmosphere (HA): above MA. It is made of superimposed layers.

The atmospheric cells are characterized by the spectral properties of the gases and aerosols they contain. The profiles of these particles are stocked in the database of DART, but they can be modified or imported by the user.

4.2.2 Elements optical properties

The optical properties define how the surfaces and volumes of the scene elements intercept, absorb and scatter the radiation. They depend on the chemical composition and structure of these elements.

Properties of surfaces

The transfer functions of surfaces are characterized by a reflectance, direct transmittance and diffuse transmittance. These spectral properties depend on the spectral band considered. They are either read in DART's internal databases, entered by the user, or generated by DART built-in models. These properties allow the calculation of the absorptance and the directional emissivity of the surfaces.
A surface's reflectance can be isotropic, constant independently of the direction (i.e lambertian) or anisotropic (analytic model: Hapke, RPV,) with possible specular term.

- Lambertian reflectance:

$$\rho(\Omega_S, \Omega_V) = \rho_{lamb} + \rho_{spec}(\Omega_S, \Omega_V) \tag{4.1}$$

The specular reflectance depends on the refractive indices of the incident medium and of the medium radiation heads to, a multiplicative factor and the angular widths of the cones where specular radiation propagates.

- Reflectance Hapke and specular:

$$\rho(\Omega_S, \Omega_V) = \rho_{Hapke}(\Omega_S, \Omega_V) + \rho_{spec}(\Omega_S, \Omega_V) \tag{4.2}$$

In the Hapke model, the ground is simulated as a plane medium containing particles, randomly distributed and large compared to the wavelengths. It is associated to a phase function that simulated backscattering and forward scattering.

- Rahman-Pinty-Verstraete reflectance (RPV) This model easier to use than that of Hapke, reproduces well the standard bidirectional reflectance distribution function BRDFs of terrestrial surfaces, even asymmetrical, and the hotspot effect.

$$\rho(\Omega_S, \Omega_V) = \rho_0 . M_I(K) . F_{HG}(\Theta) . H(\rho_c) \tag{4.3}$$

M_I is the Minnaert function, F_{HG} is based on Henyey-Greenstein functions and H is a function that simulates the hotspot.

Properties of turbid cells of vegetation

The optical properties of vegetation cells filled with turbid matter are characterized by phase functions defined by:

- The spectral optical properties of the leaf: transmittance and reflectance, and descriptive parameters of foliar specular behavior (roughness, refractive index), calculated by implemented models in DART PROSPECT-5 and PROSPECT-D, given the leaf biochemical input parameters, such as the water content and chlorophyll concentration to list few.
- Leaf dimension for hot spot
- Leaf angular distribution
- Leaf clumping or leaf agglomeration at certain points
- Temperature property for thermal emission calculation

4.2.3 Earth-atmosphere radiative transfer

The earth-atmosphere radiative transfer is simulated in five stages as shown in figure 4.4:

- Stage 1 or Illumination stage: the earth is illuminated by the sun radiation and atmosphere scattering. In case mode T is used, the thermal emission form the atmosphere is added. This stage gives the downward BOA radiance L_{BOA} ($\Omega \downarrow$), upward TOA radiance L_{TOA} ($\Omega \uparrow$) and the upward and downward sensor radiance.
- Stage 2: landscape RT with/without thermal emission, by tracking the L_{BOA} ($\Omega \downarrow$) computed in stage 1. This stage gives the landscape radiative budget, albedo and upward BOA radiance L_{BOA} ($\Omega \uparrow$).
- Stage 3 atmosphere backscattering down to the landscape by tracking the upward BOA radiance computed in stage 2.
- Stage 4 landscape RT of the radiation that the atmosphere backscatters at stage 3.
- Stage 5 Transfer of the upward fluxes of stage 2 and 4. This stage provides the radiance at sensor and the upward TOA radiance L_{TOA} ($\Omega \uparrow$).

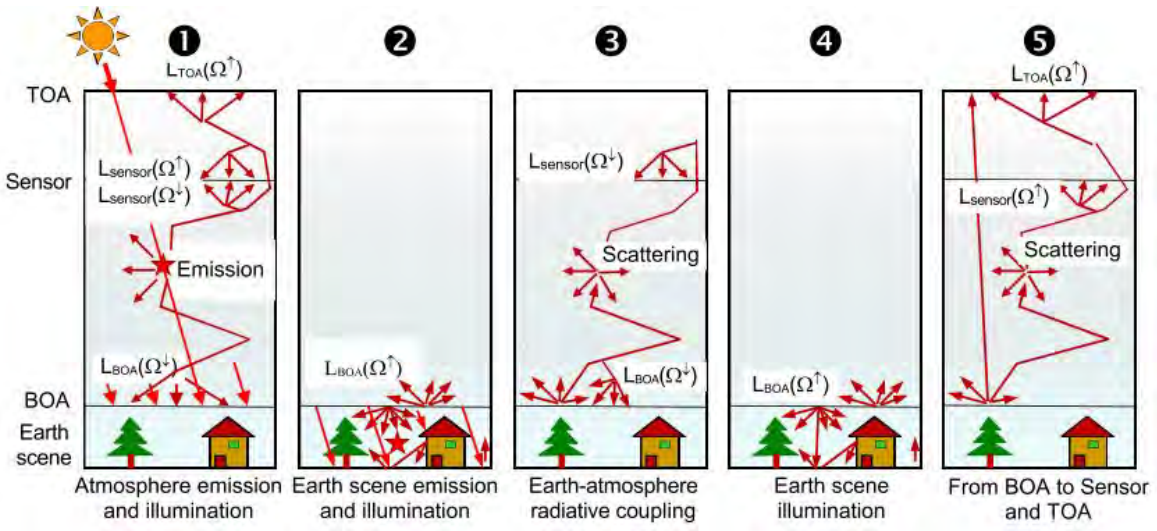

Figure 4.4: Earth-atmosphere representation

General information on radiative transfer

Radiative transfer corresponds to the propagation of radiation in a medium. Using the exact kernel and discrete ordinate methods, radiation is restricted to propagate in a finite number of directions (Ω_i) with an angular sector width ($\Delta\Omega_i$) (sr), in such way to always have $\sum \Delta\Omega_i = 4\pi$ ([92]). Any radiation that propagates along direction (Ω_i) at a position r is called source vector $W(r, \Omega_i)$. The radiative transfer equation gives the rate of variation of the radiance $L(r, \Omega)$ at position r along path dr along direction Ω of a stationary monochromatic wave. It can be written in the Cartesian coordinate system as:

$$[\zeta d/dx + \eta d/dy + \mu d/dz].L(r, \Omega_n) = -\alpha_e(r, \Omega_n).L(r, \Omega_n) + \alpha_a(r, \Omega_n).L_B(r, \Omega_n) + \sum_{m=1}^{N} \alpha_d(r, \Omega_n).P(r, \Omega_m \rightarrow \Omega_n)/4\pi.L(r, \Omega_n).\Delta\Omega_n \quad (4.4)$$

where:

- ζ, η and μ = cosine angles of the direction of propagation (Ω) wave along x, y and z.
- $\alpha_e(r, \Omega_n)$, $\alpha_a(r, \Omega_n)$ and $\alpha_d(r, \Omega_n)$ = extinction coefficients (total, absorption and scattering), $\alpha_e = \alpha_a + \alpha_d$
- $L_B(r, \Omega_n)$ = radiance emitted by a black body
- $P(r, \Omega_m \rightarrow \Omega_n)/4\pi$ = normalized phase function of the medium. It is the fraction of radiation that is intercepted along direction m that is scattered per unit solid angle along direction Ω_n.

The terms of right-hand side of the equation give the variation of $L(r, \Omega)$ per path unit $dr(\Omega)$:

- 1st term: attenuation (absorption + scattering "$\Omega \rightarrow 4\pi$") of a wave during its propagation $dr(\Omega)$.
- 2nd term: scattering along (Ω) due to scattering at point r of radiation incident from all directions of space.
- 3trd term: thermal emission.

At the top of the earth scene BOA (Refer to section Earth-Atmosphere scene), we have two components that form the irradiance: the direct sun and the atmosphere. The source vector of both components are computed as follows:

- Direct sun source vector $W(\Omega_s) = E_s(\Omega_s).|\mu_s|.\Delta x.\Delta y$
- $E_s(\Omega_s)$ is the direct sun irradiance at the top of the scene $(W/m^2/m)$
- $\mu_s = cos\theta_s$ with θ_s the sun zenith angle
- $\Delta x.\Delta y$ is the cell face area
- Atmosphere source vector $W_a(\Omega_s) = L_a(\Omega_n).|\mu_n|.\Delta x.\Delta y.\Delta\Omega_n$ due to atmosphere scattering and/or thermal emission
- $L_a(\Omega_n)$ is the atmospheric radiance $(W/m^2/sr/m)$ along direction Ω_n
- $n \in [1, N']$ with N' the number of downward discrete directions

Ray tracing approach

Ray tracing method solves numerically the above equation: N rays along N directions are traced from each source. During its propagation, a ray has its intensity that decreases by interception (absorption/scattering) and increases by thermal emission. Scattering generates, along Ndir directions, new rays $W_1(r, \Omega_n)$, the further scattering of which gives new rays $W_k(r, \Omega_n)$, and so on. With an iterative and convergent approach, the radiation intercepted by scene elements at iteration i is scattered during the following iteration i + 1. A radiation is processed until it reaches a specified threshold or is totally absorbed and scattered. The iteration process stops when the difference in scene exitance between two consecutive iterations is less than a certain value. The iteration process is a powerful feature of DART, especially when simulating urban areas, where reflections from surroundings are a major player in the total intercepted radiation by the urban forms. The ray tracing approach has three simulation modes: reflectance (R), temperature (T) and combined (R + T). In the R mode, the sun is the primary source of radiation and the atmosphere the second source. Only the shortwave optical domain is considered. In the T mode, the sun radiation is neglected and the atmosphere brightness temperature is computed. The R + T mode combines both approaches. In our case, we are only interested in computing the visible shortwave radiation as will be discussed later. Therefore, we will use the mode R in our simulations.

Simplified examples of DART radiative budget

Figure 4.5 illustrates the 3D RB at $0.56\mu m$ of a schematic building. The building is made of 4 walls with 2 windows each one, and a roof with a swimming pool. All surfaces are lambertian,

except the swimming pool that has a specular component. Sun angles are $\theta_{sun} = 30°$ and $\phi_{sun} = 225°$. Scene irradiance ($E_{BOA} = 1347W/m^2/\mu m$) is simulated with a 2mm grid. Cell size is 5cm. 3 remote sensing images are shown for 3 viewing directions (θ_v, ϕ_v): nadir ($\theta_v = 0°$), oblique $(30°, 135°)$ and "specular" $(30°, 45°)$. Reflectance and RB have a spatial variability that depends on the illumination grid and the size of triangles used to simulate the scene. For example, in the nadir image, ρ_{roof} is between 5.77 and 5.83 with an average of 5.77.

3D RB is shown at triangle level (Figure 4.5b) and cell level (Figure 4.5c) for interception at direct sun illumination (i.e., Illudir), total illumination (i.e., Illudif), and infinite scattering order (i.e., IterX). As in remote sensing images, extreme RBtriangle values appear due to a few extremely small triangles that are illuminated or not. For example, $\%f_{int,IterX}$ reaches 1.61 for a few extremely small triangles, whereas its "real" maximum is equal to 1; it occurs for the roofs. Such extreme values do not occur for RBcell since all cells have the same size. Compared to walls, windows have the same irradiance, larger absorption and smaller scattering. Figure 4.5d shows RB images for the scene and the roof. It shows also 2 vertical sections of the 3D RBcell that corresponds to a sunlit wall ($x = 20$) and a shadowed wall ($x = 60$).

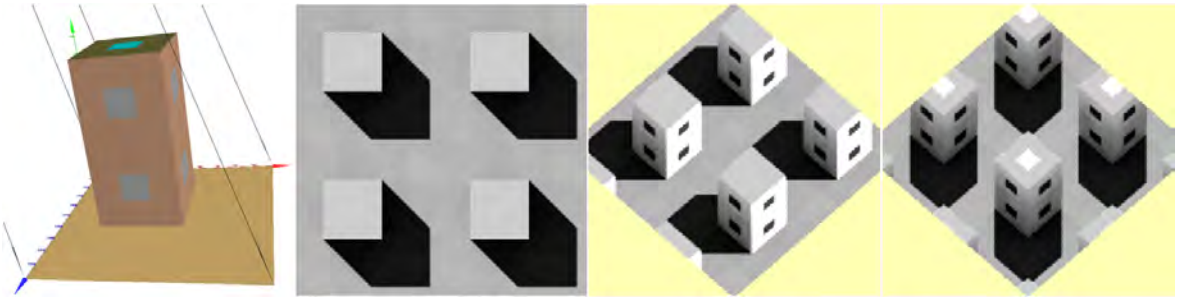

(a) Building mock-up and Remote sensing images for 3 viewing directions (v,v): nadir (v =0), (30,135) and "specular" (30,45).

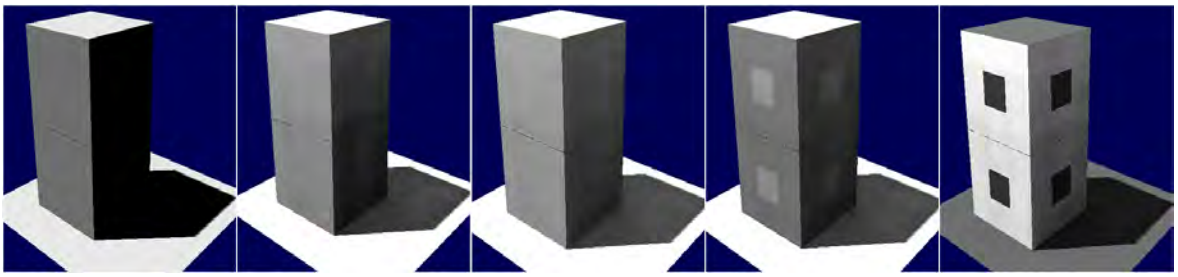

(b) 3D RB for triangles RBtriangle and for cells RBcell.

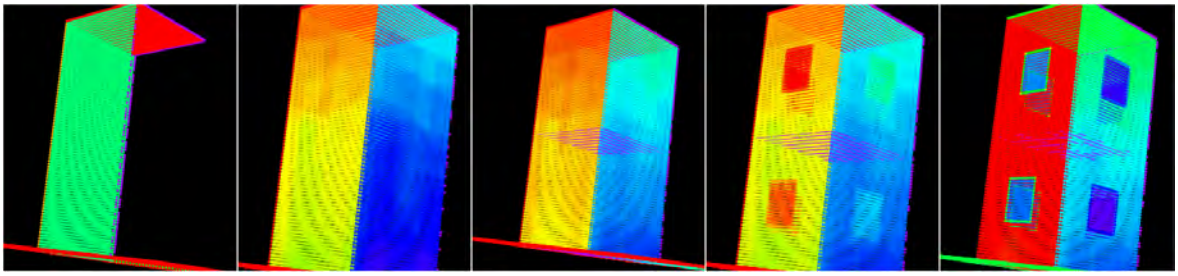

(c) intercepted radiation at Illudir, Illudif and IterX, with absorption and scattering at IterX.

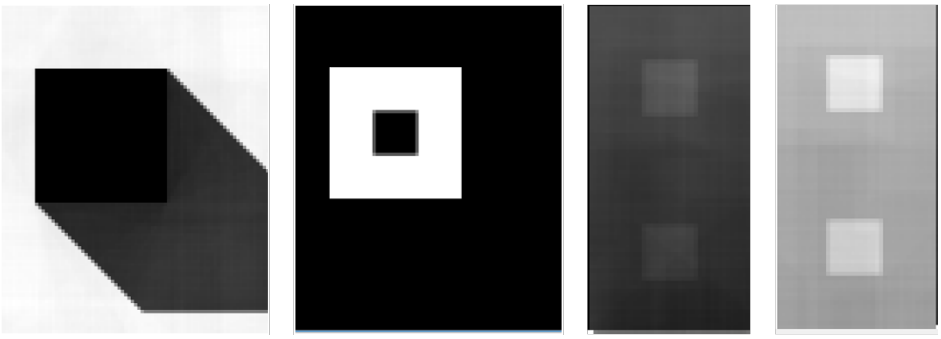

(d) RBabs images: absorption by the total scene, the roof, a sunlit wall and a shadowed wall.

Figure 4.5: Radiative budget and remote sensing images of a schematic building.

Figure 4.6 shows the 3D view of the Beirut radiative budget component "triangle

irradiance" (W/m2/μm) by triangles. The RB is simulated at 425nm, on June 21 at 17h. The illumination grid is 1cm. At 17h, sun zenith angle is 81.1°, which explains the presence of many shadows in the radiative budget for direct sun illumination only (Figure 4.6a). Indeed, the DART simulation is conducted with the "repetitive scene" option. In that case, the shadows are due to the neighboring districts of the simulated Beirut district. This effect due to neighboring districts can be removed if needed, using either the "isolated scene" option, or by setting the irradiance on one or several faces of the 3D cell array of the simulated urban scene. This latter option was introduced in DART in order to simulate the districts on the sea side. It is not used here. The large sun zenith angle (81.1°) explains that the SKYL is very large, which in turn explains that maximal direct sun irradiance is much smaller than sky irradiance. We have: $E_{directsun} = 3.7W/m^2/\mu m$. Hence, the irradiance of the roofs is $3.7W/m^2/\mu m$. The irradiance of the walls on the west side of the buildings is much larger; it is around $23.7W/m^2/\mu m$. The rectangular shapes of the ground are due to the discretization scheme that is used to simulate the digital elevation model.

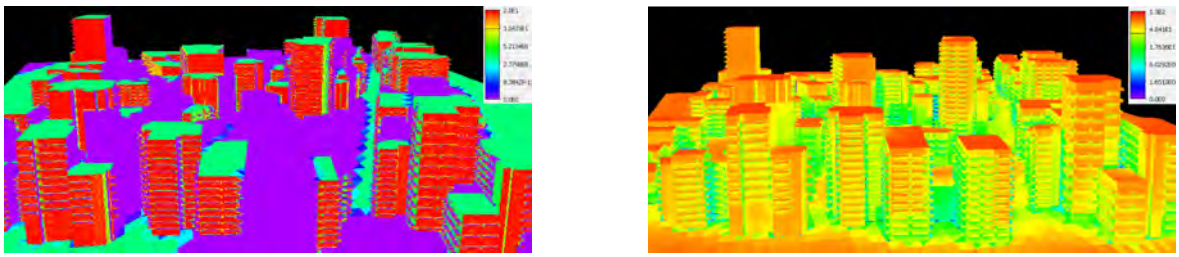

(a) Direct Illumination

(b) Infinite extrapolation

Figure 4.6: 3D view of Beirut intercepted energy ($W/m^2/\mu m$) by triangles for two different orders, on June 21 2017 at 17h (Band: 425nm).

4.3 Impact of urban development on energy budget

In the last decades, Beirut has experienced a random urban growth and the rise of high buildings above 10 floors. This wave of urbanism led to the reduction of the distances between the buildings and to their adhesion. This chaos in construction has resulted in the decrease of the incoming daylight into the apartments. The purpose of applying DART in this section is to estimate the impact of urbanization on the daylight accessibility of buildings. For this purpose, the radiative budget of windows for a small number of mixed buildings in the last

decade will be compared with that of the same district in the 1980s. Having the year of construction of each building, buildings built after 1985 were removed to represent the scene of the 1980s (see Figures 4.7 and 4.8).

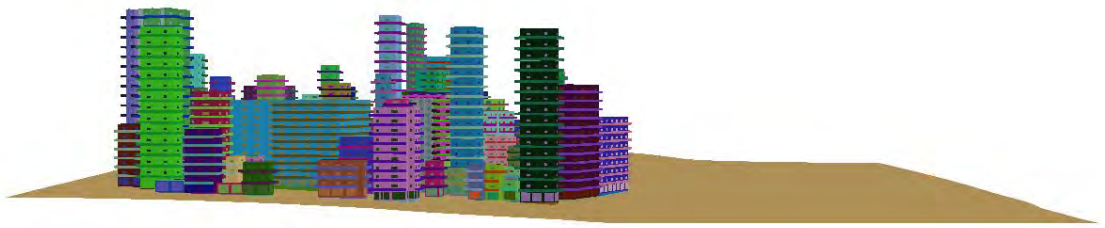

Figure 4.7: Side view of the 3D model of the district case study

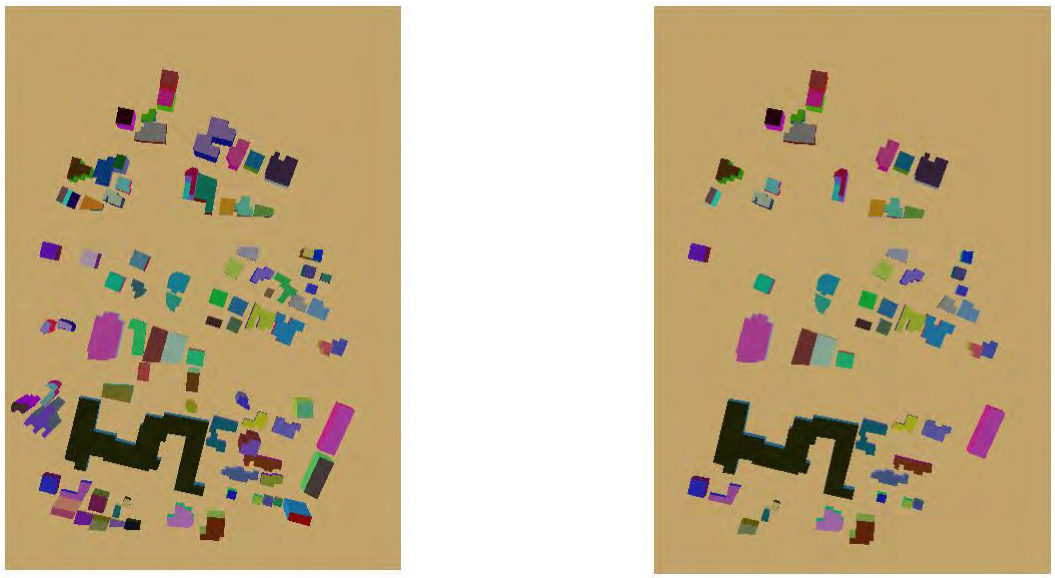

Figure 4.8: Top view figures representing the district in the 1980s (left) and recently (right).

Another exercise with DART is to assess the influence of buildings features (windows, balconies...) on the radiative budget simulation. Quantifying the influence of integrating different aspects in the 3D model is important since most of urban daylight model rely on simplification of the buildings models, without assessing the consequences of such assumption.

The intercepted energy at 3 bands is simulated each time a new feature is added to the 3D model. The increasing complexity of the model is presented in figure 4.9. Figure 4.10 represents the mean incoming radiation on the buildings facades (including walls and windows when exist) for the different models. The results of the models 0 and 1 are almost the same as shown in the figure. However, when the balconies are added in model 2, a significant decrease of the intercepted energy is noticed. The inclusion of the DEM reduces even more the intercepted energy by the facades. It is important to point that the topography of the district we are studying is not too rough, reducing its impact in our case.

In most studies, when no windows are added, the results presented are those of the facades as in model 0. To be more accurate, the intercepted energy by the windows in models 1, 2 and 3 is compared to the intercepted energy by the walls in model 0, as shown in Figure 4.11. A further decrease of the intercepted radiation is detected, especially at the middle and highest floors, since the windows surfaces' area is less than that of the walls (not all walls have windows). At lower floors, the intercepted energy is almost unchangeable because all the buildings are mixed, which means that the windows of the first floors are in fact glazed facades for shops which cover all the walls, i.e. the area of the windows is almost equal to that of the walls.

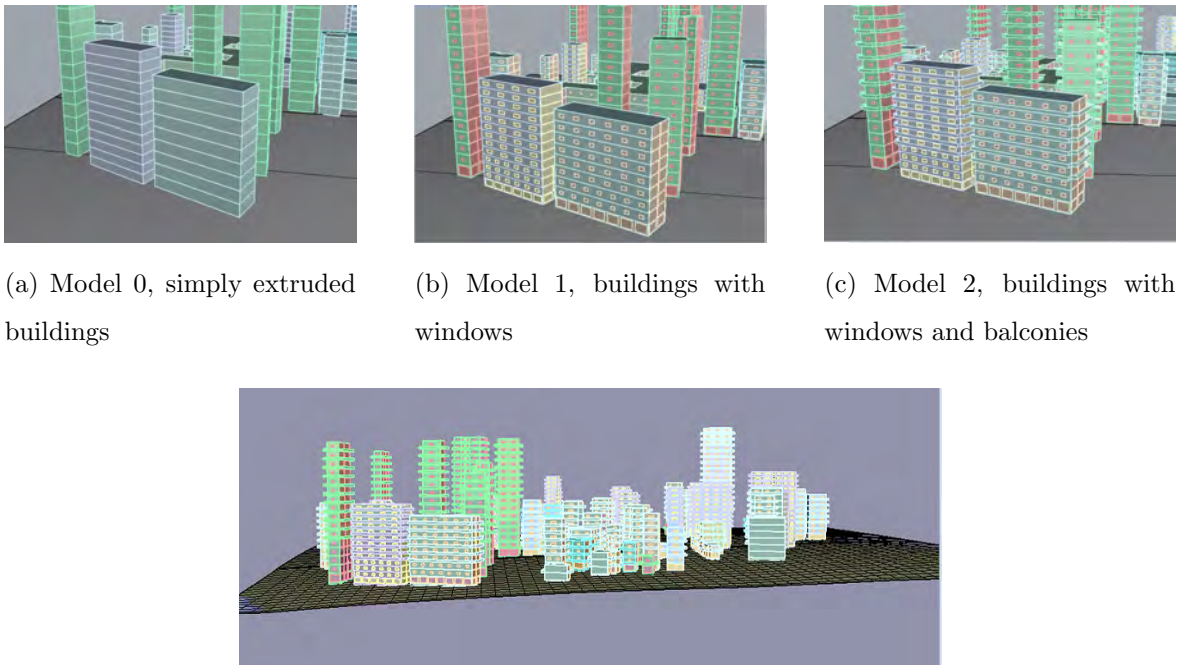

(a) Model 0, simply extruded buildings

(b) Model 1, buildings with windows

(c) Model 2, buildings with windows and balconies

(d) Model 3, final 3D model with DEM generation

Figure 4.9: Different 3D models of the urban area used in the simulation of the radiative budget in DART. The models represent different Level of Details (LoD).

Figure 4.10: Elevation profile of mean incoming radiation along the buildings' facades, at 7am on 21 June (Band $[470nm, 620nm]$.

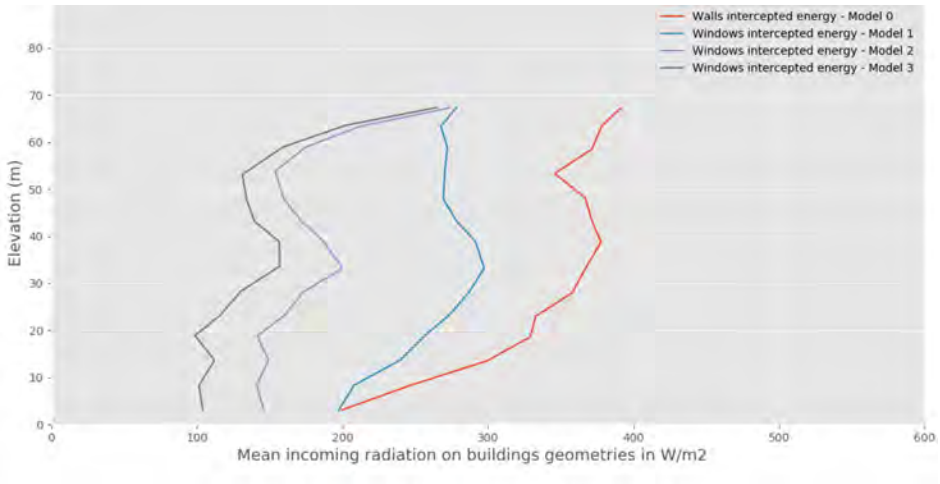

Figure 4.11: Elevation profile of windows mean incoming radiation along the buildings' heights, at 7am on 21 June (Band $[470nm, 620nm]$.

4.4 Effect of urban morphology on daylight accessibility

4.4.1 Urban morphology metrics

Compact city as a sustainable urban form is a famous trend among urban planners. Burgess defined the compact city approach as "to increase built area and residential population densities; to intensify urban economic, social and cultural activities and to manipulate urban size, form and structure and settlement systems in pursuit of the environmental, social and global sustainability benefits derived from the concentration of urban functions" [93]. Hence, planners have recognized the economic and environmental benefits of dense urban environments, such the optimal use of infrastructure and land, easy access to services and social interactions. However, the increased urban density leads to a conflict between space-use efficiency on one hand, and daylight access and walkability on the other [94, 95]. Many researchers argued about an experienced sense of compactness or compression influenced by the configuration of the urban zone. The qualification of an urban space, especially at the street level, based on this experienced compactness sense can be achieved through a range of urban design qualities [94] such as the imageability, legibility, human scale, and many others. To quantify these perceptual qualities, indicators

are implemented such as the sky view factor SVF, the aspect ratio, maximum view length, solid angle of view to list a few [96, 97, 98, 99, 100]. On the other hand, daylight is linked to buildings energy use and citizens' health. Many studies have been carried out to measure the solar access and the daylight availability in urban context [101, 102, 103] and assess its impact on the urban energy use [104]. Urban canyon geometries impact the solar access and were the subject of many studies to assess these relations [105, 26]. It was found that the location, the sky components, the width and orientation of the streets, the architecture and roof shapes of the buildings, the urban density and the optical properties of the materials of the ground and the surrounding facades are key parameters that affect the solar access [105, 26, 22, 106, 107].

In this study, focus is given to buildings' heights, orientations and the scene complexity. We also calculated the entropy of buildings and streets' orientations and the roads network's circuitry to compare the two zones.

Entropy of buildings and streets' orientations

The orientation entropies quantify the dispersal in the buildings and streets angles [105].

$$\rho_{streetorientation} = -\sum_{i}^{N} p_i log p_i \tag{4.5}$$

$$\rho_{buildingorientation} = -\sum_{i}^{N} p_i log p_i \tag{4.6}$$

where p_i is the probability that a street or a building is oriented along a direction i with respect to the North with i going from 0 to pi in steps of $pi/15$ and i from 1 to N with $N = 25$ is the number of bins.

Circuitry

The circuitry is defined as the ratio of the sum of all network's pairwise distances D to the Euclidean or straight-line distances D_e [105, 108]. It is also possible to use the great-circle distance instead of the Euclidean distance as suggested by [109]. The circuitry measures the tortuousity or the deviation from straightness of a road joining two points [105]. The average circuitry of the nework in each study area is given as below:

$$C = \frac{D}{D_e} \tag{4.7}$$

Vertical daylight profile

The vertical daylight profile corresponds to the profile of the intercepted energy by an urban component (in our case the windows) along the buildings' height. The analysis of this metric helps assessing the impact of urbanization on the daylight access on buildings' floors.

4.4.2 Radiative Budget computation - DART

Daylight Radiative Budget

For every band in the simulation, DART generates a RadiativeBudgetFigures file, that gives the radiative budget per triangle. We retrieved the information in the form of a list, where each element has the following format:

$$[surface_{type}, [x_1, y_1, z_1, x_2, y_2, z_2, x_3, y_3, z_3], [energy_{budget_values}, area]] \tag{4.8}$$

- Surface type: we have many types of triangles: Ground, Walls, Windows, Roofs, Balconies and Slabs. A number that is stored in the dart.typ file represents each type.
- The coordinates are those of the triangle vertices.
- Energy budget values: three types of energy: intercepted energy, absorbed energy and scattered energy.
- Area of each single triangle.

Since we are looking to represent the daylight, we use the standard illuminant D65 defined by the Commission Internationale de l'Eclairage (CIE) to convert the radiant energy into luminous (i.e., visible) energy. An illuminant is a mathematical representation of the light source based on human visual model, in this case the daylight. The average spectral sensitivity of human visual perception is also presented, called luminosity function. The CIE distributes standard tables with luminosity function values at $5nm$ intervals from $380nm$ to $780nm$ (the interval can be reduced to $400nm$ to $700nm$ since the values of the luminosity function becomes negligible at the wavelengths outside this interval). The following equation calculates the total luminous flux in a source of light:

$$\phi_V = \int_0^\infty \bar{y}(\lambda)\phi_{e,\lambda}(\lambda)d\lambda \tag{4.9}$$

Where

- ϕ_V is the luminous flux, in watts.
- $\phi_{e,\lambda}$ is the spectral radiant flux, in watts per nanometer.
- $\bar{y}(\lambda)$, also known as $V(\lambda)$, is the luminosity function, dimensionless.
- λ is the wavelength, in nanometers.

Formally, the integral is the inner product of the luminosity function with the power spectral density. In practice, the integral is replaced by a sum over discrete wavelengths for which tabulated values of the luminosity function are available. However, in our case, we divided the interval between $400nm$ and $700nm$ into 6 adjacent spectral bands as shown in table 4.1. Then, we calculated the mean of the luminosity function values for each spectral band as shown in the same table. Note that mean luminosity values must be divided by 100 since the relative value is 100 (for λ). Equation 4.9 becomes [110, 111]:

$$\phi_V = \sum_{i=1}^{6} \bar{y}(\Delta\lambda_i)\phi_{e,\lambda}(\Delta\lambda_i) \tag{4.10}$$

Spectral band number	Central wavelength $[nm]$	Spectral bandwidth $[nm]$	Mean Luminosity function [-]
1	425	50	93.55659
2	475	50	114.5002
3	525	50	106.5425
4	575	50	96.26877
5	625	50	86.35938
6	675	50	77.131782

Table 4.1: Central wavelength, spectral bandwidth and mean luminosity function of the 6 spectral bands of the visible spectrum defined in this study.

Description of the case study

Two zones (shown in figure 4.12) were arbitrary chosen for this study, having different urban complexity. The radiative budget on the external surfaces of 433 buildings in zone 1 and 414 buildings in B was simulated. Due to limited computational resources, the zones were subdivided into zones (6 subzones in zone1 and 3 subzones in zone 2) . The zones' boundaries

were overlapping to account for the effect of shadows from neighboring buildings. Buildings with missing function were considered residential. When no year of construction is available, it was assumed that the buildings were built after 1991.

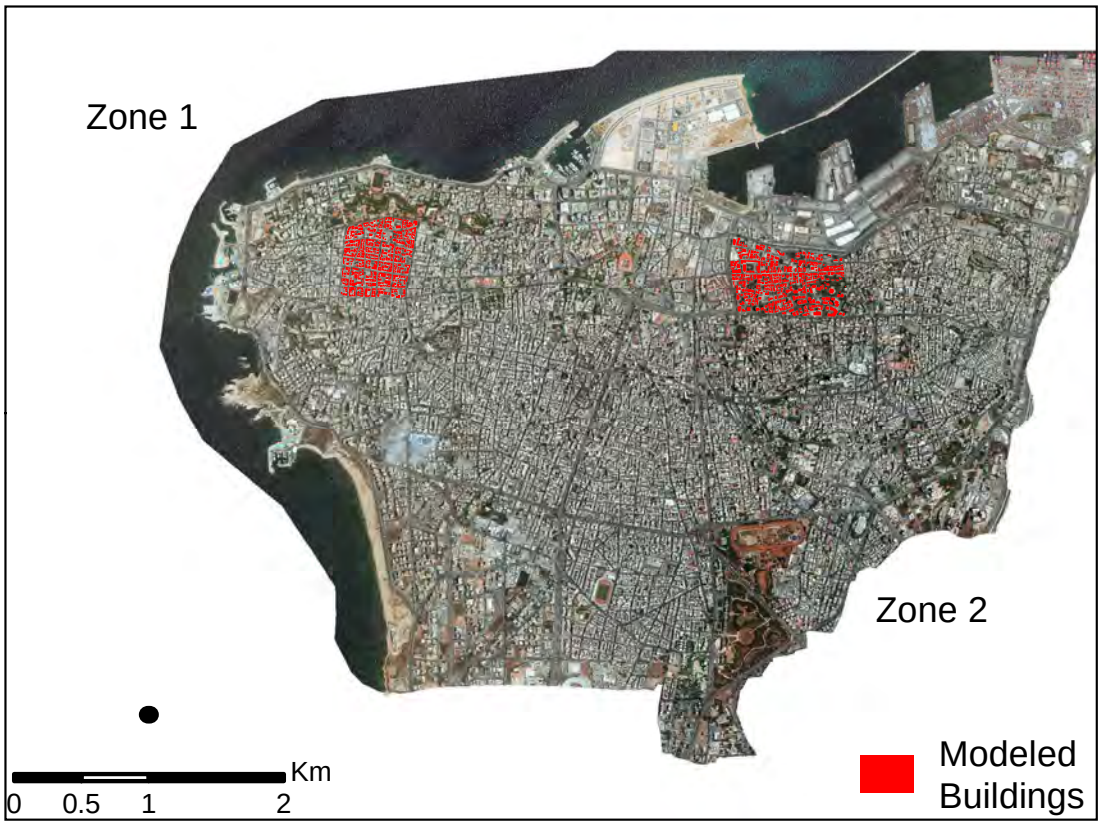

Figure 4.12: Buildings distribution in zones 1 and 2.

3D model generation

3D models of the buildings in the areas of interest were generated. Buildings were represented as flat roof models, divided into floors with windows and balconies. The window to wall ratio WWR and the optical properties of the windows, walls and roofs were identified based on the buildings'periods of construction. The latter gives insights on the construction materials and methods. A historical study of Beirut's buildings architectural aspects was achieved for this purpose. Five distinguished construction periods were identified. Spaces between buildings were assumed to be all roads, so the ground was attributed asphalt properties.

Materials' optical properties

Different types of materials characterize the buildings' components in Beirut. In the same period of construction, different materials can be encountered. For example, the roofs in 1900-1923 may be constructed of roof tiles or earth roofing recently covered by asphalt, or walls are either painted with white or beige color. Since no data regarding the materials' distribution, buildings were randomly selected and assigned the materials corresponding to their period of construction. Once the materials of the buildings components were identified, their optical properties were set. DART has an embedded library 'Lambertian database' with a large number of available materials and it was used in our case. However, the material's color is an important factor that should be considered. Therefore, the properties should be updated. A simple proportionality rule was applied based on the color's RGB for each of the six spectral bands of our simulations. Note that two dominating colors (beige and white) characterize the buildings' walls in Beirut. A python script was written to automatically assign properties to the large number of groups of the obj files.

4.5 Results and discussion

4.5.1 Zones' Urban morphology

The urban morphology of the zones is described by a set of urban metrics defined in section 4.4.1. Values of these metrics are reported in table 4.2. The two zones display similar morphology in terms of buildings and streets orientations entropies and road network circuitry. The buildings' heights distribution in Figures 4.13 and 4.14 shows that 50.5% of buildings in zone 1 have their heights between 20m and 30m while 40% of the buildings in zone 2 have their heights between 10m and 20m. The rose diagrams in figure 4.15 show that the buildings in both districts are mainly oriented north-south or east-west.

	Zone 1	Zone 2
Buildings' orientations entropy	1.06	1.08
Streets' orientations entropy	1.53	1.866
Road network circuitry	1.013	1.039

Table 4.2: Urban metrics characterizing the two zones.

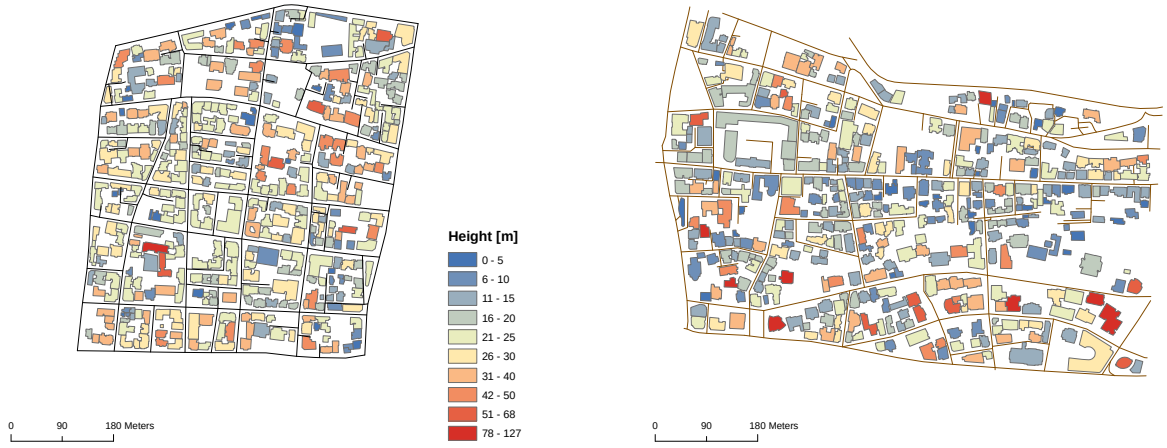

(a) Zone 1 (b) Zone 2

Figure 4.13: Spatial distribution of the buildings heights in zone 1 and 2. The driving network is also shown.

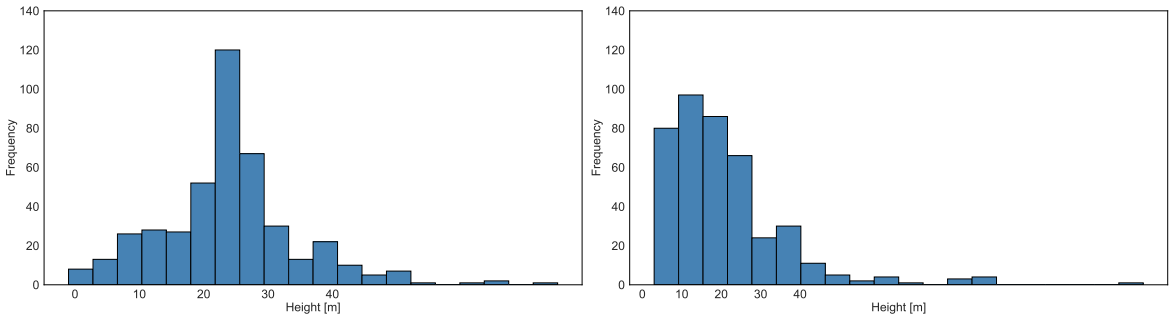

(a) Zone 1 (b) Zone 2

Figure 4.14: Buildings' heights distribution in both zones.

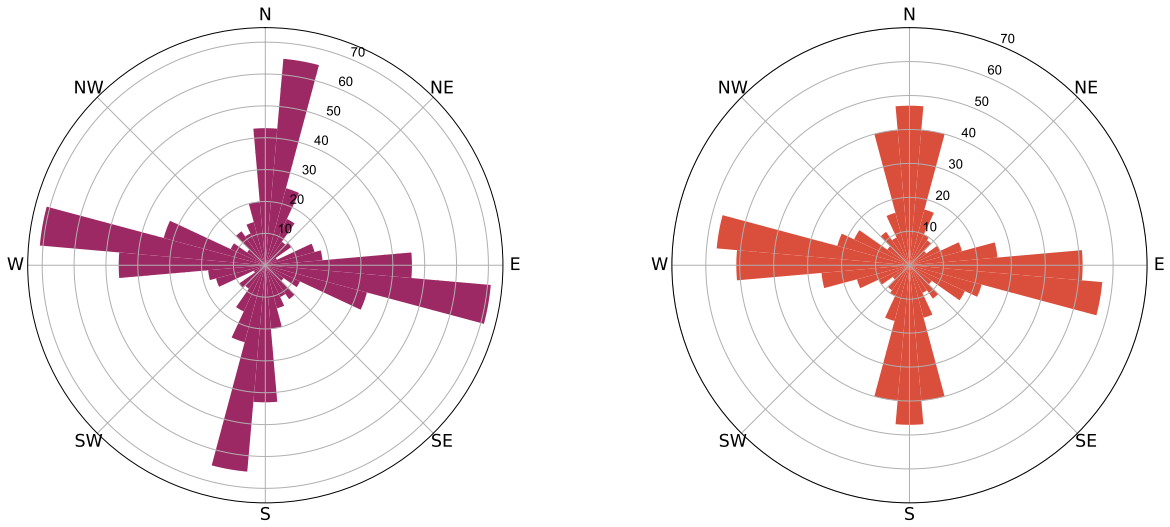

(a) Zone 1

(b) Zone 2

Figure 4.15: Buildings' orientations distribution in both zones.

4.5.2 Daylight availability and variability spatially and temporally

The mapping of the solar radiation in the subzones of zone 1 is presented in figures 4.16 at 9 am on March 21, for the spectral band $400nm - 450nm$. The 3D surface radiative budget results reveal the impact of the complex urban morphology. Walls without balconies receive higher energy compared to walls with balconies. Lower floors are less exposed to solar radiation than higher floors. These effects are more pronounced in figure 4.17.

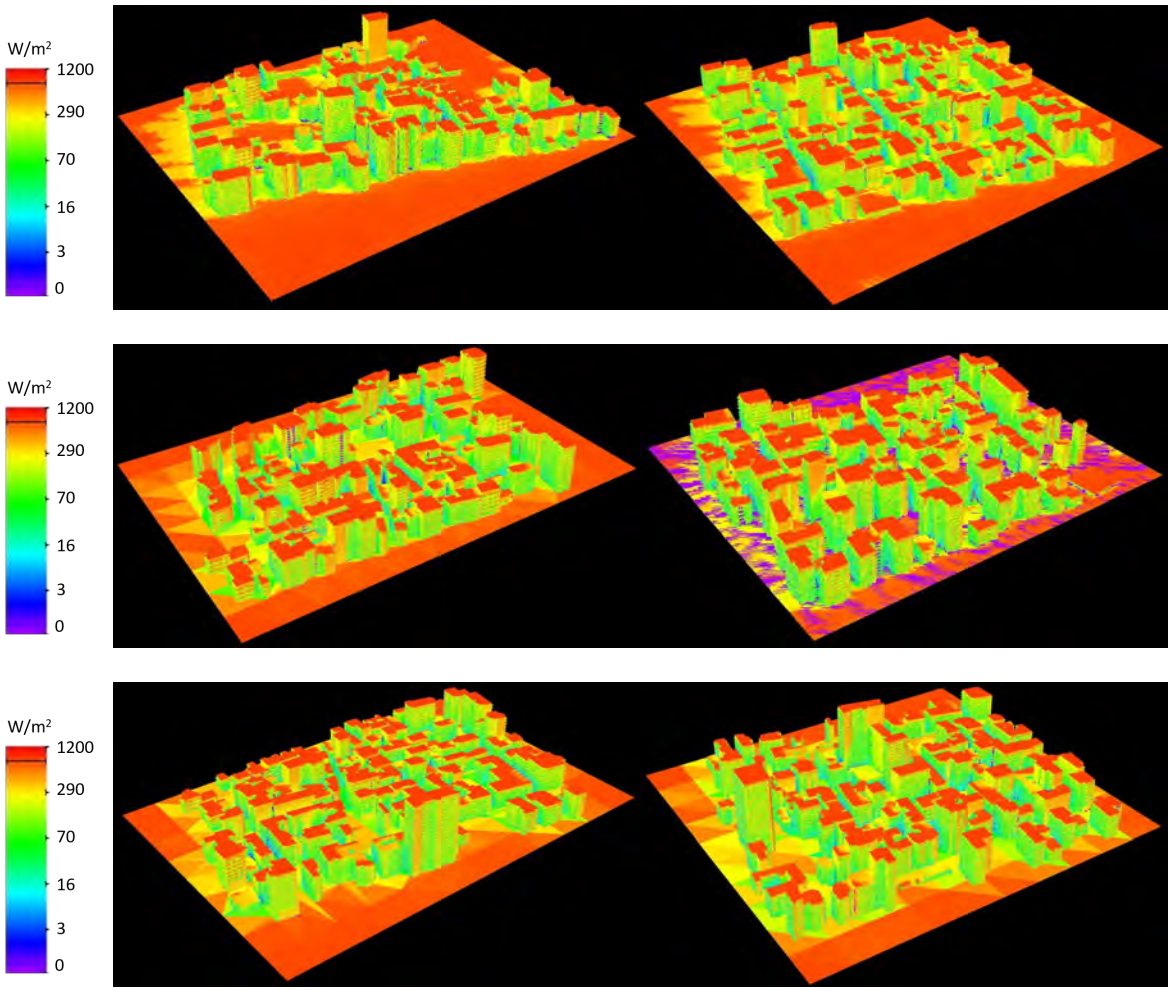

Figure 4.16: 3D surface radiative budget of the intercepted energy by buildings in the 6 subzones of zone 1, at 9am on March 21 (Band $[400nm, 475nm]$, Illumination grid = $10cm$).

To better quantify the variation of the daylight accessibility over the facades, the profiles of the windows' intercepted energy for daylight along the height of the buildings' facades are shown in figures 4.18 and 4.19 for zone 1 and 2 respectively. Their analysis demonstrates how much of the daylight accessibility is lost at the lower floors in each zone. The losses are quantified between the highest floors and the lowest ones at different hours and days of the year; the minimum loss among the simulated dates is of 74.3% at 12pm on June 21, while the maximum is of 87.8% at 9am on December 21 in zone 1. The losses are less dramatic, still high in zone 2, and ranged between 46.8% at 9am on September 21 and 58.5% at 3pm on the same day. The sudden increase at the end of each graph can be explained by the buildings having the maximum height in each zone (75m in zone 1 and 127m in zone2), as can be see in figure 4.14. These two buildings are both residential, having balconies on their floors acting

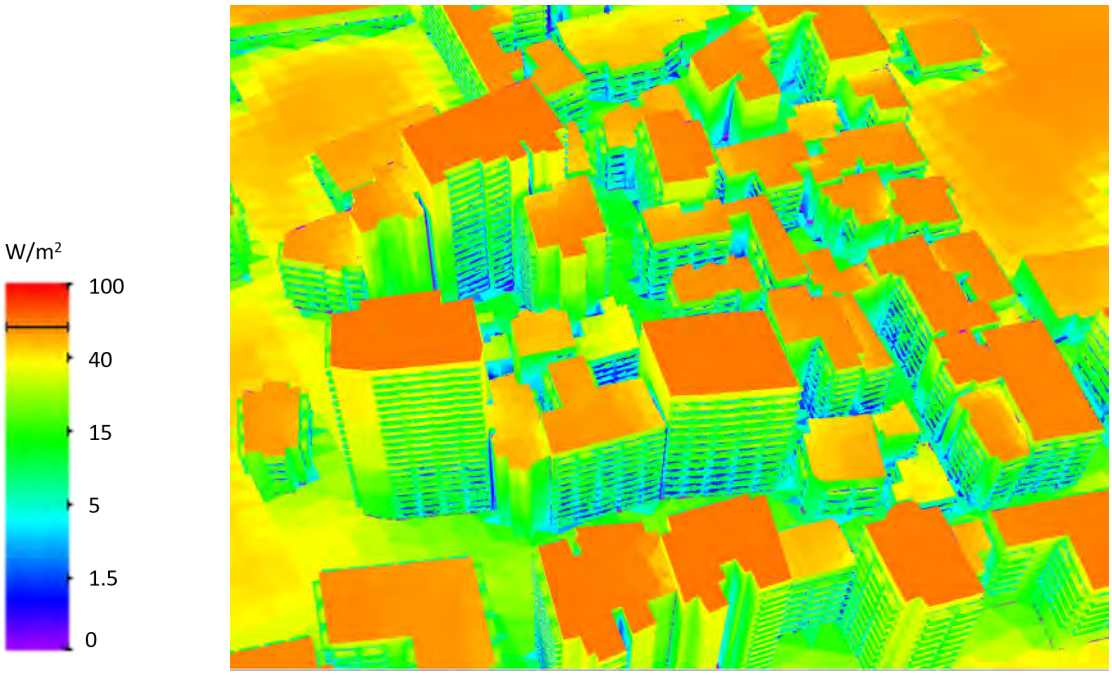

Figure 4.17: A top view of the 3D surface radiative budget of the intercepted energy by buildings in zone 1, at 5pm on September 21 (Band $[400nm, 475nm]$, Illumination grid = $1cm$).

as shading surfaces on the windows, except those of the last floors, of which the intercepted energy and therefore the daylight accessibility are not obstructed external or self-shading. Another interesting characteristic of the graphs in zone 2 is the almost steady variation of energy between 80m and 120m in zone 2, which are in fact the energy intercepted by the windows of the highest building in the scene, of 122m while the second highest building is of 87m.

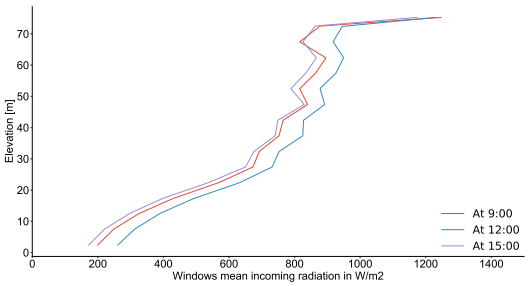

(a) 21 March

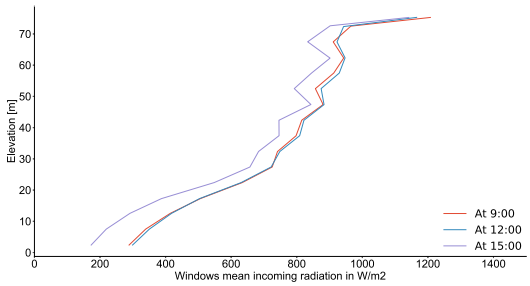

(b) 21 June

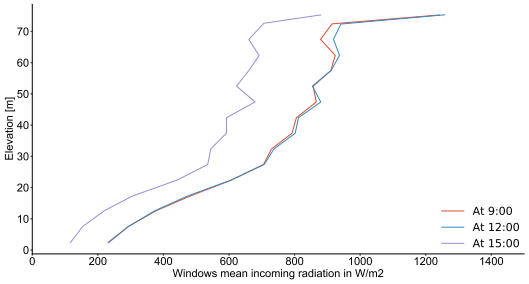

(c) 21 September

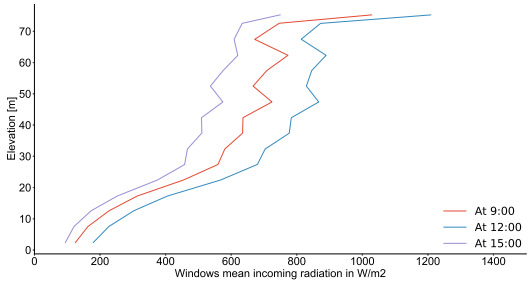

(d) 21 December

Figure 4.18: Vertical profile of the intercepted daylight energy on the buildings' windows in zone 1, at different hours of fours days of the year.

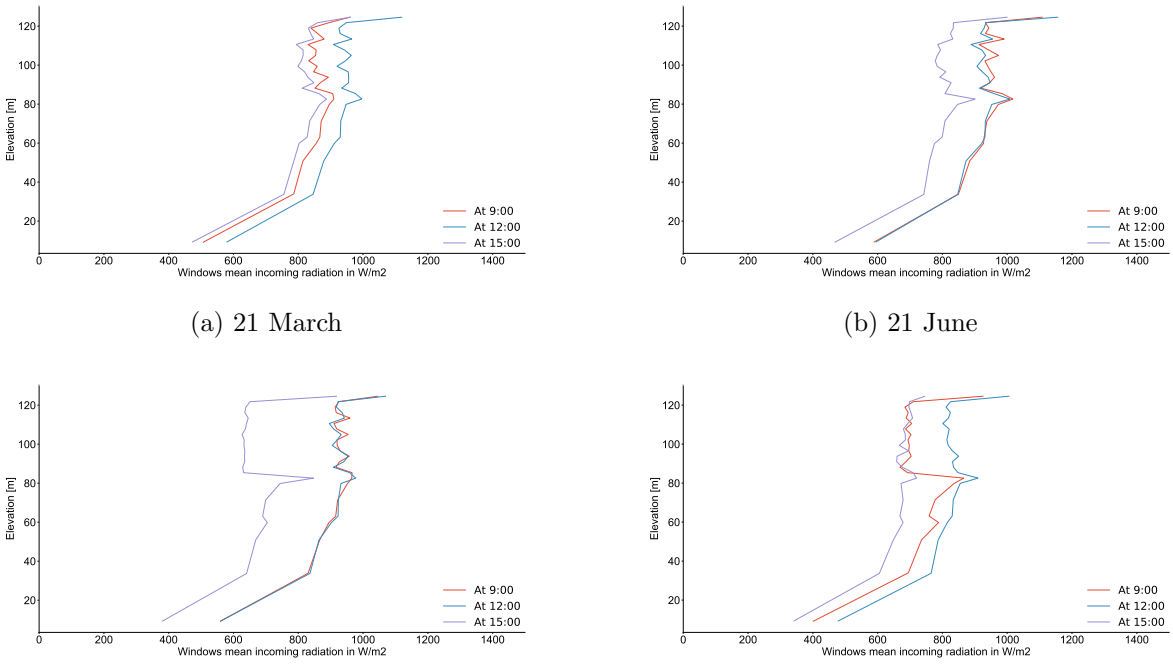

(a) 21 March

(b) 21 June

(c) 21 September

(d) 21 December

Figure 4.19: Vertical profile of the intercepted energy on the buildings' windows in zone 2, at different hours of fours days of the year.

4.5.3 Daylight potential and urban forms: Neural networks approach

Many studies have proved the impact of buildings' orientations on solar potential and daylight access [112]. The analysis of the results in the study hereby exhibits a difference of the intercepted energy of maximum 26.3% at 9am on March 21 between buildings oriented 105° from north and buildings oriented 45° from north (clockwise), for example. Figures 4.20 and 4.21 show that the variations of the daylight as function of the buildings' orientation in both districts.

Non-linear multivariate regression was performed to predict the daylight availability by correlating it to urban related variables. Neural Network NN was employed to achieve this task. It was trained an tested using Python. The first step to create a NN is to identify its input variables. In this study, quantitative variables were only used, and presented as follows:

- $\bar{H_S}$: mean height of surrounding buildings
- $\bar{O_S}$: mean orientation of surrounding buildings

- σ_{H_S}: standard deviation of surrounding buildings' heights
- σ_{O_S}: standard deviation of surrounding buildings' orientations
- H: building height
- X: building x coordinate
- Y: building y coordinate

Surrounding buildings were identified as were the shading surfaces in section 3.4.2. Briefly, a surrounding building (of height h) is a building that is $3.78h$ away from the target building within a radius of $300m$.

Due to different ranges of values of the NN features, scaling of the features was essential to bring values to the same ranges. The values of the features were standardized by removing the mean and scaling to unit variance using StandardScaler() from sklearn library, that calculates the standard score of a sample x by applying the following equation:

$$z = \frac{x - \mu}{s} \tag{4.11}$$

where μ is the mean of the training samples, and s is the standard deviation of the training samples. In this study, the multilayer perceptron (MLP) regressor neural network was adopted. The number of hidden layers was identified through an optimization process to reduce the mean absolute percentage error (MAPE). Figure 4.22 shows the variation of the MAPE as function of the number of hidden layers. The optimum number of hidden layers is one. The number of nodes of this layer is 5, representing 2/3 of the input layer nodes. The sigmoid function was chosen and the following parameters were set: the number of iterations (20 iter) and the learning rate (0.0001).

The data set was divided into a training set and a test set of 70% and 30% respectively. Simulation were carried out on the training set. Figure 4.23 illustrates the weights matrices of one of the generated neural network. By predicting the output of the test set using the generated NNs, the MAPE varied between a minimum of 18% and a maximum of 42% depending on the date on which the daylight is to assess and the representative area to study.

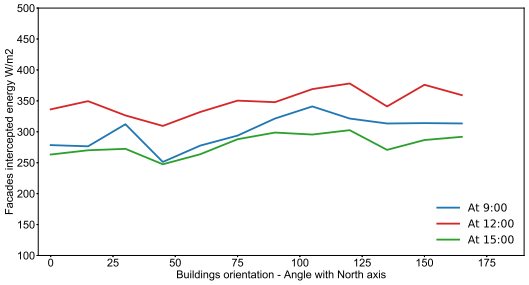

(a) 21 March

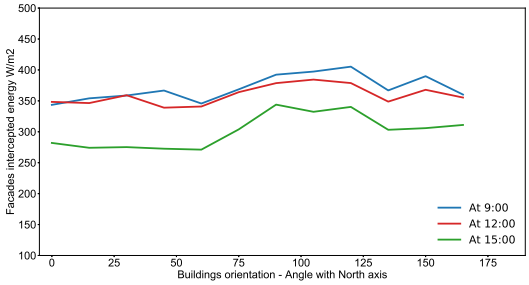

(b) 21 June

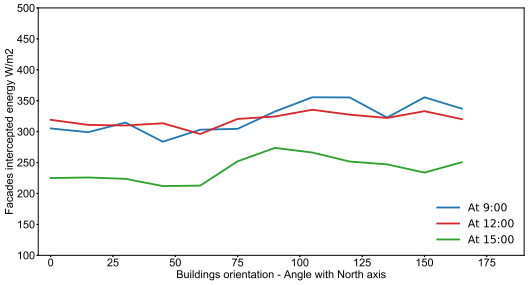

(c) 21 September

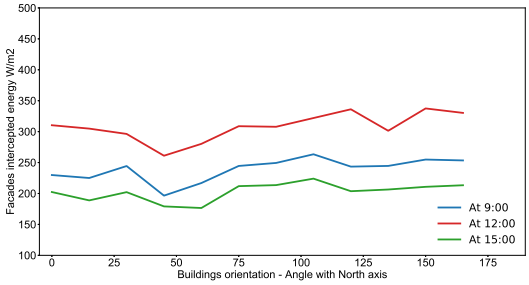

(d) 21 December

Figure 4.20: Mean facade intercepted daylight energy variation in function of buildings' orientation in zone 1.

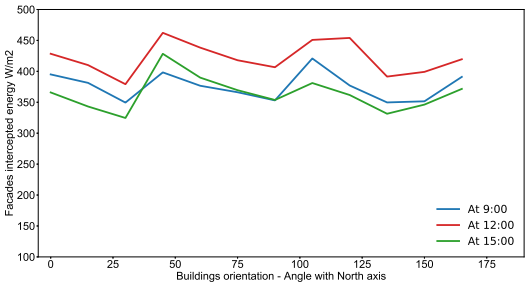

(a) 21 March

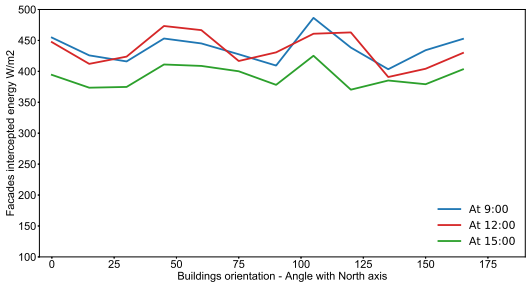

(b) 21 June

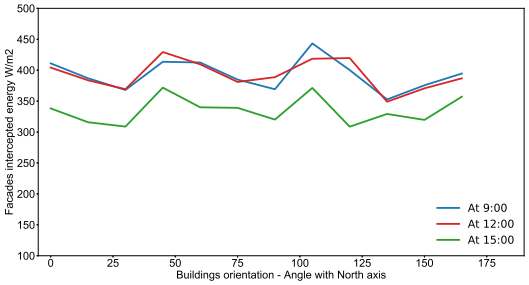

(c) 21 September

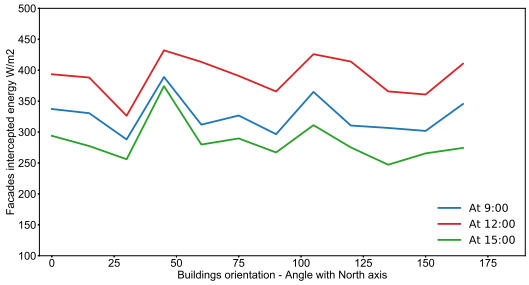

(d) 21 December

Figure 4.21: Facades intercepted energy variation in function of buildings' orientation in zone 2.

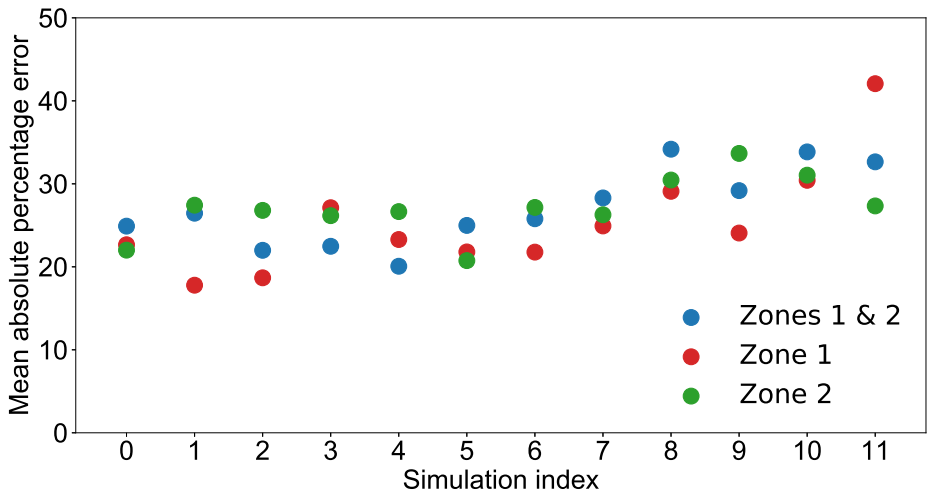

Figure 4.22: Mean absolute percentage error of the trained neural networks for each simulation. The simulation index represents the number in sequence representing different dates. For example, simulation index 1 refers to the simulation of the radiative budget at 12pm on March 21.

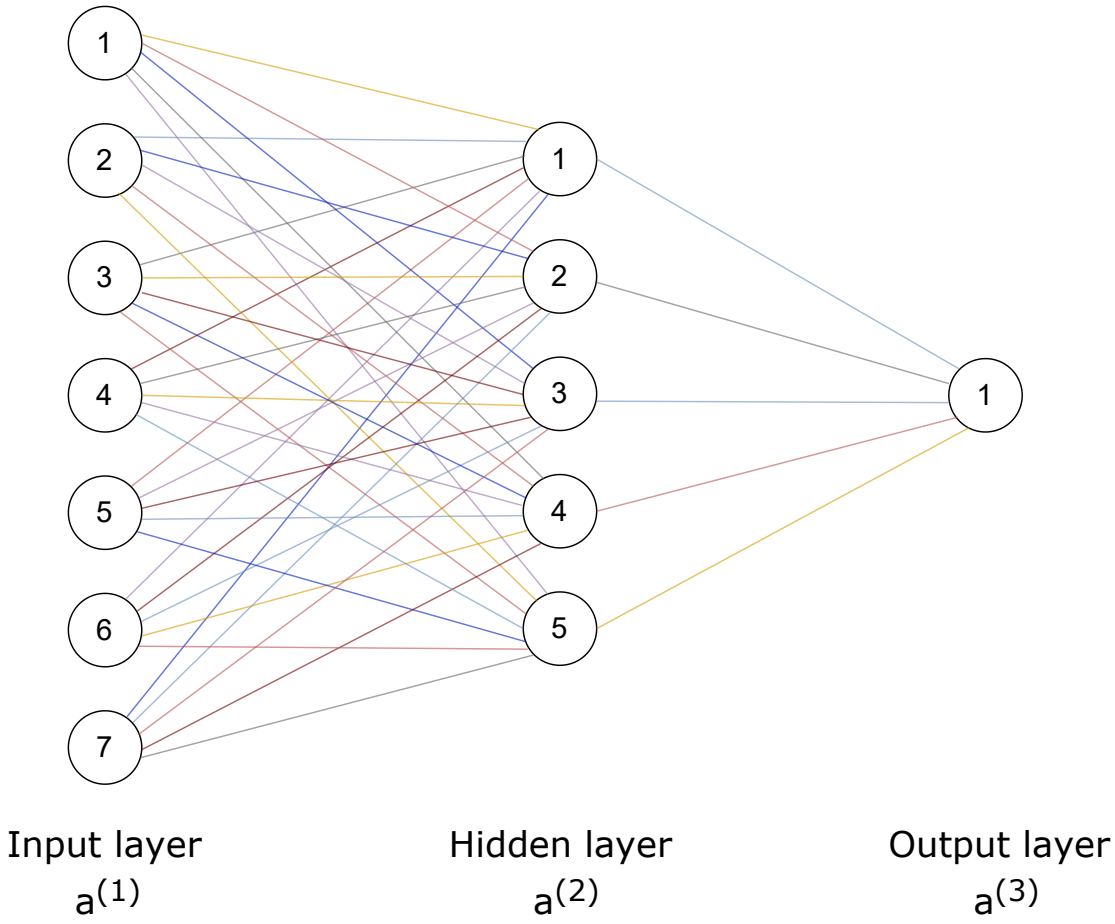

Figure 4.23: Neural Network architecture

$$\Theta^{(1)} = \begin{pmatrix} 0.53174389 & 0.06667163 & 0.23882406 & 0.64810746 & 0.01487057 \\ 0.94182258 & 0.5728948 & 0.86777523 & 0.98591874 & 0.31308534 \\ -0.21180356 & 0.35333526 & 0.16929564 & -0.40462198 & 0.30163634 \\ -1.03993562 & -0.34045903 & -0.59007595 & -1.12594992 & -0.06314182 \\ -0.89162078 & 0.0739178 & 0.27388839 & -1.12847296 & -0.22033479 \\ 3.26297866 & 0.96255204 & 1.57066297 & 3.44757584 & 0.04346199 \\ -2.01832956 & -0.93335633 & -1.1382644 & -2.1280587 & -0.17493549 \end{pmatrix}$$

$$\Theta^{(2)} = \begin{pmatrix} 30.05716245 \\ 30.84769588 \\ 31.52834707 \\ 29.10211967 \\ 28.61908975 \end{pmatrix}$$

Figure 4.23: Weights matrices of the neural network hidden and output layer, for estimating daylight at 3pm on 21December.

$$a^{(1)} = \begin{pmatrix} \bar{H}_S \\ \bar{O}_S \\ \sigma_{H_S} \\ \sigma_{O_S} \\ H \\ X \\ Y \end{pmatrix}$$

- $\bar{H}_S$: mean height of surrounding buildings
- $\bar{O}_S$: mean orientation of surrounding buildings
- σ_{H_S}: standard deviation of surrounding buildings' heights
- σ_{O_S}: standard deviation of surrounding buildings' orientations
- H: building height
- X: building x coordinate
- Y: building y coordinate

4.5.4 Relation between daylight and electricity consumption

Daylight contributes in the energy loads of a building by its capability to reduce electricity consumption by acting as a complement to artificial lighting [23]. In this section, we try to

find the relation between daylight accessibility and electricity consumption in the two zones of interest. For this purpose, we simulated the electricity consumption of buildings in both zone as described in chapter 5. Buildings with metered data were included in the calibration process of the energy model results and in the rest of the analysis, while non-metered buildings were excluded. This reduced the number of buildings from 433 to 237 in zone 1 and from 413 to 242 in zone 2. Each value of the electricity consumption of the remaining building was multiplied by its cluster average multiplicative factor to adjust it (more details in section 5.3.3 and 5.4.2). The daylight range was divided into bins, of which the mean electricity consumption was computed. Results were plotted in figures 4.24 and 4.25. The analysis of the graph showed that relation between daylight accessibility and electricity consumption is not enough clear, with a general trend of increase of electricity consumption when daylight availability increases. Two reasons can be thought of as possible explanations of these results. First, the calibration process was applied at the bimonthly level, so caution should be taken when using the calibration coefficients at the hourly level. Second, as the day progresses and therefore the daylight increases, the human activities and their cooling and heating needs increase. Anyhow, further analysis is required to understand the results and conclude the relation between daylight and electricity consumption.

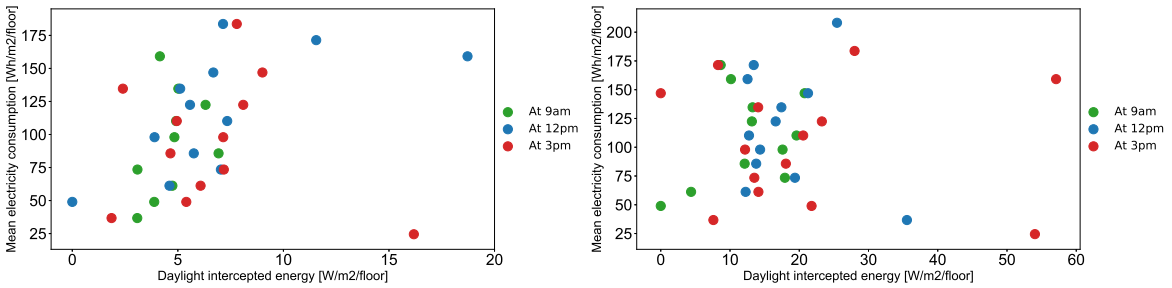

(a) 21 March

(b) 21 June

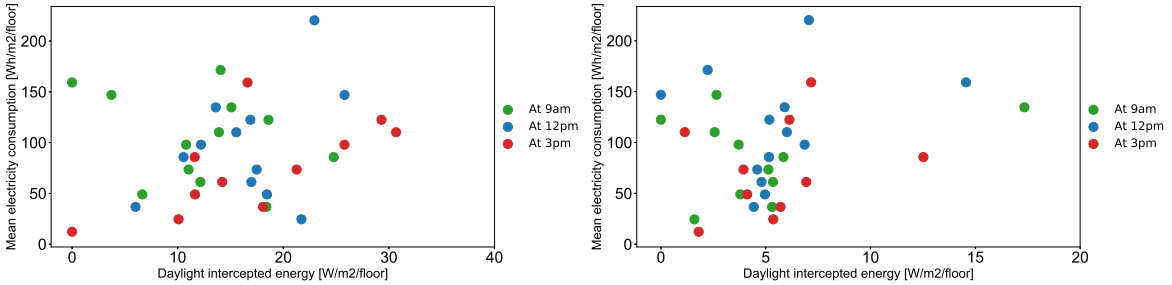

(c) 21 September

(d) 21 December

Figure 4.24: Mean electricity consumption as function of the daylight potential, normalized by floor area, in zone 1.

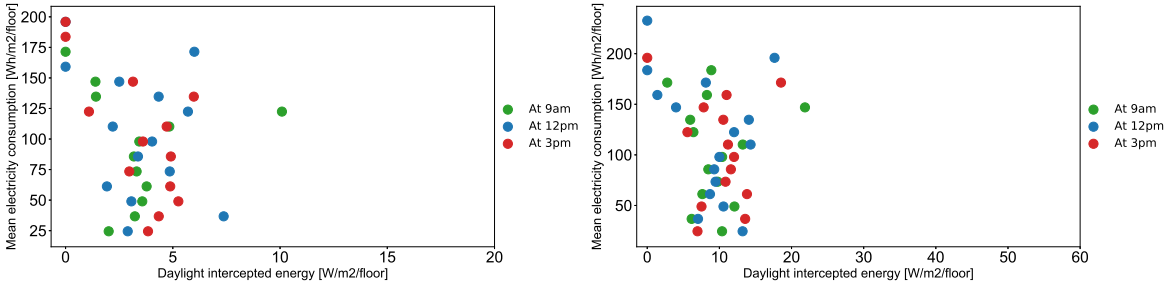

(a) 21 March

(b) 21 June

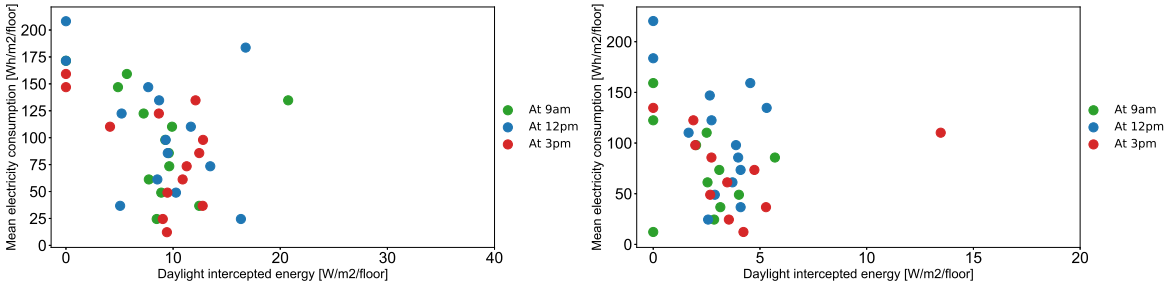

(c) 21 September

(d) 21 December

Figure 4.25: Mean electricity consumption as function of the daylight potential, normalized by floor area, in zone 2.

4.6 Conclusion

In this chapter, the radiative budget module in DART is presented, revealing its accuracy and advanced algorithms to simulate solar radiation in urban areas. Simulations of the radiative budget then its conversion to present daylight is introduced. The results of the 3D radiative budget shows the impact of the urban context and the buildings features on the assessed daylight. The vertical elevation profiles of the windows intercepted energy illustrated the expected reduction in daylight accessibility at lower floors. Moreover, neural networks are developed to link daylight to urban morphology such as buildings heights, orientations and location. The algorithm have an MAPE ranging between 17% and 40% depending on the zone and the day of study.

5. BEirut Energy Model BEEM

5.1 Introduction

This chapter introduces BEirut Energy Model BEEM, an UBEM developed for the city of Beirut. It is an automated model applied in two districts within the city due to limited input data. The chapter starts with the equations of the heat transfer and thermodynamics embedded in EnergyPlus and applied to compute the energy budget of the buildings. It is then followed by the methodology overview, which includes data preparation, parameters set-up, model execution and calibration. Results of loads profiles and the electricity consumption spatiotemporal distribution are shown to demonstrate the capabilities of the model.

5.2 Mathematical formulation

EnergyPlus, a free software tool, is a collection of modules that work together to calculate the heating and cooling loads of a building under different environmental and operational conditions. Through an integrated solution manager, EnergyPlus assures a physically realistic simulation by linking and solving the building, system, and plant simultaneously and by substitution iteration based on Gauss-Seidell numerical method [113]. The program is presented as a series of integrated elements connected by fluid loops. In our project, we tend to calculate the cooling and heating loads of our buildings, plus the electricity consumption from equipment and appliances. For this reason, the zone-system connection is only of interest and will be presented in the following section.

5.2.1 Zone and Air system integration

The heat balance equation on the zone air is the following:

$$C_z \frac{dT_z}{dt} = \sum_{i=1}^{N_{si}} \dot{Q}_i + \sum_{i=1}^{N_{surfaces}} h_i A_i (T_{si} - T_z) + \sum_{i=1}^{N_{zones}} \dot{m}_i C_p (T_{zi} - T_z) + \dot{m}_{inf} C_p (T_\infty - T_z) + \dot{m}_{sys} C_p (T_{sup} - T_z) \tag{5.1}$$

where:

- $C_z \frac{dT_z}{dt}$ = energy stored in the air
- $\sum_{i=1}^{N_{si}} \dot{Q}_i$ = sum of the convective internal loads
- $\sum_{i=1}^{N_{surfaces}} h_i A_i (T_{si} - T_z)$ = convective heat transfers from the zone surfaces
- $\sum_{i=1}^{N_{zones}} \dot{m}_i C_p (T_{zi} - T_z)$ = heat transfer due to interzone air mixing
- $\dot{m}_{inf} C_p (T_\infty - T_z)$ = heat transfer due to infiltration and ventilation
- $\dot{m}_{sys} C_p (T_{sup} - T_z)$ = system energy provided to the zone formulated from the difference between the supply air enthalpy and the enthalpy of the air leaving the zone through the system return air plenum.

Energy Plus applies a Predictor-Corrector scheme to adjust the zone temperature at each time step. The scheme is presented below:

- The load of the zone is used as a starting point since it drives the entire process. By neglecting the capacitance of the air, and by assuming that the air system has sufficient capacity to meet the zone loads requirements (i.e. $\dot{Q}_{sys} = \dot{Q}_{load}$), the equation becomes:

$$\dot{Q}_{load} = \sum_{i=1}^{N_{sl}} \dot{Q}_i + \sum_{i=1}^{N_{surfaces}} h_i A_i (T_{si} - T_z) + \sum_{i=1}^{N_{zones}} \dot{m}_i C_p (T_{zi} - T_z) + \dot{m}_{inf} C_p (T_\infty - T_z) \tag{5.2}$$

  In this case, T_z is the desired temperature of the zone defined by the control system setpoints.

- The air system is simulated to determine its actual capability. In EnergyPlus, the air system is a variable air system.

- By applying a third order backward difference algorithm to equation 3.1 , EnergyPlus then updates the actual zone temperature based on the air system calculated capabilities:

$$
\begin{aligned}
T_z^t =& (\sum_{i=1}^{N_{sl}} \dot{Q}_i + \sum_{i=1}^{N_{surfaces}} h_i A_i T_{si} + \sum_{i=1}^{N_{zones}} \dot{m}_i C_p T_{zi} + \dot{m}_{inf} C_p T_\infty + \dot{m}_{sys} C_p T_{supply} \\
& - (\frac{C_z}{t})(-3T_z^{t-t} + \frac{3}{2}T_z^{t-2t} - \frac{1}{3}T_z^{t-3t})) \\
& /(\frac{11}{6}\frac{C_z}{t} + \sum_{i=1}^{N_{surfaces}} h_i A + \sum_{i=1}^{N_zones} \dot{m}_i C_p + \dot{m}_{inf} C_p + \dot{m}_{sys} C)
\end{aligned}
\tag{5.3}
$$

By this method, the zone temperature depends on the three previous time steps. The next paragraphs present all modules and equations used by EnergyPlus to identify the different parameters of the previous equation, such the surfaces temperatures Tsi and convective coefficients hi, the infiltration and ventilation flow rates $\dot{m}_{inf}$ and $\dot{m}_{vent}$ in order to balance the equation with the zone air temperature equal to the setpoint temperature. However, it is important to present a brief overview of the air system model used in our study that allows to calculate the supply conditions (air mass flow rate, temperature and humidity).

5.2.2 Ideal Loads Air System

An ideal HVAC system model is applied to simulate the energy loads of the zones. It corresponds to an ideal VAV terminal unit with variable supply temperature and humidity, and it is not connected to a centralized source. The unit supplies cooling or heating air in sufficient quantity to meet the zone load and other constraints such the humidity if specified. The calculation procedure is presented below:

- Calculate the minimum outdoor air mass flow rate based on the specifications in the DesignSpecification: OutdoorAir Object, if specified.
- Calculate the sensible and latent impact of the outdoor air flow relative to the zone conditions.
- Determine if the unit needs to heat or cool by comparing the outdoor air sensible impact and the zone load.
- Calculate the supply air mass flow rate based on the supply temperature limit and humidification setpoint.
- Set the entering air conditions equal to the outside air conditions in case there is no economizer either heat recovery.

- Calculate the supply air temperature as function of the zone loads, entering air flow rate and temperature, but limit to the applicable temperature limit.
- Calculate the supply humidity ratio, but limit to the applicable humidity limit.
- Set the zone inlet node conditions to the supply air conditions.
- Calculate the unit output and load components.

5.2.3 Outside Surface Heat Balance

The outside surface heat balance is:

$$q''_{asol} + q''_{LWR} + q''_{conv} - q''_{KO} = 0 \tag{5.4}$$

where:

- q''_{asol} = absorbed direct and diffuse solar short wavelength radiation heat flux
- q''_{LWR} = net long wavelength radiation flux exchange
- q''_{conv} = convective flux exchange
- q''_{KO} = conduction heat flux

Conduction through the walls (Exterior/External Conduction)

EnergyPlus presents three different modules to model the conduction through walls q''_{KO}:

- Conduction Transfer Function module CTF (default module used in our project)
- Combined Heat and Moisture Transfer module HAMT
- Effective Moisture Penetration Depth module EMPD

Conduction transfer functions are time series solution that linearly relates the heat flux at either face of the surface of any generic building element to the current and some of the previous temperatures at both the interior and exterior surfaces as well as some of the previous flux values at the interior surface. To solve the CTFs, a state-space formulation is used. After calculating the coefficient matrices of the state space system, Leveriers algorithm [114] is applied to obtain the CTFs [115].

Outdoor/Exterior Convection

The heat transfer from surface convection is calculated by applying the following equation:

$$Q_c = h_{c,ext} A (T_{surf} - T_{air}) \tag{5.5}$$

where:

- Q_c = rate of exterior convective heat transfer
- $h_{c,ext}$ = exterior convection coefficient
- A = surface area
- T_{surf} and T_{air} = surface temperature and outdoor air temperature

The modeler can specify the values of the exterior convection coefficient for the surfaces, even use schedules to encounter the values variations over time. However, EnergyPlus offers a range of model equations to estimate this coefficient without the modeler intervention. The options include:

- Simple Combined
- TARP
- MoWiTT
- DOE-2
- Adaptive Convection Algorithm

The algorithms are arranged by complexity and they differ by the depending parameters they use to estimate the convection coefficient. In our model, we used the DOE-2 algorithm, which is a combination of MoWiTT and BLAST Detailed models. For very smooth surfaces, the following equation is applied:

$$h_{c,glass} = \sqrt{h_n^2 + [aV_2^b]^2} \tag{5.6}$$

where:

- $h_{c,glass}$ = convective heat transfer coefficient for very smooth surfaces
- h_n = natural convective heat transfer coefficient
- a and b = constants
- T_{surf} and T_{air} = surface temperature and outdoor air temperature

h_n is correlated to the surface orientation and the difference between the air and the surface temperatures. For less smooth surfaces, the coefficient is calculated as follow:

$$h_c = h_n + R_f(h_{c,glass} - h_n) \tag{5.7}$$

where R_f is the roughness coefficient. All the constants can be found in tables in the Engineering Reference, in addition to the details of the remaining algorithms. Note that when the outside environment indicates that it is raining, the exterior surfaces (exposed to wind) are assumed to be wet. The convection coefficient is set to a very high number (1,000) and the outside temperature used for the surface will be the wet-bulb temperature. (If you choose to report this variable, you will see 1,000 as its value.)

Longwave radiation heat flux

It is a flux exchange between the surface, the sky, and the ground. The following assumptions are adopted:

- each surface emits or reflects diffusely and is gray and opaque ($\alpha = \varepsilon$, $\tau = 0$ and $\rho = 1 - \varepsilon$)
- each surface is at a uniform temperature
- energy flux leaving a surface is evenly distributed across the surface,
- the medium within the enclosure is non-participating

The enclosure consists of building exterior surface, surrounding ground surface, and sky. The longwave radiation heat flux is given by the following equation:

$$q''_{LWR} = q''_{sky} + q''_{ground} + q''_{air} \tag{5.8}$$

By applying the Stephan-Boltzmann law, the equation becomes:

$$q''_{LWR} = \varepsilon\sigma F_{sky}(T^4_{sky} - T^4_{surface}) + \varepsilon\sigma F_{ground}(T^4_{ground} - T^4_{surface}) + \varepsilon\sigma F_{air}(T^4_{air} - T^4_{surface}) \tag{5.9}$$

where:

- ε = longwave emissivity of the surface
- σ = Stephan-Boltzmann constant
- $F_{ground} = 0.5(1 - cos\phi)$ =angle factor between the surface and the ground
- $F_{sky} = 0.5(1 - cos\phi)$ = angle factor between the surface and the sky

- $F_{air} = F_{sky}(1 - \beta)$ = view factor of wall surface to air temperature
- ϕ = tilt angle of the surface
- $\beta = \sqrt{0.5(1 + cos\phi)}$

The ground surface temperature is assumed to be the same as the air temperature. The sky temperature is calculated as follows:

$$T_{sky} = (\frac{\text{Horizontal Infrared radiation Intensity}}{\sigma})^{0.25} - 273.5 \tag{5.10}$$

The horizontal infrared radiation intensity is available in the weather file. Notes: EnergyPlus takes into consideration the variation of the temperature and the wind speed with respect to the height above ground (in the case of high buildings). For this purpose, it calculates for each floor the local air temperature and wind speed by identifying its centroid.

Shortwave radiation heat flux through surfaces

The shortwave radiation includes both direct and diffuse incident solar radiation absorbed by a surface.

Sky Radiance Model

EnergyPlus calculates the diffuse solar radiation incident on an exterior surface, taking into account, the anisotropic radiance distribution of the sky, the surface orientation and the effects of shading of sky diffuse radiation by shadowing surfaces such as overhangs. It does not account for reflection of sky diffuse radiation from shadowing surfaces or from the ground [116]. The sky diffuse irradiance on a surface is given by:

$$I_{sky} = \text{AnisoSkyMulti} \times \text{DiffuseSkyRadiation on the ground} \tag{5.11}$$

The sky radiance distribution is determined by three distributions:

1. An isotropic distribution that covers the entire sky dome
2. A circumsolar brightening centered at the position of the sun;
3. A horizon brightening

The proportion of each component depends on the sky condition, characterized by the clearness factor and the brightness factor.

$$I_{sky} = R_{horizon}I_{horizon} + R_{dome}I_{dome} + R_{circumsolar}I_{circumsolar} \tag{5.12}$$

Where:

- $I_{horizon} = I_h F_2 sinS$ = irradiance on surface from the sky horizon
- $I_{dome} = I_h(1 - F_2)(1 + cosS)/2$ = irradiance on surface from the sky dome
- $I_{circumsolar} = I_h F_1 a/b$ = irradiance on surface from circumsolar region

where:

- I_h = horizontal solar irradiance (W/m2)
- S = surface tilt (radians)
- $a = \max(0, cos\alpha)$
- $b = \max(0.087, cosZ)$
- α = incidence angle of sun on the surface (radians)
- Z = solar zenith angle (radians)
- $F_1 = f(\varepsilon, \Delta, Z)$ = circumsolar brightening coefficient
- $F_2 = f(\varepsilon, \Delta, Z)$ = horizon brightening coefficient
- $\varepsilon = (I_h + I)I_h + kZ^3(1 + kZ^3)$ = sky clearness factor (0 value means an overcast sky, 2-3 means intermediate to clear)
- $\Delta = (I_h m)I_0$ = sky brightness factor
- I = direct normal solar irradiance (available in the weather file)
- $k = 1.041$
- m = relative optic air mass
- $I_0 = 1353$ W/m2 = extraterrestrial irradiance

ε category	lower bound	upper bound
1 (overcast)	1	1.065
2	1.065	1.23
3	1.23	1.5
4	1.5	1.9
5	1.95	2.8
6	2.8	4.5
7	4.5	6.2
8 (clear)	6.2	–

Table 5.1: Discrete sky clearness categories

$R_{horizon} = R_{dome} = R_{circumsolar} = 1$ in case there is no shadowing; otherwise they are the ratio of the irradiance with obstructions over the irradiance without obstructions (the horizon is divided into intervals and the sum of the irradiance is calculated on each interval as function of the angle and incidence angle).

Reflected Sky Long-Wave Radiation

The sky long-wave radiance distribution is assumed isotropic and in case of obstructions, it is multiplied by a shading factor, R_{dome}. The long-wave radiation from these obstructions is added to the long-wave radiation from the ground; in this calculation, both obstructions and ground are assumed to be at the outside air temperature and to have an emissivity of 0.9.

Shading module

The aim of the shading module is to determine the sunlit area of a surface. The user can set the shadowing calculations frequency. The default frequency value is 20 days, which means that the solar position is averaged over twenty days to reduce runtime. Then, after determining the sun position, surfaces that sun is behind are identified as shadowing surfaces. The surfaces are then projected along the suns rays direction to the receiving surfaces. The overlap between the shadows and the receiving surfaces are determined so the sunlit area can be deduced.

Solar Gains

The combination of direct and diffuse solar radiation gives the total solar gain of an exterior surface:

$$Q_{sol} = \alpha(I_b cos\frac{S_s}{S} + I_{sky}F_{sky} + I_g F_{ground}) \tag{5.13}$$

where:

- α = solar absorptance of the surface
- θ = angle of incidence of the suns rays
- S = area of the surface
- S_s = sunlit area
- I_b = intensity of direct radiation
- I_sky = intensity of sky diffuse radiation
- I_g = intensity of ground reflected diffuse radiation (See Ground Reflectance section)
- $F_{sky} = (1 + cos\phi)/2$ = angle factor between the surface and the sky
- $F_{sky} = (1 - cos\phi)/2$ = angle factor between the surface and the ground

5.2.4 Reflections

Ground Reflectance

The diffuse radiation accounts for ground reflection even if the reflection option (WithReflection) is not used. However, if this option is turned off, shadowing of the ground by the building surfaces and neighboring buildings are ignored. $GroundReflectedSolar = (BeamSolarcos\theta + I_d) \times \rho_g round$ where I_d = diffuse solar radiation (available in the weather file)

Solar radiation reflected from exterior surfaces

In case the reflections from exterior surfaces are taken into consideration, the WithReflection option is used. Surfaces are categorized as follow:

- Shadowing surfaces: such as surrounding buildings or overhangs They are attributed diffuse and/or specular reflectance values.

- Exterior building surfaces: when a section of the building reflects solar radiation onto another section. The program considers opaque surfaces (such walls) as diffusely reflecting and calculates the reflectance values from the solar absorptance and visible absorptance values. In contrast, glazed surfaces are assumed to be specularly reflecting. Their reflectance values are calculated from the reflectance properties of the individual glass layers that make up surfaces construction assuming no shading device is present and taking into account interreflections among the layers.
- The ground surface (See Ground Reflectance Section): Beam solar and sky solar reflection from the ground is calculated even if withReflections is not used (the default). In this case, the ground plane is considered unobstructed, i.e., the shadowing of the ground by the building itself or by obstructions such as neighboring buildings is ignored. This shadowing is taken into account only if WithReflections is used in the Solar Distribution field (in Building input object). In this case, the user-input value of ground view factor is not used.

Note that the exterior solar reflection is done once and no inter-reflection is counted [116]. To calculate the beam solar and sky solar radiation reflected on the buildings exterior surfaces, a backward ray tracing method is applied.

Ray tracing method

An n-sided surface is assigned n receiving points with well-determined coordinates. The radiation received by these points presents that of the whole surface. The ray tracing method consists of sending out 90 rays into the exterior hemisphere surrounding each receiving point. The beam solar and the sky solar radiance of the surfaces hit by the rays is calculated by multiplying the total radiation by a reflection factor. The results at each receiving points are averaged and the reflected radiation onto the surface is obtained. The radiance of each hit surface is computed depending on its category.

- Sky solar radiation diffusely reflected from obstructions
- Sky solar radiation diffusely reflected from ground
- Beam solar radiation diffusely reflected from obstructions
- Beam solar radiation diffusely reflected from ground
- Beam solar radiation specularly reflected from windows

5.2.5 Inside Surface Heat Balance

The inside heat balance is:

$$q''_{LWX} + q''_{SW} + q''_{LWS} + q''_{Ki} + q''_{sol} + q''_{conv} = 0 \tag{5.14}$$

Where:

- q''_{LWX} = longwave radiant exchange flux between zone surfaces
- q''_{SW} = shortwave radiant flux to surface from lights
- q''_{LWS} = longwave radiation flux from equipment
- q''_{Ki} = conduction heat flux through the wall
- q''_{sol} = transmitted solar radiation flux
- q''_{conv} = convective heat flux to zone air

Before explaining each term in the equation, it is important to d zone internal gains, comprised of convective, radiant and latent gains, from lights, people, and equipment.

Zone internal gains

Lights

The radiant gains from lights are divided into visible, thermal and convective portions based on the light type.

People

By applying a polynomial function, the metabolic heat gain is divided sensible and latent portions.

$$SensibleGain = 6.461927 + 0.946892 \times M + 0.0000255737 \times M^2 + 7.139322 \times T - 0.0627909 \times T \times M + 0.0000589172 \times T \times M^2 - 0.19855 \times T^2 + 0.000940018 \times T^2 \times M - 0.00000149532 \times T^2 \times M^2 \tag{5.15}$$

where M is the metabolic rate (W) and the air temperature (C).

$$LatentGain = MetabolicRate - SensibleGain$$

Interior Longwave Radiation

It includes absorption and emittance of radiation sources, such as other zone surfaces, equipment, and people.

Internal Shortwave Radiation

Solar distribution of beam solar radiation through exterior windows

There are five modules:

- Minimal shadowing
- FullExterior
- FullInteriorAndExterior
- FullExteriorWithReflections
- FullInteriorAndExteriorWithReflections

In our case, we will use the FullExterior or the FullExteriorWithReflections modules. In addition to beam solar radiation entering the zone, shadowing by exterior surfaces like overhangs and exterior surfaces, and by windows and doors reveals are computed. Assuming that the entering solar radiation falls into the floor, it is then absorbed according to the floors solar absorptance. In case there is no floor, the absorption is on all interior surfaces level. The reflected radiation is added to the transmitted diffuse radiation, which is assumed to be uniformly distributed and the heat balance is applied to each surface. In addition to the aforementioned computed terms, reflections from exterior surfaces are considered in the case of FullExteriorWithReflections. However, the simulation is much slower (See Solar Radiation Reflected from Exterior Surfaces section).

Interior Solar Distribution Calculation

The interior solar radiation consists of the beam solar radiation, diffuse solar radiation, and short-wave radiation from electric lights. This radiation is apportioned as follows:

- absorbed on the inside face of opaque surfaces
- absorbed in the glass and shading device layers of the zones exterior and interior windows
- transmitted through the zones interior windows to adjacent zones
- transmitted back out of the exterior windows.

Interior convection

Many models are available within EnergyPlus to compute the inside convection coefficients and there is no way to declare one is better than another. In our case, we applied the TARP algorithm, which applies different equations for different situations depending on the surface orientation and the difference of surface and zone air temperature.

- For no temperature difference or vertical surface:

$$h = 1.31|\Delta T|^{1/3}$$

- For $\Delta T < 0$ and upward facing surface or $\Delta T > 0$ and downward facing surface:

$$h = (9.482|\Delta T|^{1/3})/(7.283 - |cos\Sigma|)$$

- For $\Delta T > 0$ and upward facing surface or $\Delta T < 0$ and downward facing surface:

$$h = (1.81|\Delta T|^{1/3})/(1.382 + |cos\Sigma|)$$

where Σ is the surface tilt angle.

Interior conduction

It represents the heat transfer to the inside face of the building element and it is calculated using the CTF formulation presented in section (Conduction through the walls).

5.2.6 Infiltration and ventilation

Infiltration Design flow rate

Infiltration is difficult to accurately model. It is the flow rate entering a zone mainly through opening and closing of exterior doors and cracks around windows. The basic equation used in EnergyPlus to calculate the infiltration rate:

$$Q_{Infiltration} = I_{design} F_{schedule}[A + B|T_{zone} - T_{odb}| + C \times windspeed + D \times windspeed^2] \quad (5.16)$$

where:

- I_{design} = Air Changes per Hour $\times$ Zone volume in m^3/s

- $F_{schedule}$ = a value for a user-defined schedule (always 1)
- T_{odb} = Outdoor air dry-bulb temperature

The coefficients A, B, C and D depends on the infiltration situation the user wants to simulate.

	A	B	C	D
Constant	1	0	0	0
Wind dependent	0.606	0.036359996	0.1177165	0

Natural ventilation

It is the ventilation caused by wind entering the zone through an open area (an open window for example). The equation used is:

$$Q_w = C_w A_{opening} F_{schedule} Windspeed \tag{5.17}$$

Where:

- Q_w = volumetric air flow rate driven by wind
- C_w = opening effectiveness
- $A_{opening}$ = opening area
- $F_{schedule}$ = user-defined schedule value

The opening effectiveness is auto calculated in EnergyPlus:

$$C_w = 0.55 - |EffectiveAngle - WindDirection|/180 \times 0.25 \tag{5.18}$$

The wind direction is available in the weather file at an hourly scale. The effective angle is the normal angle of the opening area. It is important to point out that Energy Plus also takes other parameters that act as the threshold below or above which the natural ventilation is shut off:

- Minimum and maximum indoor temperature (ArchSim only takes the minimum value and calls it Setpoint, while the maximum value is put by default at $100°C$)
- Minimum and maximum outdoor temperature
- Maximum relative humidity (40% by default)

The max relative humidity in ArchSim is not used by EnergyPlus.

Mechanical ventilation (Design Specification Outdoor air)

The mechanical ventilation is used to quantify the controlled air to enter a zone. In ArchSim, the outdoor airflow per person and the outdoor air flow per zone floor area are summed up after multiplying them by the occupancy density and floor area respectively. The result is then multiplied by a fraction schedule. If an economizer is used, the outdoor airflow will be augmented or reduced depending on limits that the user specifies. Heat recovery option is also available but not applied in our case.

5.3 Methodology

5.3.1 Data preparation

As discussed in chapter 3, the number of modeled buildings is 3,630 distributed over two districts in Beirut (figure 3.1). A topographic map was used to create the digital elevation model. Hourly weather data is obtained from the Beirut International Airport weather station, which is located along the Mediterranean coast in the southern suburbs of the city of Beirut. However, when the model had to be calibrated with actual data, many of the buildings were excluded for the following reasons:

- Null or missing electricity data as obtained from EDL.
- Unreasonable low or high electricity consumption by floor area.
- Unreliable data: the total yearly consumption is not convenient with the sum of the bimonthly consumptions. In this case, manual intervention was applied where the bimonthly electricity consumptions were adjusted by dividing the values by 1000, when it was clear that it is a problem of units.

5.3.2 Parameters Set-up and boundary conditions

The following parameters have been used for the calculations.

We took into consideration the fact that many occupants use electrical heaters during winter, which have different coefficient of performance than air conditioners, and we assumed that they represent 70% of the occupants. According to [72], reversibe split units are used in residential buildings and retail (therefore in mixed buildings). Heating and domestic hot

Building Type	Unit	Residential	Mixed	Governmental	Hospital	School
Occupant density	p/m^2	0.03	0.05	0.05	0.054	0.23
Equipment Power density	W/m^2	12	12	12	21.5	15
Lighting Power density	W/m^2	7.5	7.5	10.7	12.9	12.9
Heating Setpoint	$°C$	21	21	21	21	21
COP[1*]	-	1 or 2.3	1 or 2.3	2.3	–	2.3
Cooling Setpoint	$°C$	24	24	24	24	24
SEER[2*]	-	2.9	2.9	2.9	3.3	2.9 or 3.3
DHW demand[3*]	KWh/m^2	10	10	–	–	–

1 Coefficient of Performance, defined as the ratio between the useful heating provided and the electric energy usage.

2 Seasonal Energy Efficiency Ratio, defined as the ratio between the output cooling energy and the input electical energy.

3 Domestic Hot Water

* Values are obtained from [72].

Table 5.2: Loads and conditioning parameters used for the electricity consumption calculations.

water are assumed to be provided by diesel biolers in hospitals. Therefore, they were not considered in the electicity consumption budget. Central chiller is the main cooling system in hospitals, and we assumed it is also available in recent governmental buildings and schools.

Shading surfaces such as balconies and surrounding buildings, and the ground were set as boundary conditions.

3D geometric model was generated for each building as described in section 3.4.2. It was then fed to EnergyPlus via ArchSim tool, which stored the building's properties in an idf file, ready to run. The files were distributed on four virtual machines created on Microsoft cloud service Azure and run by EnergyPlus for the thermal model execution. For the calibration process, the results were then processed and compared to the EDL data, when available, as discussed next.

5.3.3 Model Calibration

As previously mentioned, bimonthly EDL data was available for a certain number of buildings. Outliers were removed using density-based spatial clustering of applications with noise (DBSCAN) and autoencoders algorithms, based on the buildings' area, number of

floors, type, year of construction and EDL consumption. Once outliers were identified, the remaining buildings were clustered based on their simulated electricity consumption and actual electricity consumption (EDL). This clustering helps identify buildings with similar occupancy schedules.

The offset between EDL values and those predicted by the model can be mainly attributed to behavioral patterns, HVAC systems and systematic errors. Hence, any correction to be applied must be consistent with the above categorical errors, adaptable to the city's context and justified at the same time. For this purpose, the following interventions were implemented:

- *Systematic errors*: 3 hours long electricity cutoff in Beirut accounts for a reduction factor of 1/8, when averaged across the year. Hence, the simulated electricity consumption was reduced by that amount. In addition, errors related to numerical algorithms were eliminated. These errors are the results of the Energy Plus scheme to adjust the zone temperature to meet the desired value defined by the control system set points.

- *HVAC systems architecture*: cooling in Beirut relies mostly on unitary cooling units associated to given areas. The units are rarely running at the same time. To this end, we assume that only 50% of the floor area is cooled or heated at a given time, so that the simulated cooling and heating consumption are reduced to the half. In addition, when the outdoor temperature was less than 20°C, the cooling loads were nullified.

- *Energy use and occupancy profiles*: after applying the previous corrections, we assumed that the remaining discrepancies were caused by occupancy profiles, linearly altering the total bimonthly electricity consumption by a certain factor. This assumption is justified in section 5.4.2. Therefore, the calibrated energy consumption for each building was obtained as the multiplication of model estimated energy consumption and the averaged multipliers of its cluster.

5.4 Results

5.4.1 Archetypes distribution and 3D model

The USJ data covered two districts in Beirut as shown in figure 5.1. Attributing archetypes to buildings shows that residential and mixed buildings are the two main types in the two districts with 57.9% and 38.4% respectively in district A and 62.7% and 35% respectively in district B, as shown in figure 5.1. Almost 40% of the buildings in both districts were built between 1941 and 1960 (the golden period) while 34% and 23% were built between 1961 and 1990 in district A and district B respectively, as shown in figure 5.2. The main difference between the two districts is the buildings facing the sea in the north and the west of district A. All of these buildings are residential and mixed. In addition, most schools, hospitals and governmental buildings are within district B.

The 3D model of a neighborhood in the Bachoura area in district B is shown in figure 5.3. The figure illustrates the use of archetypes to generate realistic 3D models from the thermal point of view, including windows and balconies.

5.4.2 Data processing and model calibration results

After generating the thermal model, annual hourly loads from equipment, lighting, domestic hot water, cooling and heating were aggregated into simulated electricity consumption for residential and mixed buildings. In hospitals, the electricity consumption does not account for the heating and hot water demands since they are met by steam boilers. As for schools and governmental buildings, hot water is not available in general and therefore not accounted for. The electricity consumption profiles for residential and mixed buildings are described in section 5.4.3. Note that other building types were excluded from the calibration process as we will see in the next paragraph.

Following the interventions implemented in section 5.3.3, 31% of the buildings had to be removed due to missing EDL data entries. Note that all governmental buildings and hospitals lacked EDL data and were, as such, eliminated at this stage. To ensure consistency of the calibration process, schools, representing 1.3% of the remaining dataset, were removed because their schedules are different than those of residential and mixed

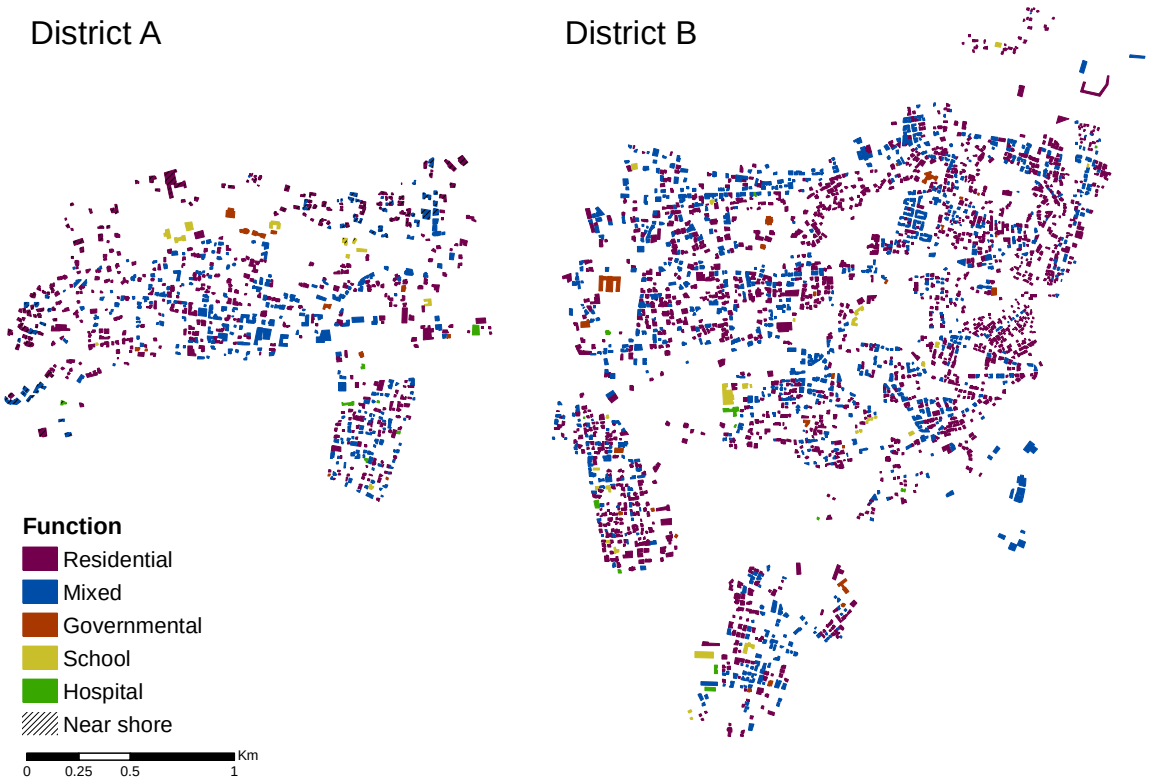

Figure 5.1: Buildings functions distribution in districts A and B

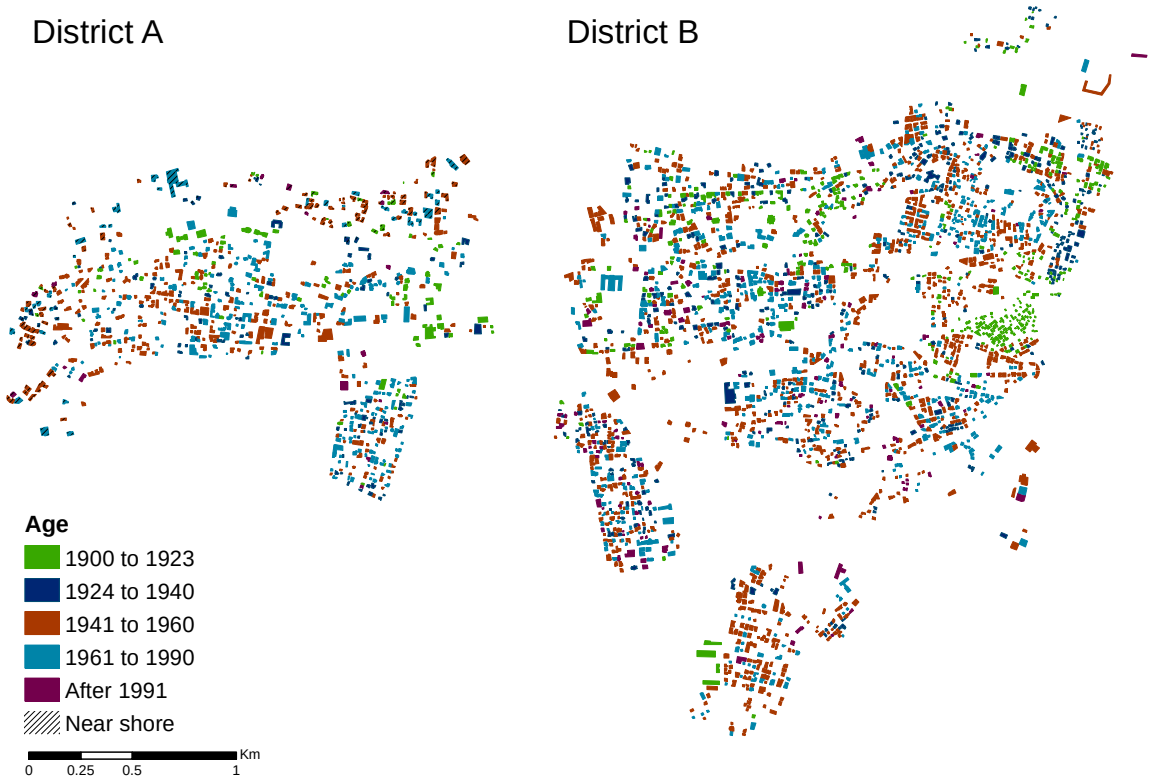

Figure 5.2: Buildings years of construction distribution in districts A and B

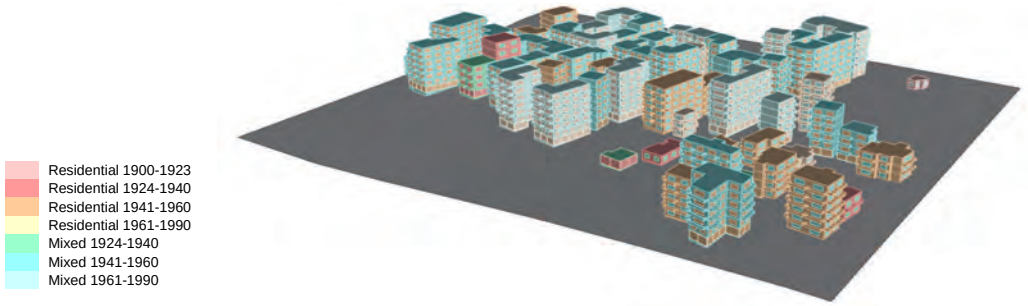

Figure 5.3: Sample of the generated 3D model of buildings in the Bachoura area, Beirut, Lebanon.

buildings.

After applying the noise detectors algorithms (dbscan and autoencoders), 64 buildings in A and 117 buildings in B were recognized as noises and therefore eliminated. The remaining data included 481 buildings in A and 1,830 in B, all residential or mixed. The average EDL electricity consumption per floor area for the final set of buildings was 69 kWh/m^2 and 83 kWh/m^2 for residential and mixed buildings respectively in district A, and 62 kWh/m^2 and 68 kWh/m^2 for the same buildings types respectively in district B. The simulated consumption was greater than the actual consumption by a minimum of 2.5% and a maximum of 236% in district A, and a minimum of 2.85% and a maximum of 262% in district B.

Model calibration is done by applying a k-means clustering to the ratio of EDL to predicted consumptions. This led to the identification of four clusters of buildings in each district, as shown in figures 5.10a and 5.11a. The number of clusters was defined based on an optimization procedure for each district. The model overestimated the electricity consumption in most buildings, mainly grouped in clusters 0 and 1 in both districts. Clusters 3 grouped buildings with EDL to simulated electricity consumption ratio ranging between 0.6 and 1.3 in district A and between 0.5 and 1.5 in district B. The consumption of only 21 and 34 buildings were underestimated in districts A and B respectively.

No specific relation between the clusters distribution and the buildings coordinates could be concluded. Moreover, the clusters distribution was shown to be independent of the buildings' type, year of construction and archetypes, as shown in figures 5.6-5.8.

Thus, energy use and occupancy profiles can be considered as the main source of the disparities between actual and predicted consumption. More specifically, maximum occupancy corresponds to buildings whose electricity consumption is the highest compared to their counterparts with the same number of floors. Figure 5.9 shows a strong correlation between the maximum actual consumption and the predicted consumption of each building normalized to its acutal consumption, which validates our hypothesis. As a result, we assumed that the discrepancies in electricity consumption between EDL and our model were related to usage profiles and hence, we adjusted the consumption of each building according to its cluster coefficients representative of specific energy patterns. Table 5.3 summarizes the clusters multipliers for both districts.

The calibrated results, plotted against EDL data in figures 5.10b and 5.11b, show that the buildings consumption of each cluster are more grouped around the identity axis.

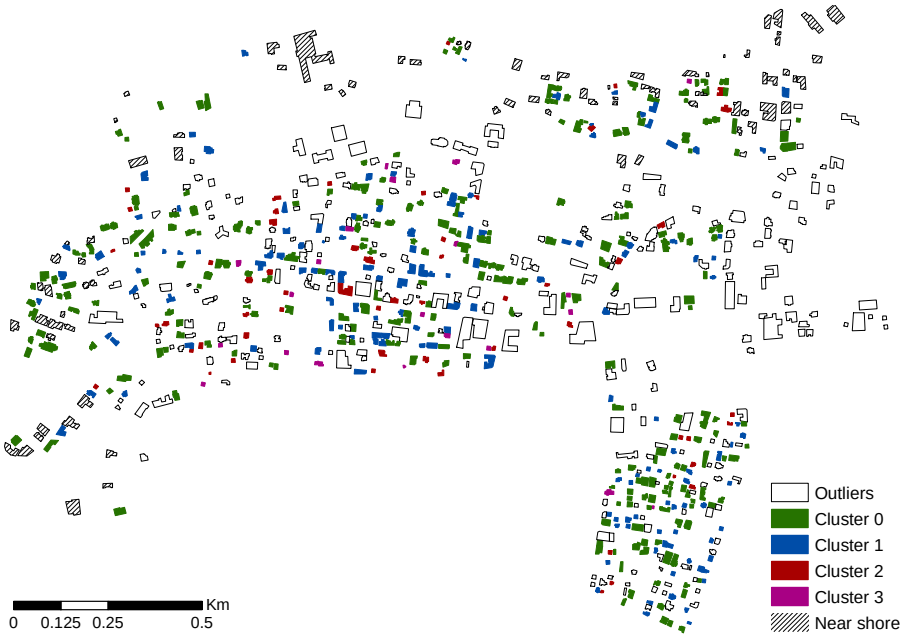

Figure 5.4: Distribution of district A buildings based on their clusters

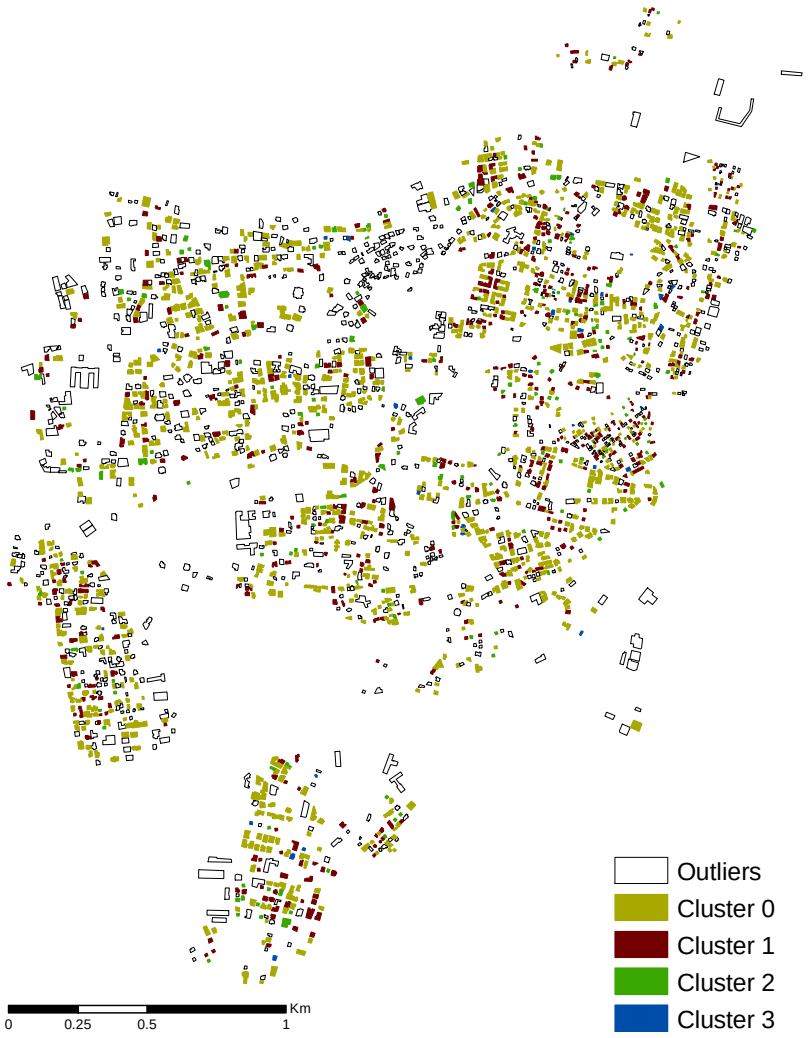

Figure 5.5: Distribution of district B buildings based on their clusters

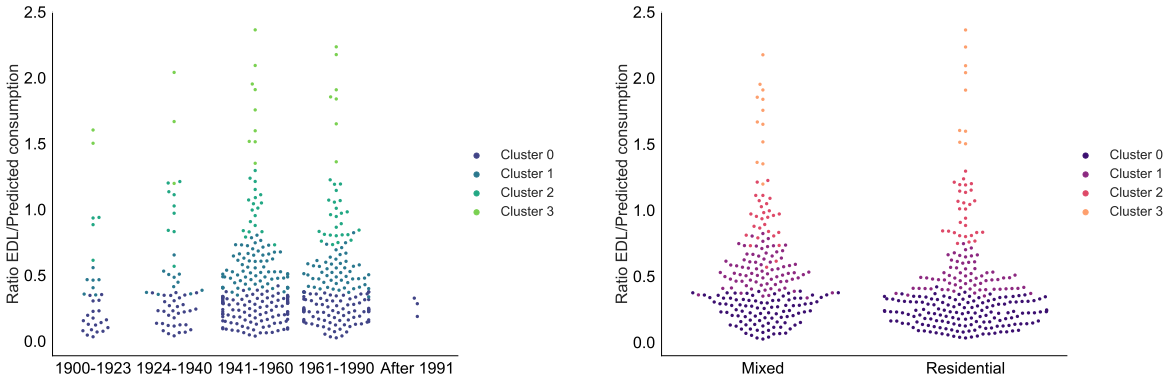

Figure 5.6: Ratio of actual consumption over predicted consumption of buildings in district A, distributed based on their year of construction (right) and their type (left)

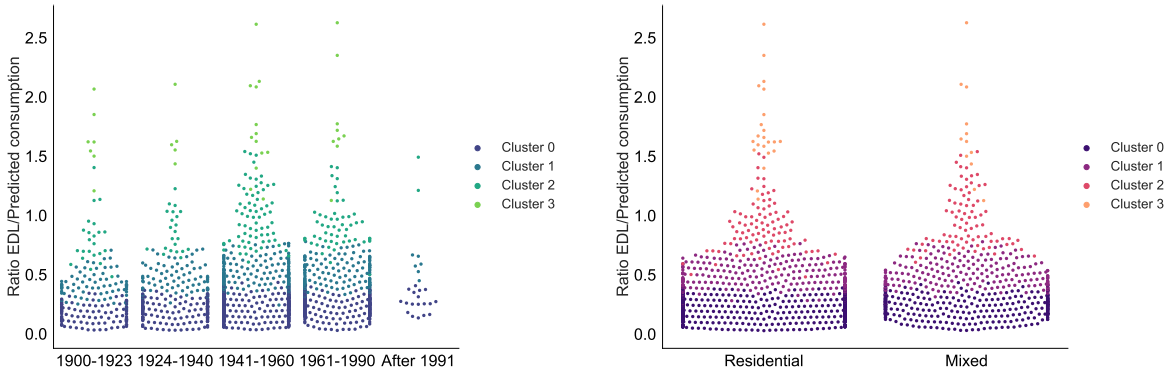

Figure 5.7: Ratio of actual consumption over predicted consumption of buildings in district B, distributed based on their year of construction (right) and their function (left)

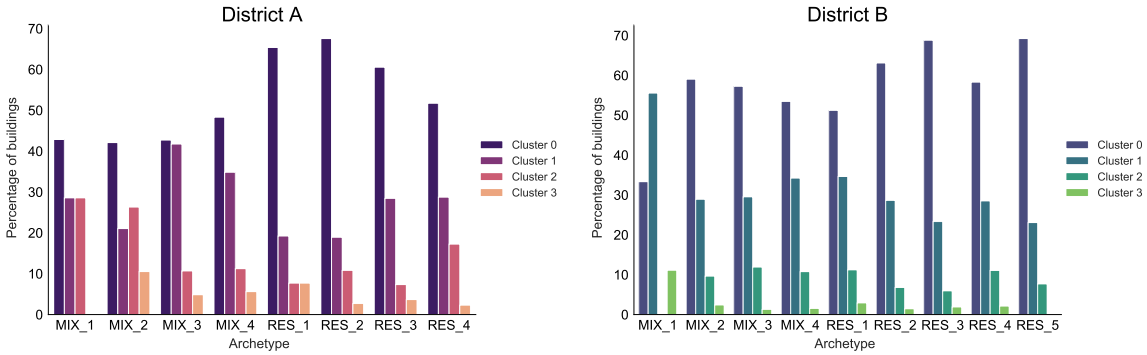

Figure 5.8: Clusters distribution as function of archetypes (District A: left, District B: right)

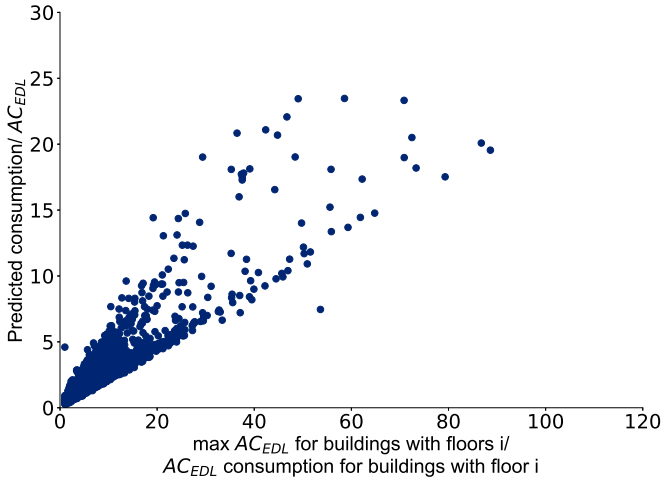

Figure 5.9: Correlation between the ratio of the maximum EDL consumption by floor to EDL consumption, and the ratio of the predicted consumption to EDL consumption.

		Jan-Feb	Mar-Apr	May-Jun	Jul-Aug	Sep-Oct	Nov-Dec
District A	Cluster 0	0.35	0.351	0.313	0.271	0.274	0.391
	Cluster 1	0.793	0.82	0.743	0.618	0.665	0.933
	Cluster 2	1.556	1.618	1.38	1.136	1.165	1.779
	Cluster 3	3.18	3.01	2.54	2.07	2.219	3.16
District B	Cluster 0	0.326	0.306	0.236	0.199	0.216	0.408
	Cluster 1	0.697	0.764	0.689	0.610	0.629	0.945
	Cluster 2	1.38	1.483	1.310	1.139	1.187	1.815
	Cluster 3	2.307	2.767	2.592	2.186	2.346	3.331

Table 5.3: Multipliers used to equate the bimonthly profile consumption with the cluster average consumption.

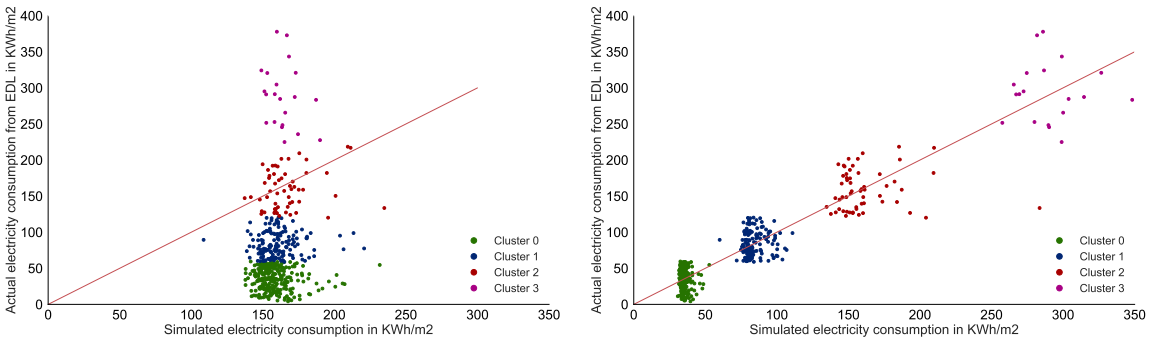

(a) Default EPlus configuration: full occupancy with ASHRAE standards

(b) Adapted EPlus results to Beirut occupancy and user behavior

Figure 5.10: Scatter plots of buildings consumption in District A for (simulated electricity consumption in kwh/m^2) in x axis versus (actual electricity consumption in kwh/m^2) in y axis after clustering.

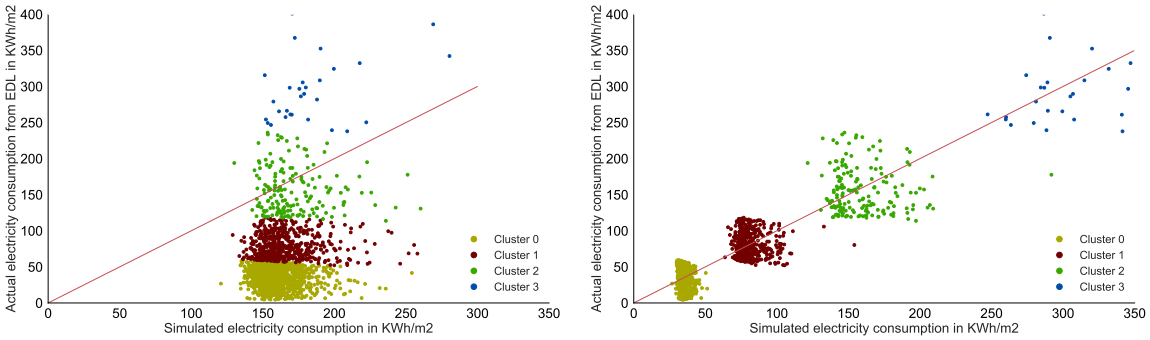

(a) Default EPlus configuration: full occupancy with ASHRAE standards

(b) Adapted EPlus results to Beirut occupancy and user behavior

Figure 5.11: Scatter plots of buildings consumption in District B for (simulated electricity consumption in kwh/m^2) in x axis versus (actual electricity consumption in kwh/m^2) in y axis after clustering.

5.4.3 Loads profiles

Comparison of the electricity consumption from EDL data with model predicted and calibrated output at a bimonthly resolution for the buildings in both districts is shown in figure 5.12. Table 5.4 illustrates the differences between the model outputs and EDL data before and after calibration.

The predicted model overestimated the electricity consumption by a minimum of 6,607 MWh in March - April and a maximum of 17,281 MWh in July- August in district A. In district B, the overestimation was much dramatic ranging between 22,757 MWh in March - April and 53,614 MWh in July- August. After calibration, the model almost attained the overall actual bimonthly consumption with an absolute difference between calibrated and actual values ranging from 33 to 132 MWh in district A and from 25 to 475 MWh in district B. The average RMSE of the yearly consumption was reduced from 105 kWh/m^2 the 25 kWh/m^2 in District A and from 112 kWh/m^2 to 22 kWh/m^2 in District B.

We found out that the monthly variation of the energy consumption predicted by the model before and after calibration follows a similar trend to that the of actual data: March and April were the months of least consumption, while peaks were detected during the hot months (July and August). The figure 5.12 also depicted the overestimation of the electricity needs variation over the year. The increase in energy demand between the less consumer months (March and April) and the most consumer months (July and August) was predicted by 97% and 107% for residential and mixed buildings respectively in district A, while in

District A	Jan-Feb	Mar-Apr	May-Jun	Jul-Aug	Sep-Oct	Nov-Dec	Yearly
EDL (Mwh)	6,302	5,675	6,674	7,506	6,650	6,413	39,220
Predicted (Mwh)	13,444	12,282	18,144	24,788	20,522	13,289	102,469
RMSE (Kwh/m^2)	15	12.5	18.8	27.5	22	13.1	105.4
Calibrated (Mwh)	6,250	5,733	6,737	7,473	6,693	6,545	39,433
RMSE (Kwh/m^2)	6.5	4	4.6	5.2	4.8	4	23.7
District B	Jan-Feb	Mar-Apr	May-Jun	Jul-Aug	Sep-Oct	Nov-Dec	Yearly
EDL (Mwh)	15,631	14,017	16,993	20,229	17,702	18,013	102,585
Predicted (Mwh)	40,989	36,774	53,977	73,844	60,904	39,632	306,119
RMSE (Kwh/m^2)	17.8	12.5	19.6	29.1	23	13.4	112
Calibrated (Mwh)	15,156	14,237	17,017	19,913	17,602	17,898	101,823
RMSE (Kwh/m^2)	4.7	3.4	4.4	5.1	4.4	4.5	22

Table 5.4: Comparison between the energy model outputs and the actual metered data before and after calibration.

reality, it was only of 32% for both buildings types in district A. Very similar trends were found in district B, except that the actual increase was of 42% between the second couple and the fourth couple of months.

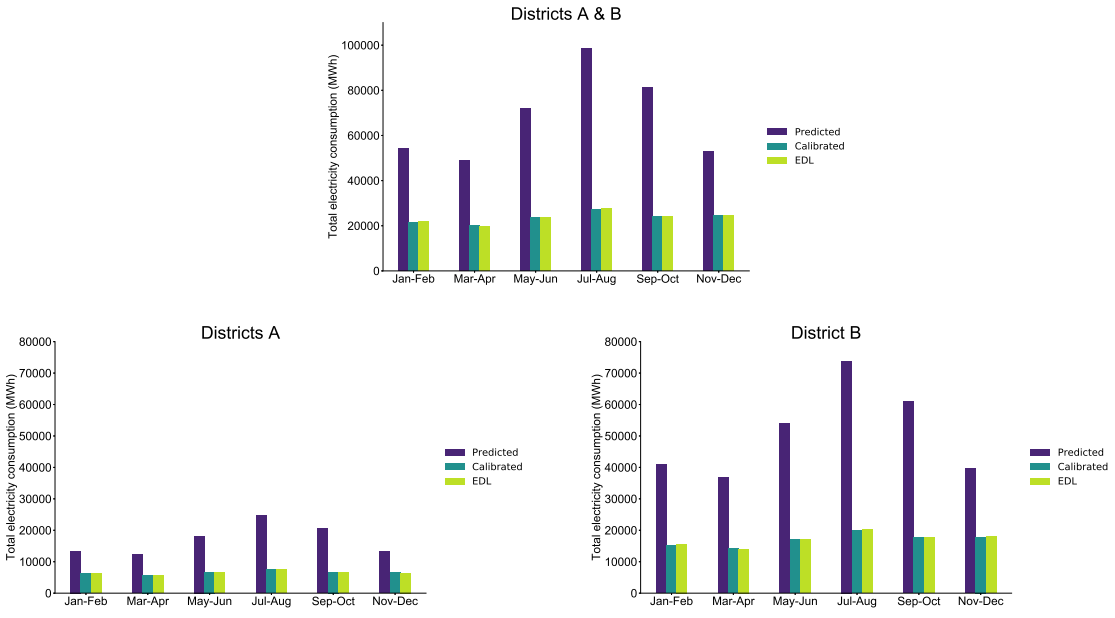

Figure 5.12: Total electricity demand in districts A and B

Figures 5.13 and 5.14 show the end-use apportionment of the bimonthly electricity consumption after calibration for residential and mixed buildings in both districts. Table 5.5 summarizes the percentage of energy consumption for each end-use in the two buildings types. Electricity consumption for cooling needs was the highest during the period from May till October, accounting for 43%, 54%, 55% and 74% of the total electricity consumption during July and August in residential and mixed buildings respectively, in district A and similarly in district B. Heating, on the other hand, reached its maximum shares during the first two months of the year with 14% and 16% in residential and mixed respectively in district A and with 16% and 15% in these buildings in district B. Equipment had almost fixed energy consumption in both buildings types, with maximum shares of 39% and 52% during March and April in residential and mixed buildings respectively, in both districts. Hot water, provided by electrical heaters in residential floors, shared the highest proportion of the total energy consumption in residential buildings during the last two months of the year with 40% and shared a lower proportion of 22% during summer in both districts. In mixed buildings, its share ranged between 10% in hot months and 23% in cold ones in both districts. Lastly, lighting needs decreased slightly during summer season and its shares were quite moderate, ranging between 9% and 18% in residential buildings, 8% and 21% in mixed buildings. However, by calculating the proportion of each component over the entire year, the equipment and hot water in residential buildings shared 32% and 31% of the total annual electricity consumption, while the cooling revealed to be of 19% in both districts. Mixed buildings, on the other hand, had 39% of their electricity consumption for appliances, followed by 31% for cooling in both districts.

District A		Jan-Feb	Mar-Apr	May-Jun	Jul-Aug	Sep-Oct	Nov-Dec	Yearly
Residential	Equipment	33	39	32	26	29	37	33
	Lighting	16	16	11	9	12	18	13
	Heating	15	3	0	0	0	4	4
	Cooling	0	4	29	44	34	0	19
	Hot water	36	38	28	22	25	40	31
Mixed	Equipment	45	53	37	28	32	53	40
	Lighting	18	17	10	8	11	21	13
	Heating	15	2	0	0	0	5	4
	Cooling	0	9	41	56	47	0	28
	Hot water	20	20	12	9	11	22	15
District B		Jan-Feb	Mar-Apr	May-Jun	Jul-Aug	Sep-Oct	Nov-Dec	Yearly
Residential	Equipment	32	39	32	25	29	37	33
	Lighting	15	16	11	9	12	18	13
	Heating	18	3	0	0	0	5	4
	Cooling	0	4	29	44	34	0	19
	Hot water	35	38	28	22	25	40	31
Mixed	Equipment	47	53	37	28	33	53	41
	Lighting	18	17	10	8	11	21	13
	Heating	17	2	0	0	0	5	3
	Cooling	0	8	41	55	46	0	28
	Hot water	19	20	12	9	11	22	15

Table 5.5: Percentage of energy consumption by end-uses for residential and mixed buildings in both districts.

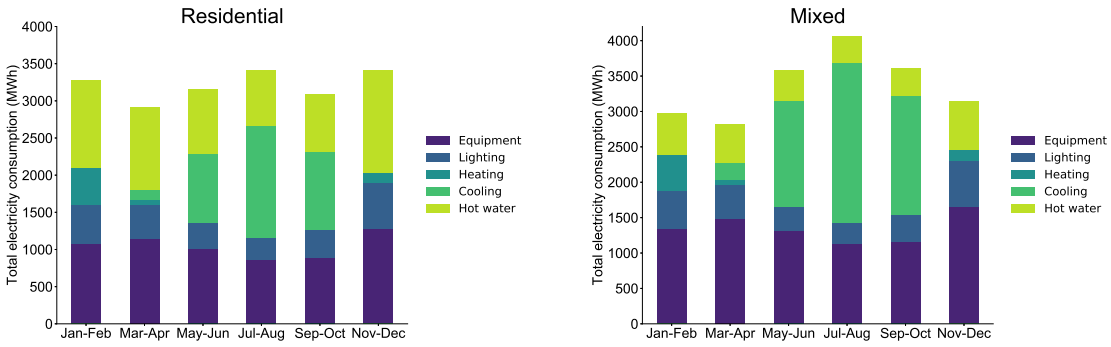

Figure 5.13: Bimonthly calibrated electricity consumption by buildings types in District A

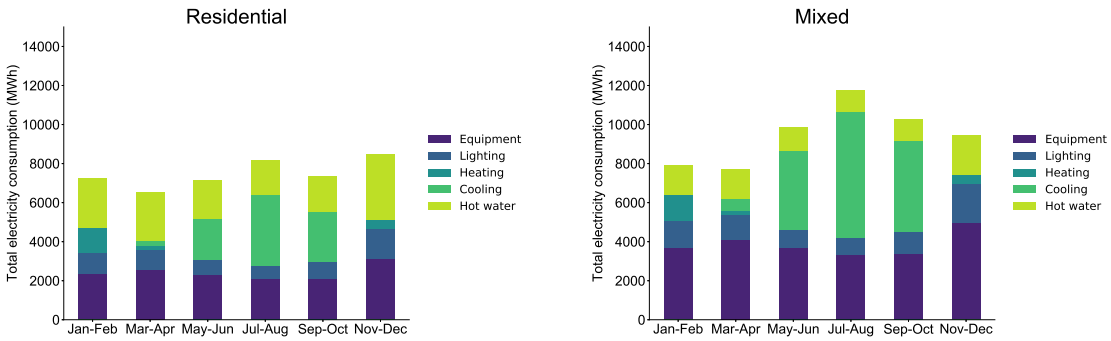

Figure 5.14: Bimonthly predicted electricity consumption by buildings types in District B

By combining the model output with GIS mapping techniques, a spatiotemporal distribution of the energy consumption is obtained, as shown in figure 5.15. Note that buildings with the highest consumption were built between 1941 and 1990.

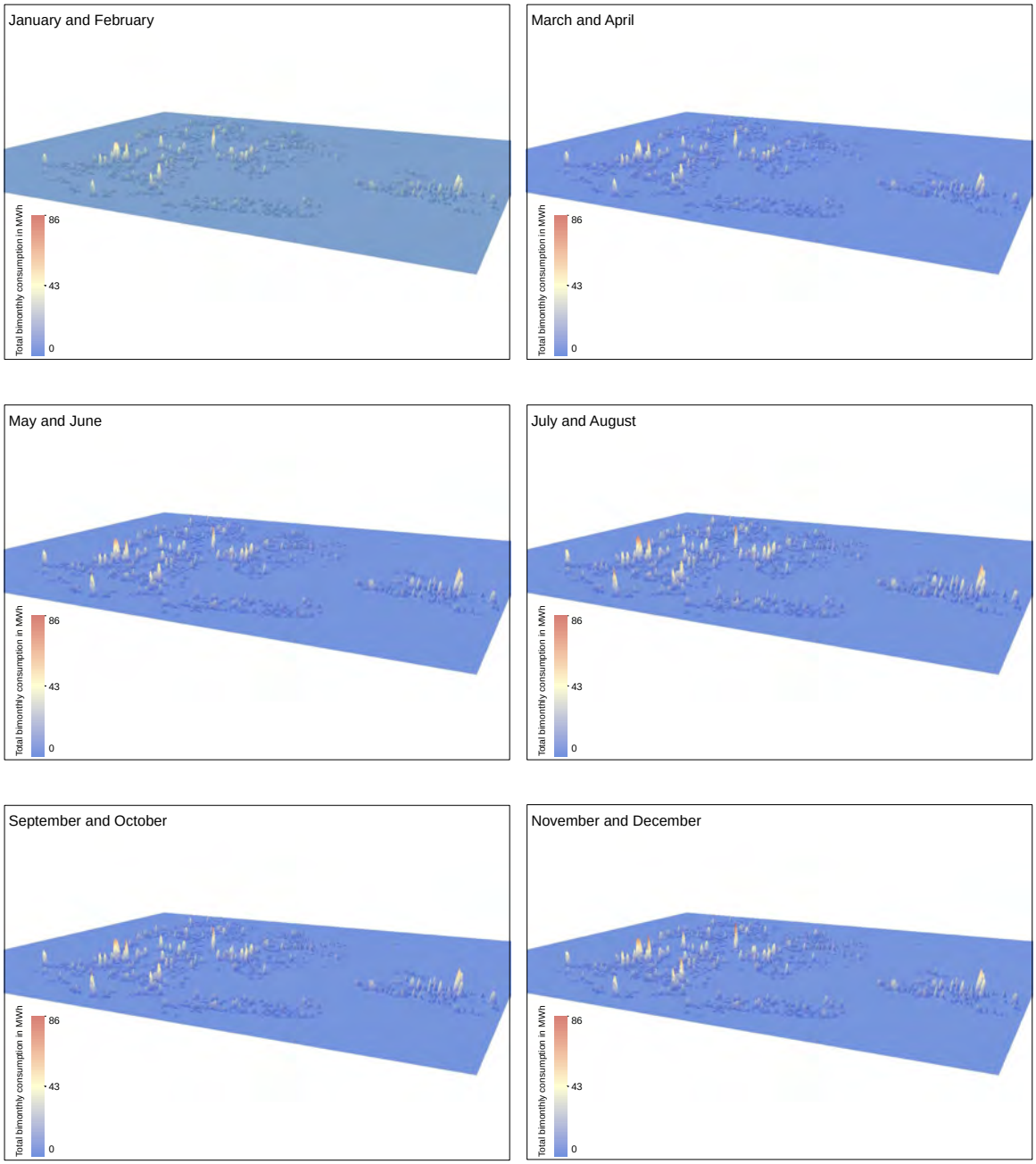

Figure 5.15: Spatio-temporal distribution of the bimonthly predicted electricity consumption of the buildings in district B

5.4.4 Spatial autocorrelation

In order to examine the spatial variation of the electricity consumption of residential and mixed buildings, we used global Moran's I to evaluate the spatial autocorrelation. Moran's

I assesses if the electricity consumption exhibits certain spatial patterns or it is random. Its values ranges from -1 to +1, where positive values indicate spatial clustering (i.e., large values are surrounded by other large values) and negative values indicate spatial dispersion (i.e., large values are surrounded by other small values). To reject the null hypothesis, a measure of uncertainty is essential with the Moran's I measure. Z-score and p-value are used for this purpose.

To determine to which extent a variable is dependent on the values observed at neighboring locations, we implement an incremental spatial autocorrelation. The analyses were based on the energy consumption per building. Results are shown in figures 5.16 and 5.17 for district A and B respectively. By comparing EDL autocorrelation results with the calibrated model results, they both appeared to be the strongest at $60m$ in district A. On the other hand, predicted energy consumption in district B showed similar results as the EDL data with the strongest correlation being at $40m$ for all end-uses. The p-value was less than 1% which indicates that the distribution of the energy consumption is not random.

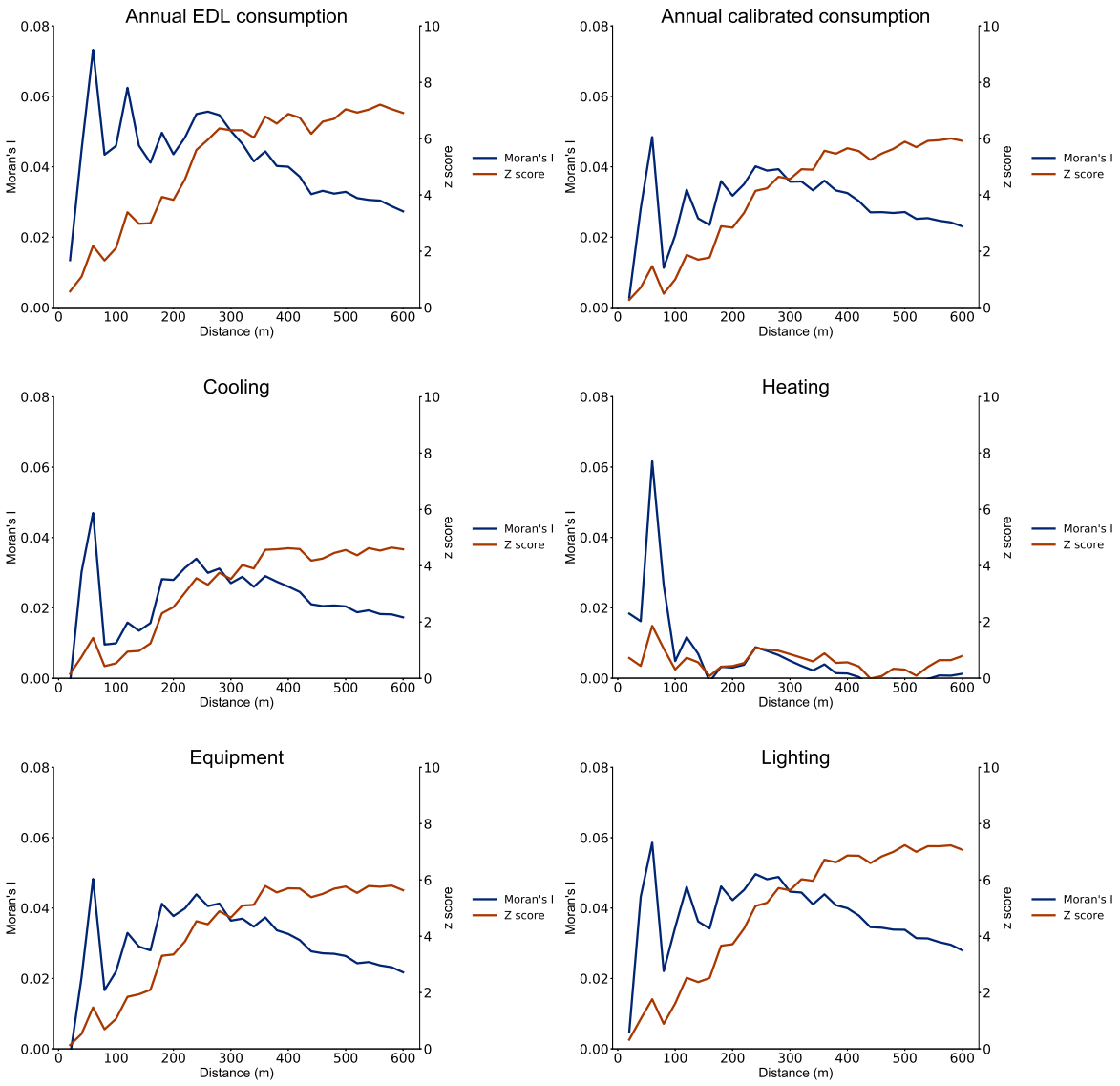

Figure 5.16: Autocorrelation analysis of electricity consumption in district A

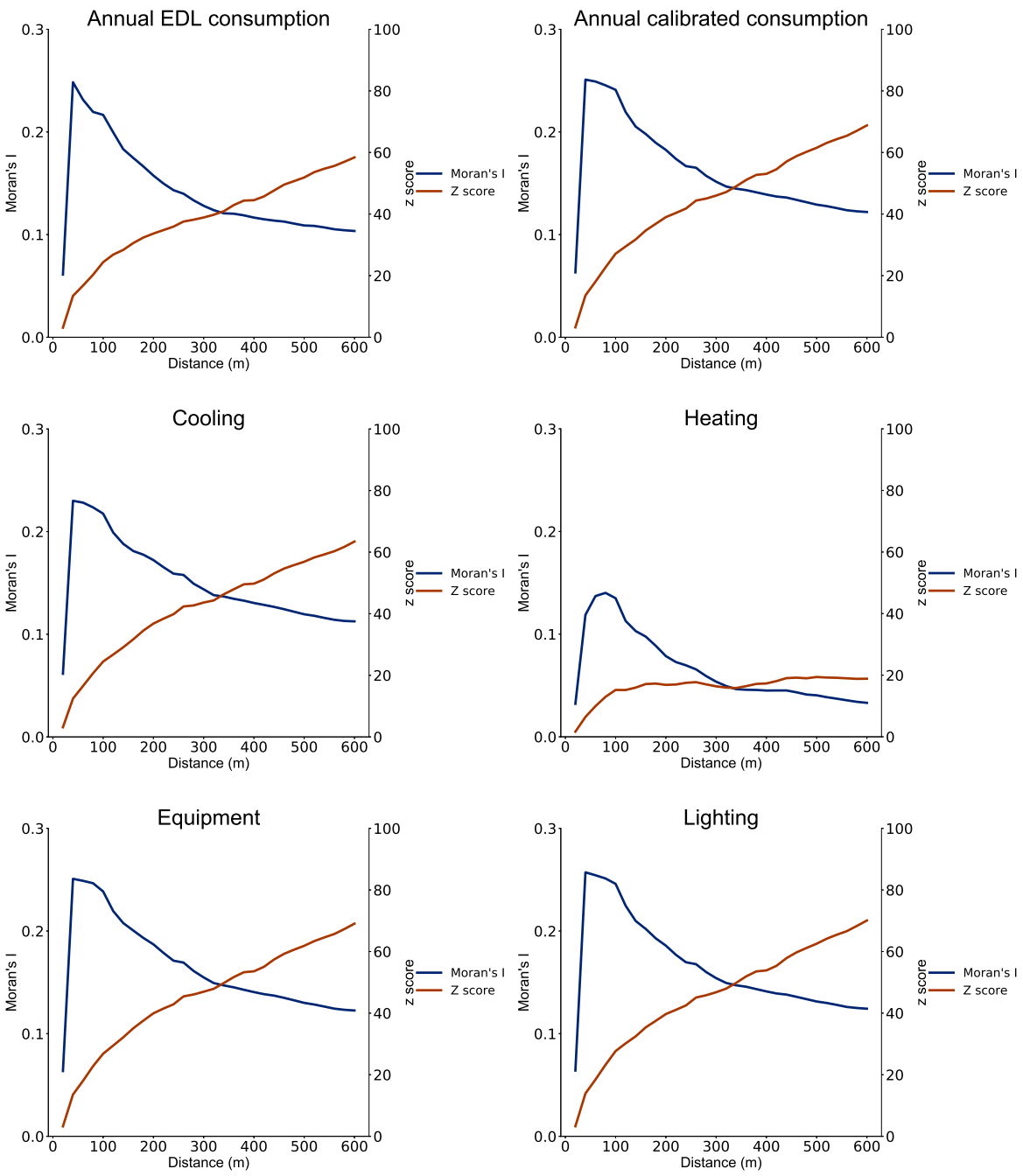

Figure 5.17: Autocorrelation analysis of electricity consumption in district B

Figure 5.18 show lumps of buildings with high consumption and other with low consumption, as proof of concept of the spatial auto-correlation clustering of buildings.

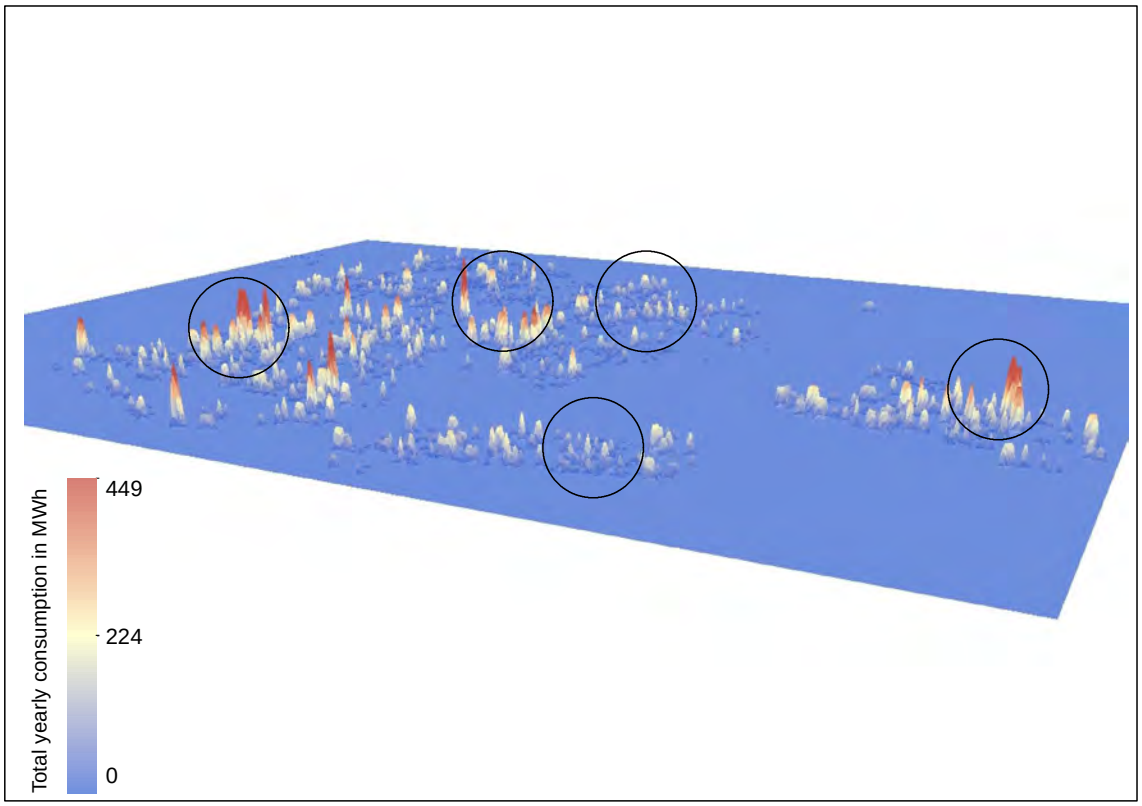

Figure 5.18: Spatial distribution of buildings energy consumption in district B

5.4.5 Archetypes Spatial correlation

In order to determine if buildings of different archetypes are linearly related in terms of electricity consumption, the Pearson coefficient was used. The value of the Pearson coefficient ranges from -1 to 1. When it approaches 0, the correlation of the two variables is weak. If the correlation factor is near 1 or -1, a strong correlation exists between the two variables. The Pearson coefficient is used to analyze the relation between a building's energy consumption with the neighboring buildings. However, the definition of neighbors buildings can vary. Therefore, we applied the correlation analysis to a radius of $1500m$ with a step of $50m$. When no buildings of the corresponding archetype reside within the given distance or no sufficient information can be deduced, null values were forced. In district A, correlation was only found between the electricity consumption of mixed buildings from the third period of construction and residential buildings from the second period on one hand and mixed buildings from the fourth period on the other hand, as shown in figure 5.19. The correlation

was quite moderate in both cases and was lost at $200m$ in the first case and at $100m$ in the second. In district B, a significant correlation was found between residential buildings of the fourth period and mixed buildings from the third period of construction ranging from 0.75 at distances less than $50m$ to 0.25 at $100m$. Furthermore, mixed buildings from the second period of construction had positive correlation with mixed and residential buildings from the third and fourth periods of construction.

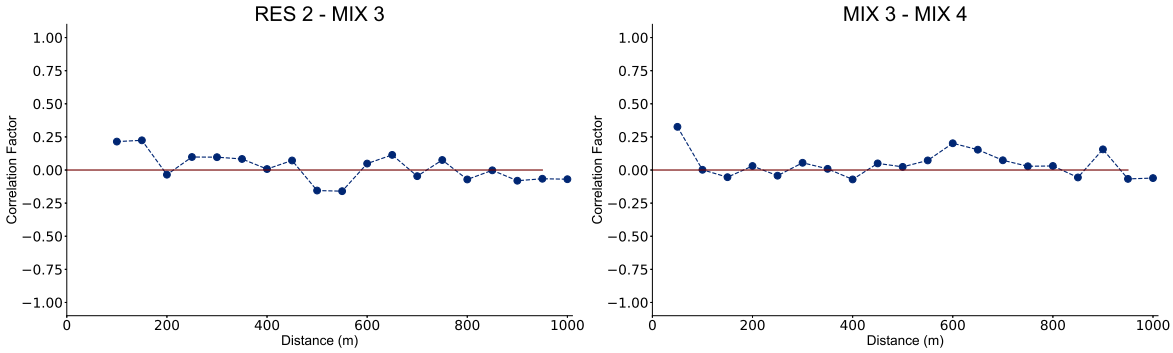

Figure 5.19: Spatial correlation between energy use of different buildings types in district A

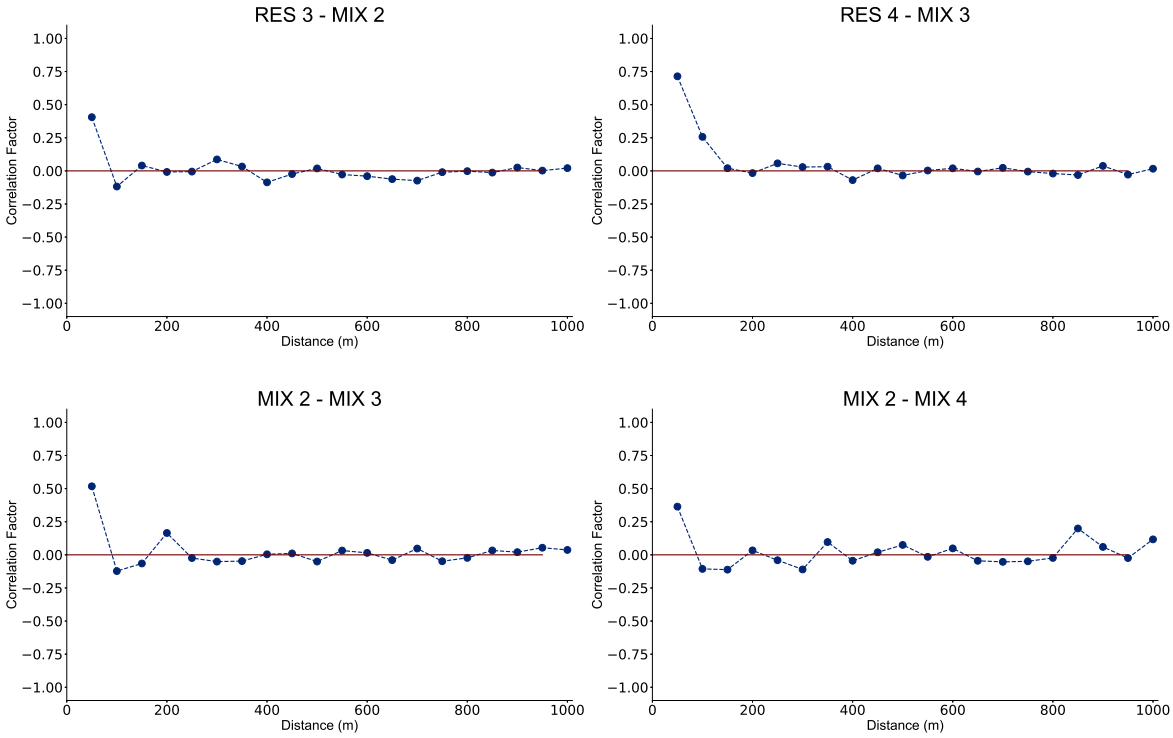

Figure 5.20: Spatial correlation between energy use of different buildings types in district B

5.4.6 Temporal correlation

In order to determine the temporal variation of the electricity consumption, we applied linear correlation analysis between the energy consumption of the different months by the use of the Pearson coefficient. The analysis was conducted at the monthly resolution (figures 5.21-5.24). As in the previous section, null values were forced when there was no consumption of electricity.

A significant correlation characterized the electricity consumption of cooling equipment in hot months. For March and April, the correlation factor was around 0.85 and 0.95 respectively in district A and 0.7 and 0.8 respectively in district B with respect to months between May and October. The cold months were also highly correlated in terms of heating.

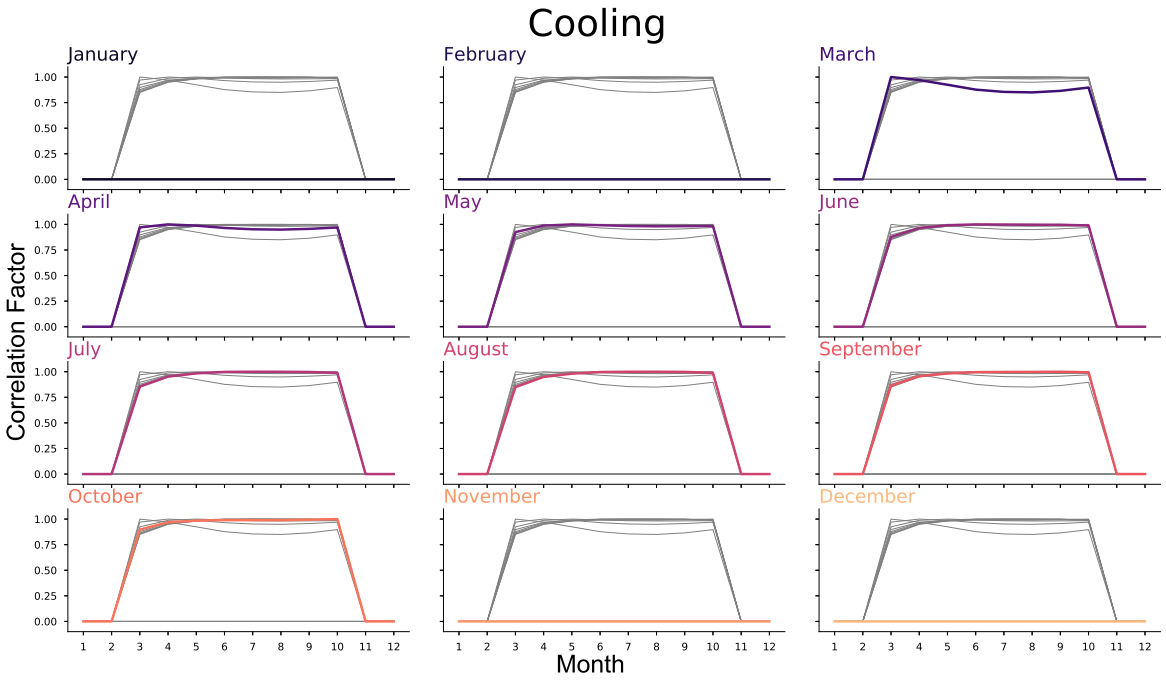

Figure 5.21: Monthly correlation of cooling loads (District A)

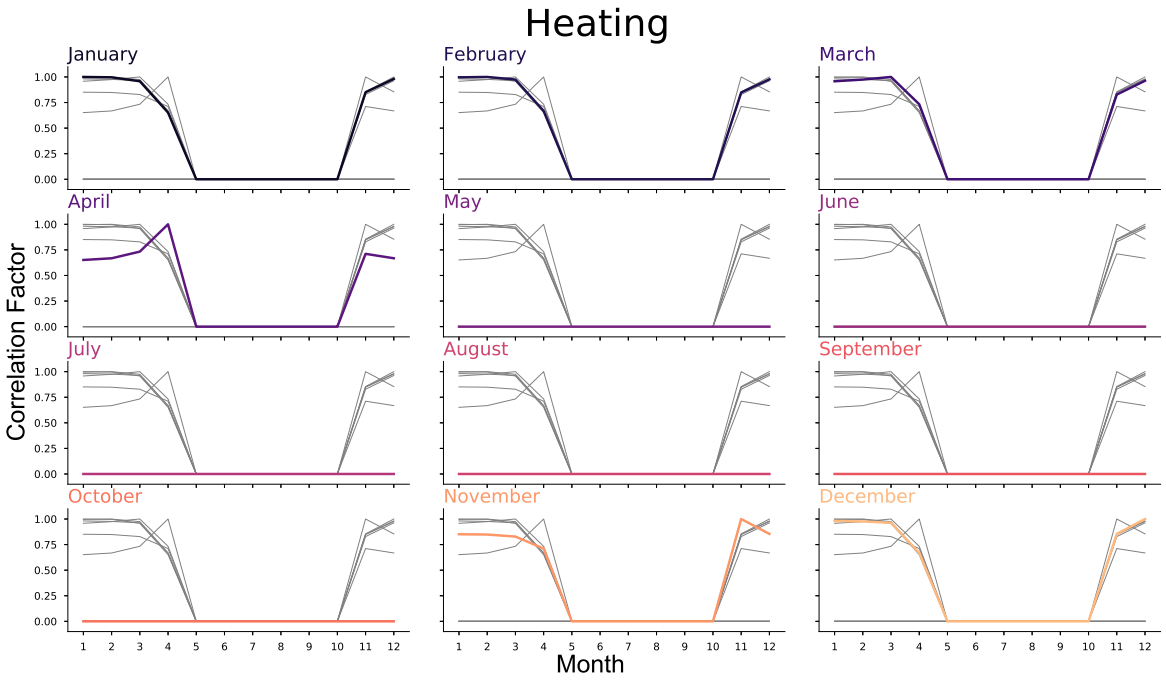

Figure 5.22: Monthly correlation of heating loads (District A)

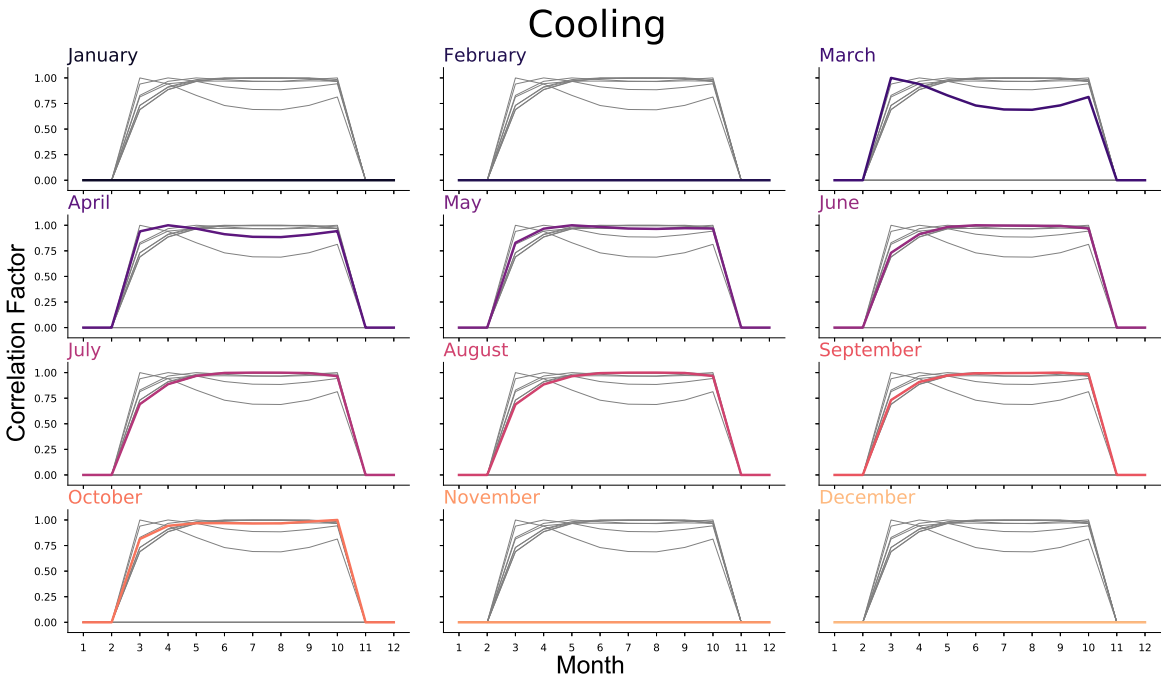

Figure 5.23: Monthly correlation of cooling loads (District B)

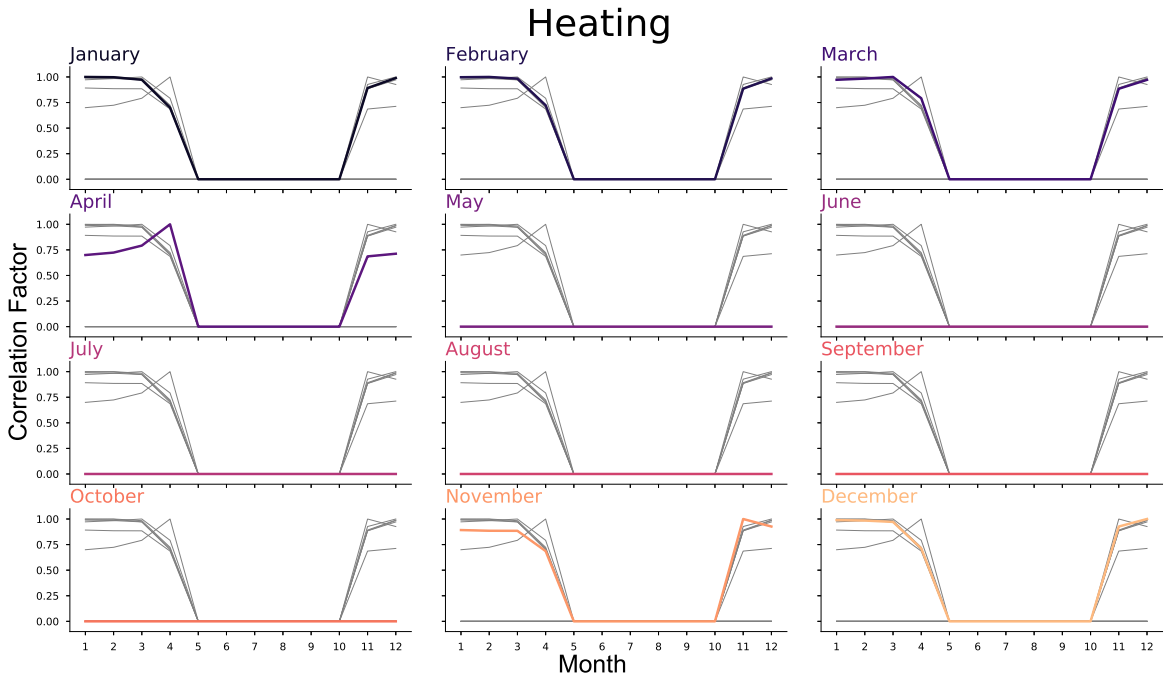

Figure 5.24: Monthly correlation of heating loads (District B)

5.5 Discussion and conclusion

The previous sections have shown how to build, generate and calibrate an UBEM, capable of predicting the electricity consumption of a city by capturing the buildings behaviors. The model takes as input, data containing buildings footprints, heights, floor area, number of floors, the corresponding archetypes as well as a weather file and a topographic map. Here, an updated weather file, encapsulating the global climate change and the UHI in Beirut is required for the full-scale energy model of the city, especially with the high density of diesel generators dispersed over the city and between buildings. Moreover, a high-resolution topographic map can reduce the complexity of the model when generating the elevation profile of the city and projecting the buildings onto the inclined plane.

The geometrical properties such the WWR and the construction materials were obtained from previous studies, while the non-geometrical properties were collected from local reports when available and existing libraries. Efforts in this regard should be carried out to create an appropriate database for Beirut that incorporates construction materials and their thermal properties. The discrepancies between BEEM predictions and actual

consumption data can be associated to the number of appliances, and occupancy schedules related to occupant's comfort and income level. In this context, most residents in Beirut tend to reduce their electricity usage for heating in winter. Moreover, during hot seasons, occupants tend to switch between different modes of cooling, including air conditioners, electric fans and natural ventilation. The penetration rates of HVAC systems and their properties should be further examined, especially in buildings built prior to 1945, characterized by their climate responsive architecture and application of sustainable concept [117]. These buildings rely on environmental conditions for indoor thermal comfort. However, these buildings may have lost their intended characteristics with the random construction and the effect of climate change. Identifying the occupancy patterns and population densities should be a first basic step to enhance the reliability of UBEMs. Moreover, extensive periodic audits are required to investigate occupant-related parameters, such as economic status, internal thermal comfort, appliances usage, daily and seasonal occupancy schedules and activities.

The main challenge faced during this study was the setup of schedules. As previously mentioned, the absence of energy use and occupancy profiles led the authors to adopt standardized schedules. The model exhibited a heavy burden on the energy sector in case citizens adopt a western expensive and comfort lifestyle. In fact, Lebanon is considered an economically weak country. Moreover, the electricity rationing already thrusts residents to modify their behavioral patterns resulting in an amount of suppressed demand. However, in presence of bimonthly metered data (EDL data), it was possible to inspect the Lebanese energy use patterns and relate them to socio-economic and political circumstances of the country. Predicted energy was adjusted by an analytical automated objective process as shown in section 5.3.3. It was clear that a lower monthly variability characterizes the electricity consumption of residential and mixed buildings, compared to the simulated one, mainly attributed to the overestimated cooling demand. This was partially corrected by the assumption that buildings floors are partially cooled (and heated). The remaining differences can be explained by the fact that many Lebanese families (up to 15%) own two or more houses [71] in other regions in the country and leave the city during summer vacation. Moreover, high numbers of residential units are unsold or vacant, owned by expatriates or investors. Up-to-date statistics of this regard are needed to correctly estimate the energy consumption per household and per capita. However, issues related to data

accessibility and privacy may be raised and should be properly addressed.

The calibration was employed at the temporal scale of the real data and yield satisfactory accuracies for the overall building energy demand. However, the authors cannot claim accuracy at hourly level with no metered data for validation and/or calibration. Efforts should be placed on recording hourly electricity consumption by EDL or by occupant behavior modeling techniques [118, 119, 120]. The calibrated electricity consumption showed similar spatial clustering as the metered data from EDL in both districts, as was found in section 5.4.4. This proves the relevance of our calibration process. The energy model can be employed to relate the observations of electricity consumption at one location to those at other locations. The main interest in revealing spatial clustering is its importance in generating zones for smart grid distribution. It is important to note that the perimeter of the neighborhood or city divided by the auto-correlation length is supposed lead to the same number of similarly behaviors clusters of buildings obtained in section 5.3.3 or the same number of archetypes. However, our district perimeter over the obtained correlation length did not match the number of clusters neither the number of archetypes for many reasons: first, our data is incomplete and many buildings were eliminated before the calibration process. Secondly, on the top of a cluster or archetype, there may be multiple classes of behaviors, especially since in our model, we are attributing each floor an archetype. Exemplary, mixed buildings include residential, offices and retail floors, each with its own schedules. Moreover, their proportions depend on the total number of floors, so a mixed building with 4 floors differ in terms of occupancy-related parameters from a mixed building with 8 floors, and so on. In addition, Beirut City represents the central administrative and commercial area of Lebanon. Human's mobility in and out the city needs to be investigated as highly possible influence on the energy demand [121], especially when extending the scope of the model to the whole city and integrating commercial and governmental buildings. Therefore, further research are required to improve the spatial auto-correlation study.

In the generation of an UBEM, each building is represented as an individual 3D thermal modeling dependent on its urban context, attributed an archetype based on a set of parameters. Temporal loads profiles are then coupled with GIS mapping techniques to support urban decision making. Considering these characteristics, no UBEM studies within the Mediterranean region was previously achieved. Bottom-up studies were mainly focusing

on defining representative buildings for the building stock and assessing their energy performance [122, 57]. In Spain, a bottom-up approach combining statistical and engineering models was used to predict the energy performance and indoor thermal comfort of a neighborhood of a city located on the Mediterranean coast of the country [123]. The methodology consisted of correlating covariates such as the urban layout geometry and solar influence to variables such as the cooling and heating energies, and discomfort heating and cooling hours. The prediction models were then applied to buildings in a neighborhood without representing them by 3D architectural thermal models. Other studies were applied to correlate the urban texture to UHI [124] with a top-down approach and a simplified representation of the urban morphology. A similar study was applied to Beirut using the Town Energy Model (TEB) [125]. TEB [11] is a conceptual model that simulates the energy and water exchanges between the city and the atmosphere by parametrizing the dynamic and thermodynamics interactions. It is based on the urban-canyon geometric model [12]. These approaches are limited to specific applications. Though they compute fast simulations, the simplified representation of the urban canyon leads to a lack of necessary details for the assessment of any future interventions at the building level and end-uses level. In addition, the model does not incorporate the stochastic occupant behaviors. The bottom-up approach presented in this paper overcomes all these drawbacks and enriches the accuracy of the model. Furthermore, its calibration concentrates on integrating the significant weight of occupant behaviors into the urban model. Its capability to handle the complexity of an urban area can be used to enhance the findings of the previous studies within the Mediterranean region. The adopted methodology can be replicated in any other districts or cities in Lebanon and the region. Its multi-scalability is recognized spatially when ranging from building to the city level, and temporally when ranging from hourly to yearly resolution. This allows for a spatiotemporal energy patterns analysis to allocate hot spots and peak times of energy demands. In this regard, 2D and 3D urban energy maps are very informative (figure 5.15) and enable critical analysis. Application of energy conservation or retrofit measures to specified buildings with high energy demands can then be explored. Moreover, the scaling down to hourly energy consumption patterns is crucial for the management of the energy distribution by smart rationing of electricity. In this context, the model may provide insights into the optimal integration strategy of the solar power on buildings rooftops, as will be studied in future research.

Policy Implications

To meet the GHG emissions reduction goals, limit the energy demand and achieve security of energy supply, the country needs to introduce energy policies to manage the energy sector and resources in the city and that are more social and environmental oriented. Energy policy can be d.efined as a strategy adopted by a given entity (often the government) to address issues related to energy development to insure its sustainability, including energy production, distribution and consumption [126, 127]. Legislation, international treaties and incentives are among the main outcomes of an energy policy.
The main purpose of UBEM is to act as a decision support tool for architects, urban planners and energy policymakers to assess the current energy demand patterns and the future impacts of energy retrofitting programs and energy supply infrastructure changes [18]. In the previous sections, the generation of an UBEM for Beirut City has been shown. Due to uncertainties related mainly to human behaviors, the model had to be calibrated for reliable results compared to metered data so that it can inform energy policies. Recommendations for the management of the energy in Beirut based on scientific evidence from this research were published in the policy brief entitled Beirut as a Smart City: Redefining Urban Energy, in collaboration with Issam Fares Institute for Public Policy and International Affairs at the American University of Beirut (Appendix B). For Lebanon, a country with chronic energy sector failings reflected by the widening deficit of power delivery and quality, this work offers three distinct policy connections that could help with resolving real and existing challenges:

- First, due to the unrefined and bi-monthly billing of electricity as well as the distorted electricity market in the country, EDL, the national power utility does not have an accurate account for consumption loads and their variations spatially and temporally. The developed model provides a powerful tool to understand better load variations, and thus plan future strategies and investments accordingly. For example, one of the main techno-policy challenges lies in estimating Lebanons real demand for electricity and its growth rate in the future due to the complex interactions between EDL and operators of private diesel generators, some of which are metered and some remain largely unregulated; and the existence of suppressed demand that is due to EDLs failure to provide power around the clock. With the help of smart metering that EDL

is starting to implement, this model can be used to scientifically calibrate, verify and estimate growing demand on a national and sub-national scales.

- Second, until EDL can provide electricity without any interruptions, power outages will continue to occur. Predicting electricity consumption patterns in Beiruts urban environment, as shown in this work, could ultimately help inform smart rationing of the electricity that provides an efficient mapping between loads and available supply capacity.
- Third, the developed model could be utilized to test various policy instruments and ideas that promote energy savings such as the implementation of building efficiency codes, installation of water heaters, etc. One particularly useful application is to test the potential of rooftop solar PV systems to meet demand, or part of it, during certain daily and yearly peak times. Separately, the authors are working on a PV supply study that can ultimately be coupled with this work to provide a real assessment of the potential of rooftop solar PV systems to provide cost savings as well as increase power coverage in Beirut.

6. Conclusion and perspectives

The raising concerns regarding cities' sustainability oriented recent research to focus on possible demand reduction and clean supply of the energy. Technologies to satisfy the twofold objective of energy management are available, but the problem is confined on how to contextualize their implementation for a specific application. This difficulty is mainly related to lack of information describing the specific demand-supply nexus. Based on the state of the art overview, urban building energy models have proved to be effective management tools for present and future energy estimations, and for assessment of possible technological interventions' impacts on urban energy, for the purpose of informing policy and programmatic decision making.

The limited application of such tools is partially explained by the availability of data. Chapter 3 focuses on the nature of data indispensable to create an urban energy model. Accordingly, an examination of the availability, completeness and usefulness of the data sources are required. This leads to an assessment of the required efforts to complete, pre-process and organize this data, considering its dispersal nature and reliability. Data management and flexible storage are two key points to facilitate its use and provide organized and clean inputs for the simulation tools. In order to construct adaptable data, remote sensing tool and machine learning algorithms were applied. An archetypal classification of buildings, based on their types and periods of construction, was adopted to reduce the complexity of dealing with large number of buildings at the urban scale. After this crucial step of data management, 3D geometrical approach was entirely developed to automatically generate the 3D thermal buildings and further subdivide them into floors. Balconies and DTM are added features to the model, and their integration was justified with a simplified example in chapter 4, as affecting parameters in the radiative budget, and hence the energy budget of buildings. Given the limited amount of useful data, the study

was limited to two districts within the city of Beirut.

In chapter 4, a new approach to simulate daylight accessibility in urban areas and thus link it to urban morphology was presented. The methodology is based on advanced computational tool to simulate the radiative budget in urban environment. Given the complexity of the 3D model of the districts involved in this chapter, the simulations were complex and time consuming. Of course this could be controlled by simplifying input parameters such as the illumination grid size and geometries meshing, but this intervention would be at the expense of results accuracy. By adopting a simplified approach, the impact of urbanization on daylight access was assessed and revealed a significant decrease. Due to unavailability of satellite images for old Beirut for 3D radiative budget comparison, another approach was adopted, where urban aspects such as the average height and orientation of surrounding buildings, their standard deviation, the building' height and position in space were associated to daylight availability on buildings' facades with artificial neural networks algorithms. With a MAPE error of 17%, the trained algorithm presents a reliable and consistent method to assess daylight accessibility for urban planning, future buildings' design and estimate its variation over the years if input features could be obtained. Chapter 5 represents the fundamental core of this thesis. The development of BEirut Energy Model was represented. The 3D model generated in chapter 3 fed a dynamic energy simulation engine to calculate the energy loads of 3,360 buildings, and then their electricity consumption. However, the limited available information and substantial uncertainties mainly related to simulation tools, energy systems and occupant behaviors should be addressed to adjust the predictable capacity of the model to study urban energy interventions and therefore avoid leading to erroneous conclusions. Accordingly, the use of metered data was indispensable to calibrate the model outputs. The calibration process was achieved by clustering the buildings based on their actual electricity and predicted consumptions, and find the multiplicative coefficients of their representative clusters centroids. These coefficients were used to correct the model outputs, but they also informed about the compatibility of the model inputs to represent the city under study. The applied methodology proved to be effective to reach acceptable accuracy in matching predicted outputs with actual data. Consequently, the analysis was pushed forward for a spatiotemporal identification of hot spots and peaks of energy demands. These energy maps are very informative for any intervention planning. Spatial autocorrelation of energy

demand was also reported, suggesting possibility for smart grid zoning. The results of BEEM were convenient to provide scientific evidence to inform policy. Recommendations based on the analysis of BEEM outputs were made and published in a policy brief, enclosed in chapter **??**.

6.1 Perspectives

The work presented in this thesis is the first UBEM at this scale in Lebanon and the region to the author's knowledge. While it has proved to present several advances, further work are still needed to promote its use in urban energy planning and some relevant developments can be considered.

Large-scale data management

Data availability was a major obstacle that limited the scope of the thesis to the one represented in this dissertation. Therefore, an inevitable need for databases is raised. Data repository should include:

- Up-to-date list of materials used in buildings' construction, along with their thermal and optical properties, in addition to construction methods such as building components' layers.
- Recent and old satellite images for cities of interest that can be used in remote sensing, not restricted to buildings' digitizing and vegetation classification, but also for urban properties' identification.
- Characteristics of energy end-uses, such as HVAC, appliances and lighting, including their rates of penetration, their efficacy and their use patterns.
- Occupant related parameters, such as their activities, behaviors and preferences. In this context, complexity raises due to the stochastic nature of humans patterns.

Data management and organization in a key factor for an efficient and less time-consuming generation of UBEMs. Common templates of information and the possibility for sharing will increase the adoption of these tools, enhance their reliability and facilitate their importation to the models.

Geometrical and non-geometrical model refinements

Many improvements can be thought of to further enhance the accuracy of the presented model and to broaden its applications. The geometrical model can be improved by considering tilted roofs, buildings' zoning into core and perimeter, trees and parks modeling, roads and pedestrian walkways, to list a few. These improvements are important for both energy model and radiative model. The archetypal classification can be improved by adding other key parameters than the building's type and year of construction. However, identification of key parameters should be based on a sensitivity analysis to avoid generation of useless archetypes.

Model functionality

BEEM model presented in chapters 3 and 5 is an automated algorithm to generate the 3D models and the ready-to-run files for energy simulations. However, the inputs and outputs of the model require huge effort to use and process. The outputs on the other hand are stored in excel files that require good programming skills to extract, analyze and visualize results. In other words, BEEM can be further developed for data management functionalities, and promoted to an effective and feasible platform for users from different backgrounds. It should adapted for compatibility with other formats, such as CityGML so it can be used in other studies. One more barrier is the computational cost of the simulations. This study was accomplished with cloud computing service. Energy simulations are time consuming unless powerful computers are in use. Therefore, attention should be taken in this regard.

Improvement of the energy budget assessment

- The radiative budget contributes in the energy budget through surfaces' solar gain and energy savings from daylight. The radiative module in EnergyPlus is simple, while that in DART is more advanced and accurate. Coupling the outputs of DART with EnergyPlus or any dynamic energy modeling software would be useful.

- Climatic parameters such as UHI, local wind conditions, evaporation near the sea and released heat from transportation should be taken into account given their influence on the energy and radiative budgets of buildings and therefore on the electricity demand. Therefore, the study could be extended to consider the effects of

microclimatic conditions by linking it to computational fluid dynamics CFD analysis, or by using urban weather generators to simulate the UHI effect..

Further studies

The presented model allows the assessment of energy demand within a spatiotemporal frame. It assess the present energy consumption and estimates future energy patterns under certain technological interventions, such as the implementation of energy conservation measures. In addition, it allows the estimation of the contribution of urban forms and energy end-uses in energy demand at building scale and city scale. The results of the energy model, the daylight model and their relation to urban metrics can be combined for a more holistic analysis of different designs, energy and low-carbon strategies, and urban planning. We started to explore these relations in sections 4.5.3 and 4.5.4, proving that the model is suitable for such analysis. Another important aspect of BEEM, is its capability to manage energy supply as well. The spatiotemporal energy maps can be coupled with solar irradiation and solar maps to estimate the potential saving from rooftop PV systems, the optimal distribution of the produced energy, and grid management to meet energy demand. It can also be used for network simulations such as district heating. Such capabilities help in informing urban planners and policy makers about possible scenarios to reduce energy demand, meet the urban needs and mitigate GHG emissions. Assessing the economical and social impacts of these interventions must be complementary to the model to provide a full adaptable plan for urban energy management.

Bibliography

[1] IEA - International Energy Agency. Lebanon: Indicators for 2014, 2016. URL `http://www.iea.org/statistics/`.

[2] United Nations Department of Economic and Social Affairs Population Division. *The World's Cities in 2016*. United Nations, Population and Vital Statistics Report, UN, New York, 2016. ISBN 978-92-1-151549-7. doi: https://doi.org/10.18356/8519891f-en.

[3] UN-Habitat. Urbanization and Development: Emerging Challenges. Technical report, UN-Habitat, Nairobi, 2016.

[4] M Santamouris. On the energy impact of urban heat island and global warming on buildings. *Energy and Buildings*, 82:100–113, 2014. ISSN 03787788. doi: 10.1016/j.enbuild.2014.07.022.

[5] Reinhard Madlener and Yasin Sunak. Impacts of urbanization on urban structures and energy demand: What can we learn for urban energy planning and urbanization management? *Sustainable Cities and Society*, 1(1):45–53, 2011. ISSN 22106707. doi: 10.1016/j.scs.2010.08.006. URL `http://dx.doi.org/10.1016/j.scs.2010.08.006`.

[6] By Bruno Osorio, Nick Mccullen, Ian Walker, and David Coley. Understanding the relationship between energy consumption and urban form. *Athens Journal of Sciences*, 4(2):115–142, 2016. doi: 10.30958/ajs.4-2-3.

[7] L Suganthi and Anand A Samuel. Energy models for demand forecasting - A review. *Renewable and Sustainable Energy Reviews*, 16(2):1223–1240, feb 2012. ISSN 13640321. doi: 10.1016/j.rser.2011.08.014.

[8] Yixing Chen, Tianzhen Hong, and Mary Ann Piette. Automatic generation and simulation of urban building energy models based on city datasets for city-scale building retrofit analysis. *Applied Energy*, 205(July):323–335, 2017. ISSN 03062619. doi: 10.1016/j.apenergy.2017.07.128.

[9] Carlos Cerezo Davila and Christoph Reinhart. Urban energy lifecycle : An analyitical framework to evaluate the embodied energy use of urban developments. In *Proceedings of BS2013: 13th Conference of International Building Performance Simulation Association, Chambéry, France, August 26-28*, pages 1280–1287, 2013.

[10] M Hajj-Hassan and H Khoury. Energy Modelling and Sustainability : A Review on Current Theories , Practices , and Challenges. *4th International Conference On Building Energy, Environment*, pages 781–786, 2018.

[11] Valéry Masson. A physically-based scheme for the urban energy budget in atmospheric models. *Boundary-Layer Meteorology*, 94(3):357–397, 2000. doi: https://doi.org/10.1023/A:1002463829265.

[12] Aude Lemonsu. Simulation of a summer urban breeze over paris. *Boundary-Layer Meteorology*, 104(3):463–490, 2002. doi: https://doi.org/10.1023/A:101650961.

[13] H. C. Ward, S. Kotthaus, L. Järvi, and C. S.B. Grimmond. Surface Urban Energy and Water Balance Scheme (SUEWS): Development and evaluation at two UK sites. *Urban Climate*, 18:1–32, 2016. ISSN 22120955. doi: 10.1016/j.uclim.2016.05.001.

[14] Carlos Cerezo Davila, Christoph F. Reinhart, and Jamie L. Bemis. Modeling Boston: A workflow for the efficient generation and maintenance of urban building energy models from existing geospatial datasets. *Energy*, 117:237–250, dec 2016. ISSN 03605442. doi: 10.1016/j.energy.2016.10.057.

[15] Jamie Bemis. *Urban Building Energy Modeling as a Dynamic Tool for Suatainability Planning*. Master thesis, Massachusetts Institute of Technology, 2016.

[16] Tianzhen Hong, Yixing Chen, Sang Hoon Lee, and Mary Ann Piette. CityBES : A Web-based Platform to Support City-Scale Building Energy Efficiency. In *Urban Computing*, number August, page 9, 2016.

[17] Stephen Evans, Rob Liddiard, and Philip Steadman. 3DStock: A new kind of three-dimensional model of the building stock of England and Wales, for use in energy analysis. *Environment and Planning B: Urban Analytics and City Science*, 44(2):227–255, 2017. ISSN 23998091. doi: 10.1177/0265813516652898.

[18] Christoph F Reinhart and Carlos Cerezo Davila. Urban building energy modeling A review of a nascent field. *Building and Environment*, 97:196–202, feb 2016. ISSN 03601323. doi: 10.1016/j.buildenv.2015.12.001.

[19] Daniel Coakley, Paul Raftery, and Marcus Keane. A review of methods to match building energy simulation models to measured data, 2014. ISSN 13640321.

[20] Hyunwoo Lim and Zhiqiang John Zhai. Review on stochastic modeling methods for building stock energy prediction. *Building Simulation*, 10(5):607–624, 2017. ISSN 19968744. doi: 10.1007/s12273-017-0383-y.

[21] Ralph T Muehleisen and Joshua Bergerson. Bayesian Calibration - What , Why And How. In *International High Performance Buildings Conference*, page 167, 2016. URL `http://docs.lib.purdue.edu/ihpbc/167`.

[22] Nazanin Nasrollahi and Elham Shokri. Daylight illuminance in urban environments for visual comfort and energy performance. *Renewable and Sustainable Energy Reviews*, 66:861–874, 2016. ISSN 1364-0321. doi: 10.1016/j.rser.2016.08.052. URL `http://dx.doi.org/10.1016/j.rser.2016.08.052`.

[23] Raphaela Walger Da Fonseca, Evelise Leite Didoné, and Fernando Oscar Ruttkay Pereira. Using artificial neural networks to predict the impact of daylighting on building final electric energy requirements. *Energy and Buildings*, 61:31–38, 2013. ISSN 03787788. doi: 10.1016/j.enbuild.2013.02.009.

[24] Christina Chatzipoulka. An Image-Based Method to Evaluate Solar and Daylight Potential in Urban Areas An image-based method to evaluate solar and daylight potential in urban areas. (June), 2018. doi: 10.22360/simaud.2018.simaud.035.

[25] C.F. Reinhart, Timur Dogan, J.A. Jakubiec, Tarek Rakha, and Andrew Sang. Umi - an Urban Simulation Environment for Building Energy Use , Daylighting and

Walkability. *Proceedings of BS2013: 13th Conference of International Building Performance Simulation Association*, pages 476–483, 2013.

[26] N. Mohajeri, A. Gudmundsson, T. Kunckler, G. Upadhyay, D. Assouline, J.H Kämpf, and J.L. Scartezzini. A solar-based sustainable urban design: The effects of city-scale street-canyon geometry on solar access in Geneva, Switzerland. *Applied Energy*, 240 (February):173–190, 2019. ISSN 03062619. doi: 10.1016/j.apenergy.2019.02.014.

[27] V. MEYRAND, Georges B. Tabet, and Oussama Kassamani. Lebanon Municipality of Beirut Sustainable energy action plan (SEAP). Technical report, CES-MED, Lebanon, 2012. URL `www.ces-med.eu`.

[28] MoE/UNDP/GEF. Lebanon's Third National Comuunication to the UNFCCC. Technical report, Beirut, Lebanon, 2016. URL `http://climatechange.moe.gov.lb/`.

[29] World Bank. Energy Efficiency Study in Lebanon. Technical Report December, Beirut, Lebanon, 2009. URL `http://climatechange.moe.gov.lb/viewfile.aspx?id=205`.

[30] Farouk Fardoun, Oussama Ibrahim, Rafic Younes, and Hasna Louahlia-Gualous. Electricity of Lebanon: Problems and recommendations. *Energy Procedia*, 19:310–320, 2012. ISSN 18766102. doi: 10.1016/j.egypro.2012.05.211.

[31] Sara Najem. Beirut Solar Map. URL `http://rredc.nrel.gov/solar/old{_}data/nsrdb/1961-1990/redbook/atlas/serve.cgi`.

[32] Loïc Frayssinet, Lucie Merlier, Frédéric Kuznik, Jean Luc Hubert, Maya Milliez, and Jean Jacques Roux. Modeling the heating and cooling energy demand of urban buildings at city scale. *Renewable and Sustainable Energy Reviews*, 81(June):2318–2327, 2018. ISSN 18790690. doi: 10.1016/j.rser.2017.06.040. URL `http://dx.doi.org/10.1016/j.rser.2017.06.040`.

[33] M. Kavgic, A. Mavrogianni, D. Mumovic, A. Summerfield, Z. Stevanovic, and M. Djurovic-Petrovic. A review of bottom-up building stock models for energy consumption in the residential sector. *Building and Environment*, 45(7):1683–1697, 2010. ISSN 03601323. doi: 10.1016/j.buildenv.2010.01.021.

[34] Morten Brøgger and Kim Bjarne Wittchen. Estimating the energy-saving potential in national building stocks A methodology review. *Renewable and Sustainable Energy Reviews*, 82(xxxx):1489–1496, 2018. ISSN 18790690. doi: 10.1016/j.rser.2017.05.239. URL `http://dx.doi.org/10.1016/j.rser.2017.05.239`.

[35] Cheng-Kai Wang. *Urban building energy modeling using a 3D city model and minimizing uncertainty through Bayesian inference - A case study focuses on Amsterdam residential heating demand simulation.* PhD thesis, Delft University of Technology, 2018.

[36] Lukas G. Swan and V. Ismet Ugursal. Modeling of end-use energy consumption in the residential sector: A review of modeling techniques. *Renewable and Sustainable Energy Reviews*, 13(8):1819–1835, 2009. ISSN 13640321. doi: 10.1016/j.rser.2008.09.033.

[37] Aurélie Foucquier, Sylvain Robert, Frédéric Suard, Louis Stéphan, and Arnaud Jay. State of the art in building modelling and energy performances prediction: A review. *Renewable and Sustainable Energy Reviews*, 23:272–288, 2013. ISSN 13640321. doi: 10.1016/j.rser.2013.03.004.

[38] A Al-ghandoor, J O Jaber, I Al-hinti, and I M Mansour. Residential past and future energy consumption : Potential savings and environmental impact. *Renewable and Sustainable Energy Reviews*, 13:1262–1274, 2009. doi: 10.1016/j.rser.2008.09.008.

[39] Deborah Wilson and Joel Swisher. Exploring the gap. Top-down versus bottom-up analyses of the cost of mitigating global warming. *Energy Policy*, 21(3):249–263, 1993. ISSN 03014215. doi: 10.1016/0301-4215(93)90247-D.

[40] V.S.K.V. S K V Harish and Arun Kumar. A review on modeling and simulation of building energy systems. *Renewable and Sustainable Energy Reviews*, 56:1272–1292, 2016. ISSN 13640321. doi: 10.1016/j.rser.2015.12.040.

[41] Hai Xiang Zhao and Frédéric Magoulès. A review on the prediction of building energy consumption. *Renewable and Sustainable Energy Reviews*, 16(6):3586–3592, 2012. ISSN 13640321. doi: 10.1016/j.rser.2012.02.049. URL `http://dx.doi.org/10.1016/j.rser.2012.02.049`.

[42] Moncef Krarti. *Energy audit of buildings systems*, volume 1. Taylor & Francis Group, second edi edition, 2011. ISBN 9788578110796. doi: 10.1017/CBO9781107415324.004.

[43] B. Howard, L. Parshall, J. Thompson, S. Hammer, J. Dickinson, and V. Modi. Spatial distribution of urban building energy consumption by end use. *Energy and Buildings*, 45:141–151, feb 2012. ISSN 03787788. doi: 10.1016/j.enbuild.2011.10.061.

[44] Giuliano Dall'o', Annalisa Galante, and Marco Torri. A methodology for the energy performance classification of residential building stock on an urban scale. *Energy and Buildings*, 48:211–219, 2012. ISSN 03787788. doi: 10.1016/j.enbuild.2012.01.034.

[45] Linda Pedersen. Use of different methodologies for thermal load and energy estimations in buildings including meteorological and sociological input parameters. *Renewable and Sustainable Energy Reviews*, 11(5):998–1007, 2007. ISSN 13640321. doi: 10.1016/j.rser.2005.08.005.

[46] U.S. Department of Energy's (DOE). EnergyPlus V8.4, 2016. URL `https://energyplus.net/`.

[47] University of Wisconsin–Madison. Solar Energy Laboratory. TRNSYS : Transient System Simulation Tool, 1975. URL `http://www.trnsys.com/`.

[48] E. H. Borgstein, R. Lamberts, and J. L M Hensen. Evaluating energy performance in non-domestic buildings: A review. *Energy and Buildings*, 128:734–755, 2016. ISSN 03787788. doi: 10.1016/j.enbuild.2016.07.018.

[49] Merih Aydinalp-koksal and V. Ismet Ugursal. Comparison of neural network, conditional demand analysis, and engineering approaches for modeling end-use energy consumption in the residential sector. *Applied Energy*, 85:271–296, 2008. doi: 10.1016/j.apenergy.2006.09.012.

[50] Mohammad Saad Al-Homoud. Computer-aided building energy analysis techniques. *Building and Environment*, 36(4):421–433, 2001. ISSN 03601323. doi: 10.1016/S0360-1323(00)00026-3.

[51] Luana Filogamo, Giorgia Peri, Gianfranco Rizzo, and Antonino Giaccone. On the classification of large residential buildings stocks by sample typologies for energy

planning purposes. *Applied Energy*, 135:825–835, 2014. ISSN 03062619. doi: 10.1016/j.apenergy.2014.04.002.

[52] Érika Mata, Angela Sasic Kalagasidis, and Filip Johnsson. A modelling strategy for energy, carbon, and cost assessments of building stocks. *Energy and Buildings*, 56: 100–108, 2013. ISSN 03787788. doi: 10.1016/j.enbuild.2012.09.037.

[53] Ilaria Ballarini, Stefano Paolo Corgnati, and Vincenzo Corrado. Use of reference buildings to assess the energy saving potentials of the residential building stock: The experience of TABULA project. *Energy Policy*, 68:273–284, 2014. ISSN 03014215. doi: 10.1016/j.enpol.2014.01.027.

[54] I Ballarini, S P Corgnati, and V Corrado. Improving energy modeling of large building stock through the development of archetype buildings. 2011.

[55] Carlos Cerezo Davila, Christoph Reinhart, and Jamie Bemis. Modeling Boston: A workflow for the generation of complete urban building energy demand models from existing urban geospatial datasets. *Energy*, 2016. ISSN 03605442. doi: 10.1016/j.energy.2016.10.057.

[56] Adesoji Albert Famuyibo, Aidan Duffy, and Paul Strachan. Developing archetypes for domestic dwellings An Irish case study. *Energy & Buildings*, 50:150–157, 2012. ISSN 0378-7788. doi: 10.1016/j.enbuild.2012.03.033.

[57] Shady Attia, Arnaud Evrard, and Elisabeth Gratia. Development of benchmark models for the Egyptian residential buildings sector. *Applied Energy*, 94(2012):270–284, 2012. ISSN 03062619. doi: 10.1016/j.apenergy.2012.01.065.

[58] Claudia Sousa Monteiro, André Pina, Carlos Cerezo, Christoph Reinhart, Paulo Ferrão, Claudia Sousa Monteiroa, André Pinaa, Carlos Cerezo, Christoph Reinhart, and Paulo Ferrãoa. The Use of Multi-detail Building Archetypes in Urban Energy Modelling. *Energy Procedia*, 111(September 2016):817–825, 2017. ISSN 18766102. doi: 10.1016/j.egypro.2017.03.244. URL `http://linkinghub.elsevier.com/retrieve/pii/S1876610217302771`.

[59] Anil Parekh. Development of Archetypes of Building Characteristics Libraries for Simplified Energy Use Evaluation of Houses. In *Ninth International IBPSA Conference*, pages 921–928, 2005.

[60] Shem Heiple and David J. Sailor. Using building energy simulation and geospatial modeling techniques to determine high resolution building sector energy consumption profiles. *Energy and Buildings*, 40(8):1426–1436, 2008. ISSN 03787788. doi: 10.1016/j.enbuild.2008.01.005.

[61] Julia Sokol, Carlos Cerezo Davila, and Christoph F. Reinhart. Validation of a Bayesian-based method for defining residential archetypes in urban building energy models. *Energy and Buildings*, 134:11–24, 2017. ISSN 03787788. doi: 10.1016/j.enbuild.2016.10.050.

[62] Nelson Fumo. A review on the basics of building energy estimation, 2014. ISSN 13640321. URL `http://dx.doi.org/10.1016/j.rser.2013.11.040`.

[63] Jimeno A. Fonseca and Arno Schlueter. Integrated model for characterization of spatiotemporal building energy consumption patterns in neighborhoods and city districts. *Applied Energy*, 142:247–265, 2015. ISSN 03062619. doi: 10.1016/j.apenergy.2014.12.068. URL `http://dx.doi.org/10.1016/j.apenergy.2014.12.068`.

[64] ESRI. ArcGIS V10.3, 2014. URL `https://www.arcgis.com/features/index.html`.

[65] Robert McNeel & Associates. Rhinoceros 3D V5, 2015. URL `https://www.rhino3d.com/6`.

[66] Carlos Cerezo, Julia Sokol, Christoph Reinhart, and Adil Al-mumin. Three Methods for Characterizing Building Archetypes in Urban Energy Simulation A Case Study in Kuwait City. *14th International Conference of the International Building Performance Simulation Association*, pages 2873–2880, 2015.

[67] Ian Richardson, Murray Thomson, and David Infield. A high-resolution domestic building occupancy model for energy demand simulations. 40:1560–1566, 2008. doi: 10.1016/j.enbuild.2008.02.006.

[68] Miaomiao He, Timothy Lee, Simon Taylor, Steven K Firth, and Kevin Lomas. Coupling a Stochastic Occupancy Model to EnergyPlus to Predict Hourly Thermal Demand of a Neighbourhood. pages 2101–2108, 2015.

[69] Ghina Annan, Nesreen Ghaddar, and Kamel Ghali. Natural ventilation in Beirut residential buildings for extended comfort hours. *International Journal of Sustainable Energy*, 35(10):996–1013, 2016. ISSN 1478646X. doi: 10.1080/14786451.2014.972403.

[70] Z Ghaddar, K Ghali, and N Ghaddar. The Impact of the Air-Conditioning Systems on the Urban Microclimate of Beirut City Key words. 1(14):882–885, 2017.

[71] Sorina Mortada. The First Energy Indicators Report of the Republic of Lebanon. Technical report, MEW; LCEC, 2018.

[72] Sven Schimschar and Joseph Al Assad. A Roadmap for developing Energy Indicators for Buildings in Lebanon. Technical Report July, MED-ENEC, Energy Efficiency in the Construction Sector in the Mediterranean: Cairo, 2013.

[73] Agnès Bégué, Damien Arvor, Beatriz Bellon, Julie Betbeder, Diego de Abelleyra, Rodrigo P.D. Ferraz, Valentine Lebourgeois, Camille Lelong, Margareth Simões, and Santiago R. Verón. Remote sensing and cropping practices: A review. *Remote Sensing*, 10(1):1–32, 2018. ISSN 20724292. doi: 10.3390/rs10010099.

[74] Amin Shaban, Ghaleb Faour, Mohamad Khawlie, and Chadi Abdallah. Remote sensing application to estimate the volume of water in the form of snow on Mount Lebanon. *Hydrological Sciences Journal*, 49(4):643–653, 2004. ISSN 02626667. doi: 10.1623/hysj.49.4.643.54432.

[75] Graeme L. Stephens and Christian D. Kummerow. The Remote Sensing of Clouds and Precipitation from Space: A Review. *Journal of the Atmospheric Sciences*, 64 (11):3742–3765, 2007. ISSN 0022-4928. doi: 10.1175/2006JAS2375.1. URL `http://journals.ametsoc.org/doi/abs/10.1175/2006JAS2375.1`.

[76] Jan de Leeuw, Yola Georgiadou, Norman Kerle, Alfred de Gier, Yoshio Inoue, Jelle Ferwerda, Maarten Smies, and Davaa Narantuya. The function of remote sensing in support of environmental policy. *Remote Sensing*, 2(7):1731–1750, 2010. ISSN 20724292. doi: 10.3390/rs2071731.

[77] Lucas Landier. *Modélisation 3D du Bilan Radiatif des Milieux Urbains par Inversion d ' Images Satellites en Cartes de Réflectance et de Température des Matériaux Urbains.* PhD thesis, Université Toulouse 3 Paul Sabatier (UT3 Paul Sabatier), 2018. URL `https://tel.archives-ouvertes.fr/tel-01907888`.

[78] Stamatios Aggelos N. Alexandropoulos, Sotiris B. Kotsiantis, and Michael N. Vrahatis. *Data preprocessing in predictive data mining*, volume 34. 2019. ISBN 0269888918. doi: 10.1017/S026988891800036X.

[79] Hawkins D. *Identification of Outliers*. 1980.

[80] S.M.A. Bettencourt. Outlier Detection: Applications And Techniques. *IJCSI International Journal of Computer Science Issues*, 9(1):307–323, 2012.

[81] Hans-Peter Kriegel, Peer Kroger, and Arthur Zimek. Outlier Detection Techniques. *Tutorial at KDD*, 10, 2010.

[82] Jinghui Chen, Saket Sathe, Charu Aggarwal, and Deepak Turaga. Outlier Detection with Autoencoder Ensembles. In *Proceedings of the 2017 SIAM International Conference on Data Mining*, pages 90–98, 2017. doi: 10.1137/1.9781611974973.11.

[83] Gautam Bhattacharya, Koushik Ghosh, and Ananda S. Chowdhury. Outlier detection using neighborhood rank difference. *Pattern Recognition Letters*, 60-61:24–31, 2015. ISSN 01678655. doi: 10.1016/j.patrec.2015.04.004. URL `http://dx.doi.org/10.1016/j.patrec.2015.04.004`.

[84] Ifigeneia Theodoridou, Agis M Papadopoulos, and Manfred Hegger. A typological classification of the Greek residential building stock. *Energy & Buildings*, 43(10):2779–2787, 2011. ISSN 0378-7788. doi: 10.1016/j.enbuild.2011.06.036.

[85] Georges Joseph Arbid. *Practicing modernism in Beirut architecture in Lebanon 1946-1970*. PhD thesis, Cambridge, Massachusetts : Harvard University, 2002.

[86] UNDP/GEF and MPWT/DGU. Groundwork for a Technical Guide for the application of the Thermal Standard for Buildings in Lebanon. Technical report, UNDP/GEF and MPWT/DGU, Beirut, Lebanon, 2005.

[87] Timur Dogan. Archsim - energy modeling tools for grasshopper, 2016. URL www.archsim.com.

[88] Ralf Plag. Ubakus - U-value calculator, 2009. URL www.ubakus.de.

[89] ANSI/ASHRAE/IES. Standard 90.1-2010-Energy Standard for Buildings Except Low-Rise Residential Buildings. Technical report, ASHRAE, Atlanta:ASHRAE; 2012, 2010.

[90] Jean Philippe Gastellu-Etchegorry, Tiangang Yin, Nicolas Lauret, Thomas Cajgfinger, Tristan Gregoire, Eloi Grau, Jean Baptiste Feret, Maïlys Lopes, Jordan Guilleux, Gérard Dedieu, Zbynek Malenovsk, Bruce Douglas Cook, Douglas Morton, Jeremy Rubio, Sylvie Durrieu, Gregory Cazanave, Emmanuel Martin, and Thomas Ristorcelli. Discrete anisotropic radiative transfer (DART 5) for modeling airborne and satellite spectroradiometer and LIDAR acquisitions of natural and urban landscapes. *Remote Sensing*, 7(2):1667–1701, 2015. ISSN 20724292. doi: 10.3390/rs70201667.

[91] J. P. Gastellu-Etchegorry. 3D modeling of satellite spectral images, radiation budget and energy budget of urban landscapes. *Meteorology and Atmospheric Physics*, 102 (3-4):187–207, 2008. ISSN 01777971. doi: 10.1007/s00703-008-0344-1.

[92] Eloi Grau and Jean Philippe Gastellu-Etchegorry. Radiative transfer modeling in the Earth-Atmosphere system with DART model. *Remote Sensing of Environment*, 139: 149–170, 2013. ISSN 00344257. doi: 10.1016/j.rse.2013.07.019. URL http://dx.doi.org/10.1016/j.rse.2013.07.019.

[93] Rod Burgess. The compact city debate: A Global Perspective. In Mike Jenks and Rod Burgess, editors, *Compact Cities: Sustainable Urban Forms for Developing Countries*, pages 9–24. SPON PRESS, London and New York.

[94] Reid Ewing, Susan Handy, Ross C. Brownson, Emily Winston, and Otto Clemente. Identifying and Measuring Urban Design Qualities Related to Walkability. *Journal of Physical Activity and Health*, 3(s1):S223–S240, 2016. ISSN 1543-3080. doi: 10.1123/jpah.3.s1.s223.

[95] Timur Dogan and Maksis Knutins. CitySeek: Towards Urban Daylight Models Based on GIS Data and Semi-Automated Image Processing. In *SimAUD*, number June, Delft, the Netherlands, 2018. doi: 10.22360/simaud.2018.simaud.036.

[96] Zhong-Hu Jiao, Huazhong Ren, Xihan Mu, Jing Zhao, Tianxing Wang, and Jiaji Dong. Evaluation of Four Sky View Factor Algorithms using Digital Surface and Elevation Model Data. *Earth and Space Science*, 6:222–237, 2019. ISSN 23335084. doi: 10.1029/2018ea000475.

[97] Ariane Middel, Jonas Lukasczyk, Ross Maciejewski, Matthias Demuzere, and Matthias Roth. Sky View Factor footprints for urban climate modeling. *Urban Climate*, 25 (May):120–134, 2018. ISSN 22120955. doi: 10.1016/j.uclim.2018.05.004.

[98] Žiga Kokalj, Klemen Zakšek, and Krištof Oštir. Application of sky-view factor for the visualisation of historic landscape features in lidar-derived relief models. *Antiquity*, 85 (327):263–273, 2011. ISSN 0003598X. doi: 10.1017/S0003598X00067594.

[99] Jérémy Bernard, Erwan Bocher, Gwendall Petit, and Sylvain Palominos. Sky View Factor Calculation in Urban Context: Computational Performance and Accuracy Analysis of Two Open and Free GIS Tools. *Climate*, 6(3):60, 2018. ISSN 2225-1154. doi: 10.3390/cli6030060.

[100] Houda Belgacem, Thomas Leduc, and Marjorie Musy. Mesure et représentation cartographique de l'impression de confinement d'un piéton immergé dans la ville. In *SHS Web of Conferences*, volume 47, page 01011, 2018. doi: 10.1051/shsconf/20184701011.

[101] Michele Morganti, O Le Corre, I Andri Agnese, A Pina, P Ferrão, and J Coch. Effects of urban compactness on the building energy performance in Mediterranean climate. In *Energy Procedia*, volume 122, pages 499–504. Elsevier B.V., 2017. doi: 10.1016/j.egypro.2017.07.303.

[102] Timur Dogan and Maksis Knutins. CitySeek: Towards Urban Daylight Models Based on GIS Data and Semi-Automated Image Processing. (June), 2018. doi: 10.22360/simaud.2018.simaud.036.

[103] Francesco De Luca, Andrei Nejur, and Timur Dogan. Facade-Floor-Cluster . Methodology for Determining Optimal Building Clusters for Solar Access and Floor Plan Layout in Urban Environments. Number June, 2018. doi: 10.13140/RG.2.2.34765.13287.

[104] J Strømann-andersen and P A Sattrup. The urban canyon and building energy use : Urban density versus daylight and passive solar gains. 43:2011–2020, 2011. doi: 10.1016/j.enbuild.2011.04.007.

[105] Sara Najem. Streets and buildings' orientation entropies and the city's rooftops' solar potentials. *European Physical Journal Plus*, 134(2), 2019. ISSN 21905444. doi: 10.1140/epjp/i2019-12494-4.

[106] Haniyeh Sanaieian, Martin Tenpierik, Kees Van Den Linden, Fatemeh Mehdizadeh Seraj, and Seyed Majid Mofidi Shemrani. Review of the impact of urban block form on thermal performance, solar access and ventilation. *Renewable and Sustainable Energy Reviews*, 38:551–560, 2014. ISSN 13640321. doi: 10.1016/j.rser.2014.06.007.

[107] Gabriele Lobaccaro, Salvatore Carlucci, Silvia Croce, Rossana Paparella, and Luca Finocchiaro. Boosting solar accessibility and potential of urban districts in the Nordic climate : A case study in Trondheim. *Solar Energy*, 149:347–369, 2017. ISSN 0038-092X. doi: 10.1016/j.solener.2017.04.015. URL `http://dx.doi.org/10.1016/j.solener.2017.04.015`.

[108] David Levinson. Network structure and city size. *PLoS ONE*, 7(1), 2012. ISSN 19326203. doi: 10.1371/journal.pone.0029721.

[109] Geoff Boeing. The Morphology and Circuity of Walkable and Drivable Street Networks. *The Mathematics of Urban Morphology; D'Acci, L., Ed.; Birkhäuser: Basel, Switzerland*, 2019. doi: 10.1007/978-3-030-12381-9.

[110] J. E. Saunders, J. R. Jarvis, and C. M. Wathes. Calculating luminous flux and lighting levels for domesticated mammals and birds. *Animal*, 2(6):921–932, 2008. ISSN 17517311. doi: 10.1017/S1751731108002012.

[111] Hsien-Che Lee. *Introduction to Color Imaging Science*. Cambridge University Press, Cambridge, 2005. ISBN 9780511614392. doi: 10.1017/CBO9780511614392. URL `http://ebooks.cambridge.org/ref/id/CBO9780511614392`.

[112] Dapeng Li, Gang Liu, and Shengming Liao. Solar potential in urban residential buildings. *Solar Energy*, 111:225–235, 2015. ISSN 0038092X. doi: 10.1016/j.solener.2014.10.045.

[113] US Department of Energy. EnergyPlus Engineering Reference: The Reference to EnergyPlus Calculations. *US Department of Energy*, pages 1–847, 2010. ISSN 03787788. doi: citeulike-article-id:10579266. URL `http://scholar.google.com/scholar?hl=en{&}btnG=Search{&}q=intitle:EnergyPlus+Engineering+Reference,+The+Reference+to+EnergyPlus+Calculations{#}1`.

[114] D M Wiberg. *Theory and Problems of State Space and Linear Systems*. 1971.

[115] Xiang Qian Li, Youming Chen, J. D. Spitler, and D. Fisher. Applicability of calculation methods for conduction transfer function of building constructions. *International Journal of Thermal Sciences*, 48(7):1441–1451, 2009. ISSN 12900729. doi: 10.1016/j.ijthermalsci.2008.11.006. URL `http://dx.doi.org/10.1016/j.ijthermalsci.2008.11.006`.

[116] Solar Radiation Distribution. URL `http://designbuilder.co.in/programhelp/solar{_}radiation{_}distribution.htm`.

[117] Aram Yeretzian. Beirut a sustainable dimension of the city and its buildings. *Al Mohandes*, mar 2010.

[118] Da Yan, William O'Brien, Tianzhen Hong, Xiaohang Feng, H. Burak Gunay, Farhang Tahmasebi, and Ardeshir Mahdavi. Occupant behavior modeling for building performance simulation: Current state and future challenges. *Energy and Buildings*, 107:264–278, 2015. ISSN 03787788. doi: 10.1016/j.enbuild.2015.08.032.

[119] Urs Wilke, Frédéric Haldi, Jean Louis Scartezzini, and Darren Robinson. A bottom-up stochastic model to predict building occupants' time-dependent activities. *Building and Environment*, 60:254–264, 2013. ISSN 03601323. doi: 10.1016/j.buildenv.2012.10.021.

[120] F Haldi and D Robinson. The impact of occupants' behaviour on building energy demand. *Journal of Building Performance Simulation*, 4(4):323–338, 2011. ISSN 1940-1493. doi: 10.1080/19401493.2011.558213.

[121] Neda Mohammadi and John E Taylor. Urban Energy Flux : Human Mobility as a Predictor for Spatial Changes. *arXiv*, 2016.

[122] S Yathreb. Analysis of a Residential Building Energy Consumption as Base Model in Tripoli, Lebanon. *Energy Prod. & Mgmt*, 1(4):359–370, 2016. ISSN 19961073. doi: 10.3390/en4030475.

[123] Marta Braulio-gonzalo, María Dolores Bovea, María José Ruá, and Pablo Juan. A Methodology for Predicting the Energy Performance and Indoor Thermal Comfort of Residential Stocks on the Neighbourhood and City Scales. A Case Study in Spain. *Journal of Cleaner Production*, pages 646–665, 2016. ISSN 0959-6526. doi: 10.1016/J.JCLEPRO.2016.08.059.

[124] Agnese Salvati, Paolo Monti, Helena Coch, and Carlo Cecere. Climatic performance of urban textures : Analysis tools for a Mediterranean urban context. *Energy & Buildings*, 185:162–179, 2019. ISSN 0378-7788. doi: 10.1016/j.enbuild.2018.12.024.

[125] Noushig Kaloustian and Youssef Diab. Effects of urbanization on the urban heat island in Beirut. *Urban Climate*, 14:154–165, 2015. ISSN 22120955. doi: 10.1016/j.uclim.2015.06.004.

[126] K. H. Solangi, M. R. Islam, R. Saidur, N. A. Rahim, and H. Fayaz. A review on global solar energy policy. *Renewable and Sustainable Energy Reviews*, 15(4):2149–2163, 2011. ISSN 13640321. doi: 10.1016/j.rser.2011.01.007. URL `http://dx.doi.org/10.1016/j.rser.2011.01.007`.

[127] Eraldo Banovac, Marinko Stojkov, and Dražan Kozak. Designing a global energy policy model. *Proceedings of the Institution of Civil Engineers - Energy*, 170(1):2–11, 2016. ISSN 1751-4223. doi: 10.1680/jener.16.00005.

A. Appendix: Energy Policy brief

AUB POLICY INSTITUTE

CNRS
المجلس الوطني للبحوث العلمية

POLICY BRIEF #3/2019
March 2019

BEIRUT AS A SMART CITY: REDEFINING URBAN ENERGY

Alaa Krayem
Lebanese University, Beirut, Lebanon and Université de Toulouse, Toulouse, France

Ahmad Al Bitar
Centre d'Etudes Spatiales de la Biosphère, Université de Toulouse, CNES/CNRS/IRD/UPS, Toulouse, France

Ghaleb Faour
National Center for Remote Sensing, National Council for Scientific Research, CNRS-L

Ali Ahmad
Issam Fares Institute for Public Policy and International Affairs, American University of Beirut

Sara Najem
National Center for Remote Sensing, National Council for Scientific Research, CNRS-L

Summary

Global efforts are exerted to improve energy supply-demand balance in urban environments which are characterized by higher population density and levels of energy consumption. Beirut, Lebanon's capital, is no exception in facing such urban challenges, which are compounded by the regular power outages. As such, developing an urban scale energy model for energy management is essential to achieve this goal. This policy brief presents a model developed for the Bachoura area to determine its buildings energy performance. The results are integrated to report the hourly energy use profile spatially distributed over the city, which leads to identifying hotspots and peak hours of energy demands. The model can be used to estimate the potential savings from rooftop solar energy production and recommend targeted energy-use policies to alleviate peaks and ensure an optimal and efficient distribution of resources.

MAIN RECOMMENDATIONS

- Predicting spatial and temporal peak-loads could ultimately help in informing smart rationing of the electricity by the power utility company, EDL when the grid is strained. Additionally, it could match local demand to supply from solar energy through smart distribution and optimization of demand management
- The developed model could be utilized to test various policy instruments that promote energy savings such as the implementation of building efficiency codes, installation of water heaters, etc.

Introduction

The expansion of cities worldwide is accompanied by socio-economic problems that range from challenges in providing services to compounding the impact of climate change. One major issue cities face is soaring demand for energy. Consequently, designing energy efficient cities will go a long way in reducing demand for power while also reducing emissions and air pollution. As such, energy modeling has been adopted to simulate buildings' energy consumption at early design stage, evaluate the efficacy of various design options, and optimize the overall performance of building systems in Beirut.

When extending the scope of the energy performance simulation to the urban scale, two main categories of urban energy models can be found: top-down models and bottom-up models. Top-down models are mainly used to explore the interrelations between the energy sector and variables like socio-economic indicators, energy price, and climate. However, they lack technical details and hence fail to study the impacts of new technologies and intervention. Bottom-up models, on the other hand, estimate individual end-uses then aggregate results to get the urban energy consumption.

They are suitable for improvement and technological intervention studies. They can be further subdivided into statistical and engineering models. The former relies on a large amount of historical dataset to estimate energy consumption at the metered data scale. Engineering models apply thermodynamic and heat transfer equations at the building level, leading to high accurate results, and offer the maximum flexibility to test end-use energy conservation measures.

The work presented in this policy brief has been extended from the individual building scale to the urban scale, allowing for the assessment of building to building interactions as well as of buildings to other urban forms interactions.

Methods

Urban Building Energy Model UBEM, which has been utilized in this study, combines the bottom-up statistical and engineering models and communicates results with GIS platform for energy maps generation, used for results analysis and comparison with measured data or surveys to help designers and policy makers.

Data collection and processing

The conducted analysis utilized data collected from a range of sources to create the model's dataset, namely:

- Hourly weather data from Beirut International Airport.
- Topographic map to create the digital elevation profile.
- GIS data incorporating buildings' footprints, area, number of floors, year of construction, function.

Cleaning the data was a crucial step to ensure model's consistency and accuracy. Buildings with the following drawbacks were removed from the data set:

- Mismatch of buildings' footprints with their corresponding position in the satellite image.
- Missing entries such as the number of floors, function or EDL electricity consumption.

Buildings' segmentation: Beirut buildings were grouped based on two parameters, the building function and the year of construction based on a historical architectural study of the buildings. Building's function helps in setting a building's occupancy patterns and determining internal heat loads, while its year of construction informs about construction materials and methods.

For the specific case of Beirut, five distinguished construction periods were identified based on Georges Arbid's study: 1900 to 1923, 1924 to 1940, 1941 to 1960, 1961 to 1990, and after 1991. Regarding the function, the buildings were grouped into six classes (residential, mixed, hospitals, schools and governmental buildings). In total, 30 archetypes were generated.

Buildings' Characterization: Thermal properties were obtained from the Technical Guide for the application of the Thermal Standard for Buildings in Lebanon published in 2005, the simulation software's default library and online libraries.

A priori, non-geometrical properties such as the occupancy and use schedules were set by referring to The American Society of Heating, Refrigerating and Air-Conditioning Engineers (ASHRAE) standards and previous studies. The apriori values were then modified to take into consideration the Beirut context (working hours, occupancy, and heating/cooling systems)

Thermal model generation and calibration

Each building was represented by a 3D thermal model, divided into floors, with windows on facades and balconies if residential.

When simulating the energy consumption of each building, discrepancies between the predicted model outputs and the actual metered data from EDL were found. They can be attributed to three categorical errors as follows:

- Systematic errors resulted from the daily 3 hours of blackouts not accounted for during simulations, and from the constraints on indoor temperature and humidity that need to be met despite them being behaviorally unrealistic, such as keeping indoor temperature at 21°C in winter.
- Heating, Ventilation, and Air Conditioning (HVAC) systems operating when they are not supposed to, for example covering all floor's area and operating even under 20°C for cooling.
- Variation of equipment use and occupancy profiles.

A Case Study: The City of Beirut

Beirut city, the capital of Lebanon, holds with its suburbs 50 percent of the urban population. It consumes 12 percent of the total national energy produced while it only covers 0.2 percent of the country's total area. Its building sector accounts for almost all of its electricity consumption. The city and its residents suffer from a minimum of 3 hours of blackouts per day. These key indicators demonstrate that Beirut is an energy-starved city.

In 2015, during the 2015 United Nations Climate Change Conference (COP21), Lebanon pledged to reduce its emissions by 30 percent by 2030 within a conditional commitment. Four years later, the country is still facing a significant challenge to manage its energy sector and integrate renewable energy. Therefore, developing an urban scale energy model could prove to be a very useful tool to assess Beirut's energy resources and provide insights for the management of its energy supply. The developed model could serve as a decision support system by estimating energy consumption patterns and identifying grid peak demands with a spatiotemporal distribution. The latter, integrated with the potential solar production findings, will offer a great potential in estimating the savings and recommending targeted energy-use policies to alleviate peaks and ensure an efficient and optimal resources distribution.

Another feature of the energy model for Beirut is its capability to project energy consumption under normal conditions. Currently, estimates of demand do not account for the suppressed amount of electricity, since during outages, occupants modify their behaviors and alter their energy consumption patterns and preferences.

Therefore, one of the major advantages of the developed model is to provide projected estimates for demand, which are currently underestimated.

Results

Data for buildings in the Bachoura area was obtained. After the cleaning process and removal of outliers (buildings with abnormal EDL electricity consumption), 1830 residential and mixed buildings were represented by thermal models. Most of these buildings were built between 1940 and 1990. The difference between the metered data and the predicted data was of 203534 MWh, representing an overestimation of 200 percent. After eliminating the impacts of the systematic errors and the HVAC systems related errors, we found that the remaining disparity was independent of the buildings position and archetype.

More than 70 percent of mixed buildings' floors are residential. Therefore, the majority of the floors in the Bachoura area are residential, sharing similar occupancy schedules.

Accordingly, we could think about energy use and occupancy profiles as the main reason behind the disparities and mismatch between actual and predicted consumption. More specifically, maximum occupancy corresponds to buildings whose electricity consumption is the highest compared to their counterparts with the same number of floors. Therefore, the ratio of the latter consumptions is an indicator of the occupancy level and should explain the aforementioned mismatch. Results showed a strong correlation between this indicator and the ratio of the model's predictions to the actual consumptions, which validates our hypothesis.

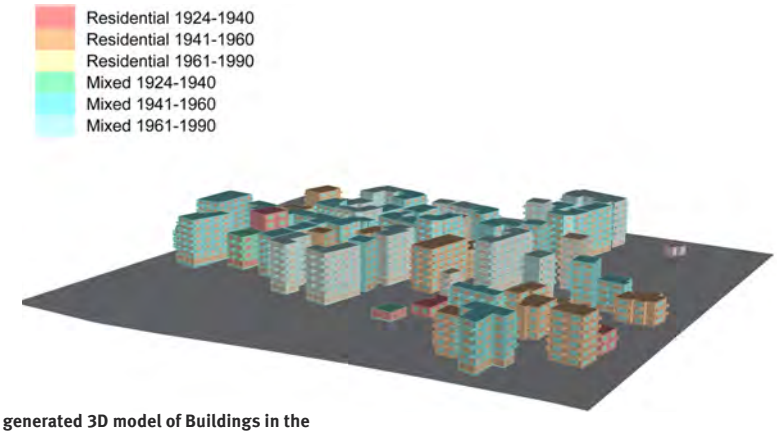

Figure 1: Sample of the generated 3D model of Buildings in the Bachoura area, Beirut, Lebanon

"The developed model could serve as a decision support system by estimating energy consumption patterns and identifying grid peak demands"

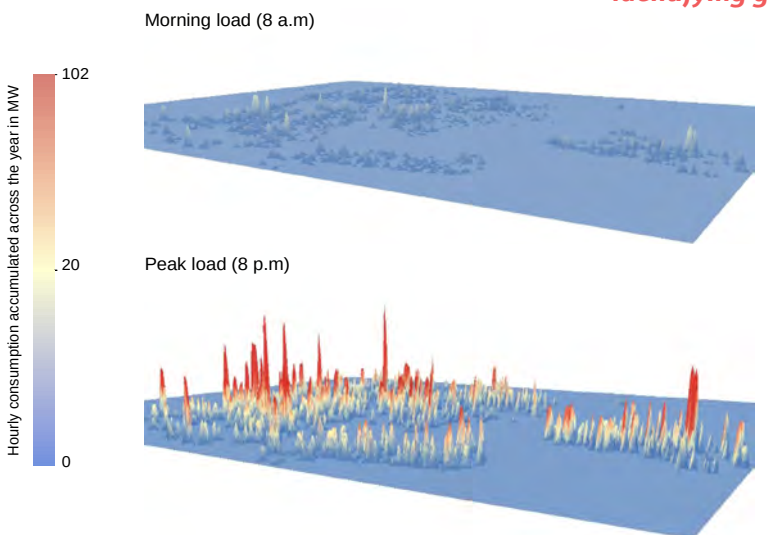

Figure 2: Hourly electricity consumption accumulated across the year during the morning (at the top) and at peak time (at the bottom) for the buildings in the Bachoura area

In terms of load profiles, the model could replicate the overall bimonthly electricity consumption of the buildings. March and April are the least consumption-intensive months while July and August are the highest. The equipment and hot water in residential buildings shared around a third of the total annual electricity consumption, while cooling's share has been estimated to be around 20 percent. Mixed buildings, on the other hand, had 39 percent of their electricity consumption for appliances, followed by 31 percent for cooling.

The electricity consumption results also showed similar spatial clustering as the metered data from EDL with the strongest correlation at 40 meters, i.e. the energy consumption of two buildings is most similar when they are 40 meters apart. Hence, the energy model can be employed to relate the observations of electricity consumption at one location to those at other locations.

Model Applicability

The model multi-scalability is recognized spatially when ranging from building to the city level, and temporally when ranging from hourly to yearly resolution. This allows for spatiotemporal energy patterns analysis to allocate hot spots and peak times of energy demands, as shown in Figure 2. Therefore, energy measures can be optimized to specified buildings with high energy demands. Figure 2 shows peak consumptions across the study area in residential and mixed buildings constructed between 1941 and 1990.

Acknowledgement

We acknowledge the Lebanese University's support through which we were granted access to Microsoft Azure cloud computing.

The Energy Policy and Security Program

The Energy Policy and Security Program at the Issam Fares Institute for Public Policy and International Affairs at AUB was launched in 2016 as a Middle East-based, interdisciplinary platform to examine, inform and impact energy and security policies, regionally and globally. The Program closely monitors the challenges and opportunities of the shift towards alternative energy sources with focus on nuclear power and the Middle East. The Program has been established with a seed grant support from the John D. and Catherine T. MacArthur Foundation to investigate the prospects of nuclear power in the Middle East and its potential to promote regional cooperation as a way to address the security concerns associated with the spread of nuclear power.

Issam Fares Institute for Public Policy and International Affairs at the American University of Beirut

The Issam Fares Institute for Public Policy and International Affairs at the American University of Beirut (AUB Policy Institute) is an independent, research-based, policy-oriented institute. Inaugurated in 2006, the Institute aims to harness, develop, and initiate policy-relevant research in the Arab region.

We are committed to expanding and deepening policy-relevant knowledge production in and about the Arab region; and to creating a space for the interdisciplinary exchange of ideas among researchers, civil society and policy-makers.

We thank Prof. Haitham Zaraket for his assistance all throughout, Prof. Jocelyne Gerard for sharing the surveyed data of Beirut, and the technical team at the National Center for Remote sensing.

Special thanks to Prof. Aram Yeretzian for his major assistance in archetype generation.

This work is part of Alaa Krayem's PhD thesis funded by the CNRS-L.

References

ANSI/ASHRAE/IES, 2010. Standard 90.1-2010-Energy Standard for Buildings Except Low-Rise Residential Buildings, Atlanta:ASHRAE.

Arbid, G.J., 2002. Practicing modernism in Beirut architecture in Lebanon 1946-1970. Cambridge, Massachusetts : Harvard University.

Cerezo Davila, C., Reinhart, C.F. & Bemis, J.L., 2016. Modeling Boston: A workflow for the efficient generation and maintenance of urban building energy models from existing geospatial datasets. Energy, 117, pp.237–250. Available at: http://dx.doi.org/10.1016/j.energy.2016.10.057.

Kavgic, M. et al., 2010. A review of bottom-up building stock models for energy consumption in the residential sector. Building and Environment, 45(7), pp.1683–1697. Available at: http://dx.doi.org/10.1016/j.buildenv.2010.01.021.

Meyrand, V. et al. , 2012. Lebanon Municipality of Beirut Sustainable energy action plan (SEAP), Lebanon. Available at: www.ces-med.eu.

Schimschar, S. & Al Assad, J., 2013. A Roadmap for developing Energy Indicators for Buildings in Lebanon, Energy Efficiency in the Construction Sector in the Mediterranean: Cairo.

Swan, L.G. & Ugursal, V.I., 2009. Modeling of end-use energy consumption in the residential sector: A review of modeling techniques. Renewable and Sustainable Energy Reviews, 13(8), pp.1819–1835.

UNDP/GEF & MPWT/DGU, 2005. Groundwork for a Technical Guide for the application of the Thermal Standard for Buildings in Lebanon, Beirut, Lebanon.

United Nations, Department of Economic and Social Affairs & Population Division, 2016. The World's Cities in 2016 – Data Booklet (ST/ESA/ SER.A/392), Available at: www.unpopulation.org.

Issam Fares Institute for Public Policy and International Affairs (AUB Policy Institute)American University of Beirut P.O.Box 11-0236
Riad El-Solh / Beirut 1107 2020
Lebanon

Issam Fares Institute Building
AUB
961-1-350000 ext. 4150
+961-1-737627
ifi.comms@aub.edu.lb
www.aub.edu.lb/ifi
aub.ifi
@ifi_aub

B. Appendix: French Summary (30 pages)

Révéler l'utilisation énergétique spatio-temporelle d'une ville côtière méditerranéenne: le cas de Beyrouth

1 Introduction

En 2016, 54,5% de la population mondiale vivait en zone urbaine. D'ici 2030, les villes devraient abrite 60% de la population mondiale [1]. Les zones urbaines connaissent une croissance sans précédente raison de l'exode rural dû à des facteurs socio-économiques tels que la recherche de meilleures opportunités d'emploi ou niveaux d'enseignement supérieur. En outre, le développement de l'économie ainsi que l'industrialisation concentrée dans certaines régions au détriment d'autres, avec migration de pays pauvres souffrant de problèmes économiques ou asile de citoyens s'échappant des guerres et des zones de crise politique sont tous des facteurs contribuant à l'augmentation de la population urbaine. L'urbanisation a le potentiel de rendre les villes plus prospères et des pays plus développés, en créant de la richesse et des emplois et en stimulant le progrès humain. Cependant, de nombreuses villes du monde souffrent de problèmes persistants: l'augmentation du nombre de résidents dans les taudis et les quartiers informels, la difficulté d'approvisionnent en services urbains, le changement climatique, l'exclusion et la montée des inégalités et de l'insécurité durant les migrations internationales [2]. Le réchauffement urbain est l'un des défis climatiques en milieu urbain, mesuré dans de nombreuses villes du monde en plus des émissions des gaz à effet de serre (GES) [3]. L'un des facteurs de l'augmentation des températures urbaines est la prédominance du caractère artificiel des villes aux dépenses des fractions vertes naturelles qui s'y trouvent. Un autre aspect de l'urbanisation est le changement structurel économique du pays. La concentration des activités économiques dans les villes

amène la main-d'œuvre à passer du secteur agricole aux secteurs industriels ou de services de la ville, phénomène bien connu comme tertiarisation. Ce transfert qui accompagne l'exode rural contribue indirectement à l'augmentation de la consommation d'énergie. Tout d'abord, en raison du manque de main-d'œuvre, les produits agricoles doivent être mécanisés et transportés des zones de production vers les villes. Deuxièmement, les besoins en services de transport augmentent, entraînant une augmentation de la demande des combustibles fossiles et donc de ses impacts sur le climat urbain. Dernier point mais non le moindre, le développement économique des villes affecte les comportements et les modes de vie des habitants qui ont tendance à poursuivre les produits et services commerciaux, par exemple appareils électriques et accessoires, augmentant ainsi la consommation d'énergie [4]. La ville étant un grand consommateur d'énergie et contributeur aux émissions des GES, une compréhension pertinente de son métabolisme est essentielle au développement des stratégies d'efficacité énergétique [5]. Afin d'assurer l'optimisation et la priorisation des mesures de conservation d'énergie à appliquer, une prise de décision programmatique ou alors la gestion de l'énergie est nécessaire. Elle consiste en la planification, la mise en œuvre et le suivi de l'approvisionnement en énergie, sa distribution et son utilisation de manière efficace et efficiente pour réduire ses pertes et sa consommation. En outre, elle étudie les ressources alternatives et environnementales, l'organisation technique, le rapport coût-efficacité et changement de comportement pour améliorer la qualité de l'énergie, sa disponibilité et ses impacts sur l'environnement et la nature [6]. Cependant, comprendre comment le système énergétique d'une ville évolue dans le temps et dans l'espace sous ces interventions est cruciale pour soutenir le processus de prise de décision. Le secteur des bâtiments a été identifié comme responsables de 30% à 70% de la consommation d'énergie primaire dans les villes [7] et de 30% des émissions en GES [8]. Par conséquent, développer des modèles

d’énergie des bâtiments (BEM) au niveau de la ville est essentiel pour la gestion de l'approvisionnement en énergie. Ces modèles ont été développés et ont servi comme étant des outils de conception au niveau des bâtiments [9]. Ils sont généralement utilisés à la phase de conception initiale et tout au long du processus de conception pour évaluer diverses options de conception et optimiser la performance globale des systèmes de construction. L’extension de la portée de la modélisation énergétique à l'échelle urbaine permet d'évaluer les interactions entre les bâtiments (ombrage, échange de chaleur, etc.), et d’interactions avec des composantes urbaines telles que l'îlot thermique urbain et le trafic. Les modèles de bilan énergétique à l’échelle de la ville peuvent être basés sur une approche « top-down » [10]–[12]. Dans ce cas, ils sont utilisés pour la modélisation climatique, mais ne fournissent pas les détails nécessaires pour tester des scénarios innovants à l'échelle du bâtiment. D'autre part, les modèles « bottom-up » de simulation physique ont été introduits comme outils de simulation efficaces pour modéliser l’impact du contexte urbain sur la demande énergétique des bâtiments [13]–[16]. Dans ce contexte, Reinhart et Davila [17] ont présenté les modèles énergétiques des bâtiments urbains (UBEM), qui sont des modèles de simulation physique ascendant utilisés comme outils de simulation efficaces pour simuler l'impact du contexte urbain sur la demande énergétique des bâtiments. Ils permettent de surmonter les lacunes des modèles statistiques et techniques en leur capacité à fournir des hypothèses d’énergie horaire, à estimer les impacts des nouvelles technologies, et incorporer les comportements des occupants [13]. Une autre caractéristique de UBEM est la possibilité de les combiner avec une plateforme GIS. Les cartes d'énergie résultantes sont ensuite utilisées pour l'analyse des résultats et la comparaison avec des données mesurées ou des enquêtes pour aider les concepteurs et les décideurs. UBEM applique des équations de transfert de chaleur dans et autour des bâtiments représentés un en tant que modèle thermique dynamique 3D individuel.

UBEM est donc capable de supporter développement de scénarios complexes. En outre, ils peuvent être combinés avec la simulation énergétique programmes. Le flux de travail de modélisation énergétique d'un UBEM nécessite beaucoup d'effort et de temps ressources étant donné la quantité massive de données pour potentiellement des milliers de bâtiments. Assembler, gérer et automatiser le flux de travail est essentiel. À cette fin, le stock de bâtiments est divisé en archétypes pour réduire la complexité et les exigences de calcul [13].

Le modèle de Boston développé par le MIT Sustainable Lab est un exemple illustrant UBEM [18]. Le modèle a été réalisé à l'aide d'un ensemble d'outils comprenant des systèmes GIS pour l'importations des polygones des bâtiments, Rhinoceros 3D [19] en tant qu'environnement de CAO et EnergyPlus en tant que le moteur de simulation thermique. Le workflow consiste à générer les archétypes à partir de l'année de construction et les types de bâtiments, en extrudant l'empreinte du bâtiment pour créer la forme tridimensionnelle, en la divisant en étages, en générant des fenêtres et en assignant les propriétés thermiques spécifiques en fonction de l'archétype du bâtiment. Les surfaces d'ombrage étaient déterminées et chaque bâtiment a ensuite été représenté par un modèle thermique et son énergie la performance a été simulée dans EnergyPlus. Une étude suivante, où le même flux de travail a été appliqué pour un quartier de Boston, a exploré différents ECM pouvant être appliqués à réduire la consommation d'énergie [14].

BEM et UBEM doivent être fiables et adaptables en ce sens qu'ils doivent fournir des estimations de la performance énergétique des bâtiments. Cependant, des divergences se produisent souvent entre le modèle prédit et la consommation énergétique réelle mesurée du bâtiment, principalement en raison des imprécisions/incertitudes dans la paramétrisation et la structure du modèle [20]. Par conséquent, l'étalonnage de modèles énergétiques est essentiel pour atteindre un niveau de confiance dans les prévisions des modèles et encourager leur

adoption. Ils vont du réglage itératif manuel déterministe [20], [21], au processus d'étalonnage automatique utilisant des techniques d'optimisation, des algorithmes d'apprentissage automatique ou la calibration bayésienne [22]. Une fois calibré, UBEM peut être utile pour estimer les impacts de nouvelles technologies et politiques pour lesquelles aucune donnée mesurée n'est disponible et pour révéler modèles d'occupants inconnus.

Parmi les sources de consommation d'énergie dans les bâtiments, le rayonnement solaire et l'éclairement sont considérées comme des ressources renouvelables pour accroître l'efficacité énergétique des bâtiments par des techniques passives et l'utilisation de la lumière du jour. Ce dernier, associé à un éclairage artificiel, a fait l'objet de nombreuses études dans le cadre d'une stratégie de développement durable visant au confort visuel, l'optimisation énergétique et l'aspect architectural des bâtiments [23]–[25]. La lumière du jour et le confort en plein air sont des indicateurs du confort et du bien-être des résidents [25]. La quantité d'énergie solaire et de lumière du jour atteignant un environnement urbain est fortement liée à la compacité urbaine, parmi ses indicateurs, la géométrie du canyon urbain et les blocs urbains, l'orientation des rues et des bâtiments. Evaluer les effets de ces indicateurs sur le potentiel d'énergie solaire et la lumière du jour fournissent des lignes directrices pour l'optimisation de la forme urbaine dans relation avec les interventions de modernisation des enveloppes de bâtiment et des applications de l'énergie solaire dans zones urbaines denses [26].

Le district administratif de Beyrouth, la Capitale du Liban, situé dans le Grand Beyrouth, présente un intérêt particulier dans cette étude. La ville a connu une expansion horizontale et verticale au fil des ans. Cette densification a entraîné d'énormes défis liés principalement à la fourniture des services urbains tels que l'énergie et l'atténuation des effets du changement climatique. La ville comptait 50,7% de la population urbaine du pays et 44,6% de la population totale en 2016 [1], et consomme 12% de l'énergie nationale totale produite alors

qu'elle ne couvre que 0,2% de la superficie totale du pays. Son secteur tertiaire (secteur commercial, bureaux publics, hôtels et hôpitaux) et le secteur résidentiel représentent 73% et 26% de sa consommation d'électricité respectivement. Celles-ci représentent 39% et 14% des émissions de GES de l'électrification respectivement [27]. Alors que la demande en énergie augmente, le Liban souffre depuis de nombreuses années, d'une crise dans le secteur de l'énergie. Le pays compte sur les produits pétroliers importés pour satisfaire ses besoins en énergie, ce qui place le pays dans un état de grande vulnérabilité. Les importations nettes sont passées de 5,45 millions de tep (tonnes d'équivalent pétrole) en 2008 à 7,61 millions d'euros en 2014, dont 43% ont été utilisés pour la production d'électricité en 2014 [28]. La capacité disponible pour la production d'électricité est de 2670 MW [29], dont seulement 1500 MW jusqu'à un maximum de 2000 MW sont assurés par EDL (Electricité du Liban) [30], la seule institution publique responsable de la production, la transmission et la distribution de l'énergie électrique au Liban [31]. En d'autres termes, un maximum de 65% de la puissance générée est émise par l'État et le reste par des générateurs privés de secours. Même si Beyrouth est soumis à la plus faible période de rationnement (seulement 3 heures alors que celle-ci dure jusqu'à 12 heures certaines régions du pays), réduire sa demande en énergie peut atténuer les coupures de courant quotidiennes dans les autres régions.

Cette situation remet en cause l'engagement pris par le Liban de réduire ses émissions de gaz à effet de serre de 30% d'ici 2030. Le pays est alors confronté à un défi important pour gérer son secteur énergétique et intégrer les énergies renouvelables. Il est donc essentiel de développer un modèle énergétique à l'échelle urbaine pour la gestion des ressources et de l'approvisionnement en énergie à Beyrouth. Un tel modèle sert de système de support de décision en estimant les schémas de consommation d'énergie et en identifiant le pic de demandes du réseau avec une distribution spatio-temporelle. Ce dernier, intégré aux résultats

du potentiel solaire produit [32], aide à estimer les économies et à recommander des politiques d'utilisation de l'énergie visant à réduire les pointes et à assurer une distribution efficace des ressources. Une autre caractéristique du modèle énergétique de Beyrouth est sa capacité à projeter la consommation d'énergie dans des conditions normales. Actuellement, les estimations de la demande ne tiennent pas compte la quantité d'électricité supprimée, car lors des pannes, les occupants modifient leurs comportements et leurs habitudes et préférences de consommation d'énergie.

2 BEirut Energy Model

BEEM, BEirut Energy Model, est un modèle énergétique urbain pour Beyrouth, et dont l'organigramme est présenté ci-dessous.

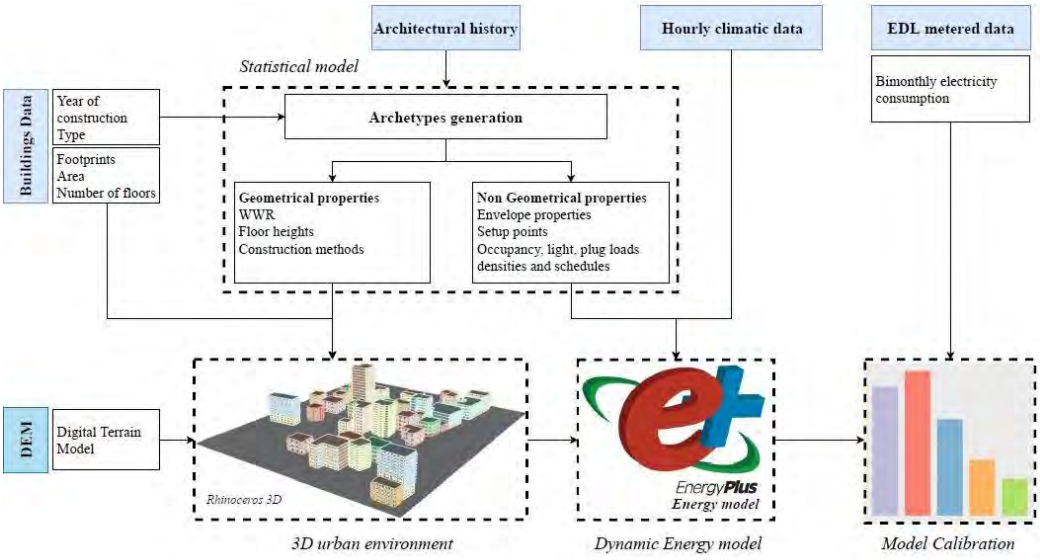

Figure 1: Organigramme de la méthodologie de BEEM

Les informations nécessaires pour créer BEEM sont :

- Les polygones des bâtiments et leur position dans l'espace.

- Leurs types, leurs années de construction, leurs élévations et leurs nombres d'étages.
- Le profil d'élévation de la ville DEM.
- Des données météorologiques horaires pour une année.

Ces données sont collectées de plusieurs sources :

- Par télédétection et traitement des images satellites pour la segmentation des bâtiments, la détermination de leurs élévations et du DEM.
- Sondage effectué par l'université Saint Joseph pour 7120 bâtiments dont seulement 3630 avaient des données suffisantes et par la suite utilisés dans les simulations.
- La station de météo à l'aéroport international de Beyrouth.

Pour représenter ces bâtiments, une série d'archétypes, ou des bâtiments représentatifs devaient être développés. Les archétypes consistent en un ensemble de propriétés géométriques caractérisant les performances thermiques d'un bâtiment, telles que la résistance thermique des murs, etc. La génération d'archétype comprend deux étapes: la segmentation, ou le regroupement de bâtiments ayant des propriétés similaires, et la caractérisation, ou la définition de l'ensemble complet des propriétés thermiques pour chaque archétype. Les bâtiments de Beyrouth ont été segmentés en fonction de deux paramètres clés: d'une part, le type et d'autre part, l'année de construction fondée sur une étude architecturale des bâtiments. Le type est un facteur important dans la détermination des charges aux prises et des gains de chaleur internes d'un bâtiment, tandis que l'année de construction d'un bâtiment fournit des hypothèses sur les méthodes de construction et les matériaux utilisés. Pour identifier les propriétés de chaque groupe de bâtiments, nous nous référons tout d'abord au guide technique de base publié par le ministère des Travaux publics et des Transports en 2005 (Technical Guide for the application of the Thermal Standard for Buildings in Lebanon [33]) avec les

propriétés thermiques d'un large éventail de matériaux utilisés dans la construction au Liban. Les propriétés manquantes ont été identifiées à partir de la bibliothèque du logiciel utilisé comme interface avec EnergyPlus nommé ArchSim. Nous avons également utilisé les sites Web de la même bibliothèque. Pour les horaires d'occupation et les chargements de fiche, nous avons utilisé ceux définis par ASHRAE et nous les avons mis à jour pour répondre au mieux au cas libanais.

Après la préparation des données, les bâtiments ont été divisés en étages et un archétype a été attribué à chacun. Le processus de modélisation de la géométrie est présenté dans la figure ci-dessous.

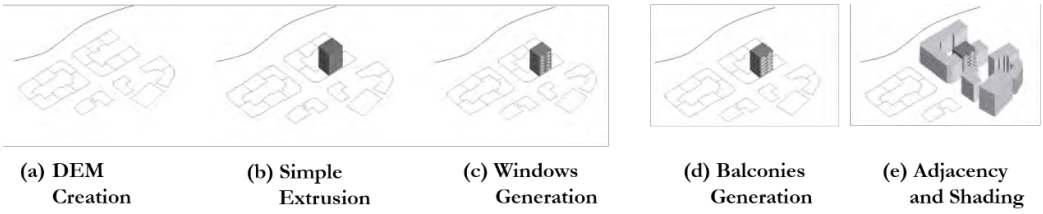

Figure 2: La figure (a) montre la création du DTM, suivie d'une extrusion simple illustrée à la figure (b), puis de la génération de fenêtres et de balcons respectivement en (c) et (d), et enfin, les contours et les ombrages sont illustrés en (e).

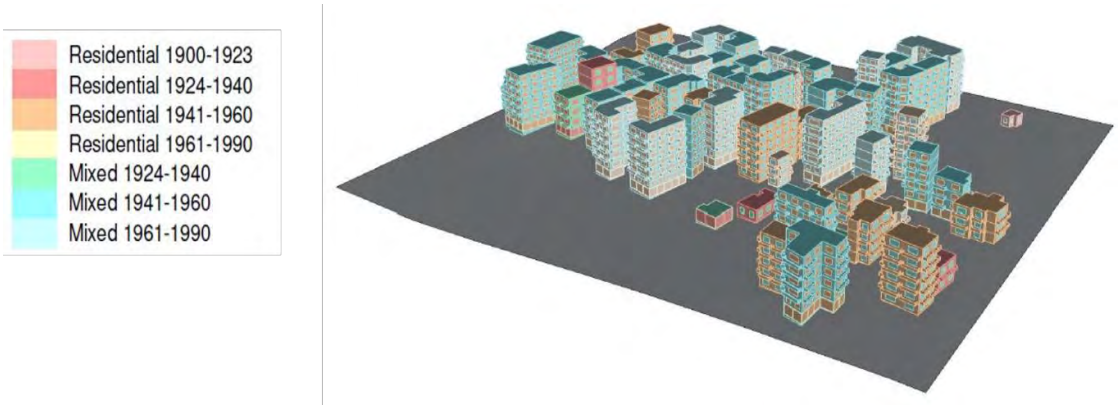

Figure 3: Exemple du modèle 3D généré de bâtiments dans la région de Bachoura, Beyrouth, Liban.

Une fois le modèle 3D terminé, les paramètres de simulation de la base de données des bâtiments ont été attribués à chaque zone thermique et stockés dans des fichiers constituant des entrées à EnergyPlus. Le modèle énergétique a été simulé et les résultats obtenus ont été ensuite analysés.

2.1 Calibration du modèle

Après avoir généré le modèle thermique, les charges horaires annuelles provenant des équipements, de l'éclairage, de l'eau chaude sanitaire, du refroidissement et du chauffage ont été agrégées dans une consommation électrique simulée pour les bâtiments résidentiels et mixtes. En comparant les résultats obtenus aux données réelles bimensuelles de l'Electricité du Liban (EDL) disponibles pour un certain nombre d'immeubles, des différences ont été identifiés. Ce décalage entre les valeurs EDL et celles prédites par le modèle peut être principalement attribué aux modèles de comportement, aux systèmes CVC et aux erreurs systématiques. Par conséquent, toute correction à appliquer doit être compatible avec les erreurs catégoriques ci-dessus, être adaptable au contexte de la ville et justifiée en même temps. À cette fin, les interventions suivantes ont été mises en œuvre:

- Erreurs systématiques: une coupure de courant de 3 heures à Beyrouth représente un facteur de réduction de 1/8, calculé sur une moyenne annuelle. Par conséquent, la consommation d'électricité simulée a été réduite de ce montant. De plus, les erreurs liées aux algorithmes numériques ont été éliminées. Ces erreurs sont les résultats du programme EnergyPlus permettant d'ajuster la température de la zone afin d'atteindre la valeur souhaitée définie par les points de consigne du système de contrôle.
- Architecture des systèmes HVAC: le refroidissement à Beyrouth repose principalement sur des unités de refroidissement unitaires associées à des zones données. Les unités fonctionnent rarement en même temps. À cette fin, nous supposons que seulement 50% de la surface du sol est refroidie ou chauffée à un moment donné, de sorte que la consommation simulée de refroidissement et de chauffage est réduite de moitié. En outre, lorsque la température extérieure était inférieure à 20 ° C, les charges de refroidissement étaient annulées.
- Consommation d'énergie et profil d'occupation: après application des corrections précédentes, nous avons réalisé que les écarts restants ont été causés par des profils d'occupation, modifiant de manière linéaire la consommation totale bimestrielle d'électricité d'un facteur déterminé. Par conséquent, la consommation d'énergie calibrée pour chaque bâtiment a été obtenue en multipliant la consommation d'énergie estimée par le modèle et les multiplicateurs moyens de sa grappe.

  Les valeurs aberrantes ont été supprimées à l'aide d'un clustering spatial basé sur la densité d'applications avec bruit (DBSCAN) et d'auto-encodeurs, en fonction de la superficie des bâtiments, du nombre d'étages, du type, de l'année de construction et de la consommation EDL. Une fois les valeurs aberrantes identifiées, les bâtiments restants ont été regroupés en fonction de leur consommation d'électricité simulée et de leur consommation d'électricité

réelle (EDL). Ce regroupement aide à identifier les bâtiments avec des horaires d'occupation similaires.

La calibration du modèle est effectuée en appliquant une classification k-means au rapport entre EDL et les consommations prédites. Cela a conduit à l'identification de quatre groupes de bâtiments dans chaque district, comme indiqué dans les figures 4 et 5. Le nombre de clusters a été défini en fonction d'une procédure d'optimisation pour chaque district. Le modèle a surestimé la consommation d'électricité dans la plupart des bâtiments, principalement dans les groupes 0 et 1 des deux districts. Les clusters 3 regroupaient les bâtiments avec EDL avec un ratio de consommation d'électricité simulé compris entre 0,6 et 1,3 dans le district A et entre 0,5 et 1,5 dans le district B. La consommation de seulement 21 et 34 bâtiments a été sous-estimée dans les districts A et B, respectivement.

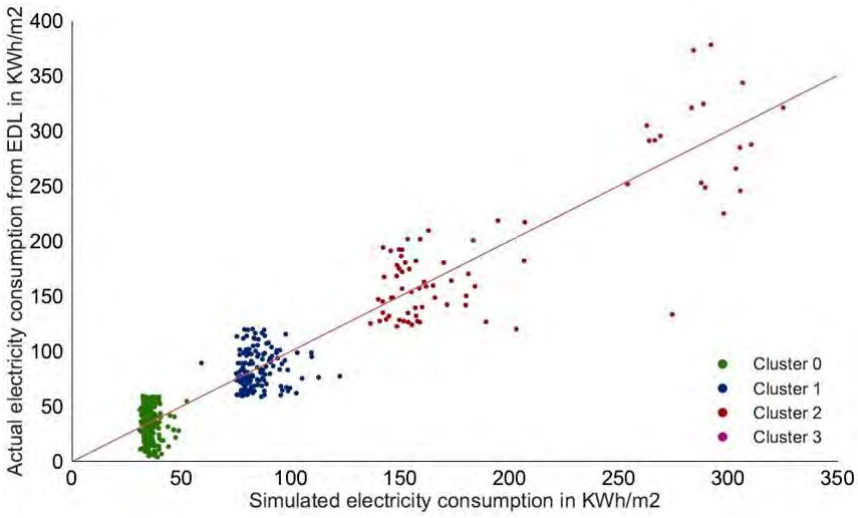

Figure 4: Configuration EPlus par défaut: occupation complète avec les normes ASHRAE

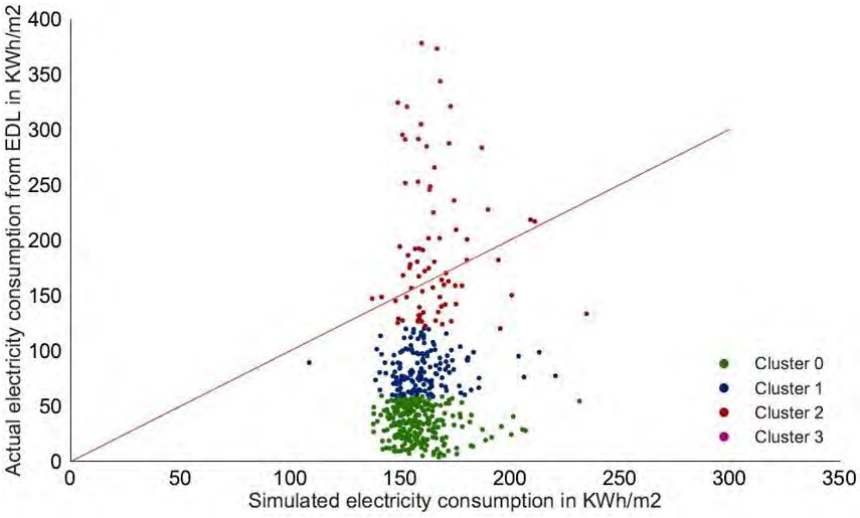

Figure 5: Résultats EPlus adaptés à l'occupation de Beyrouth et au comportement des utilisateurs

En combinant les résultats du modèle avec les techniques de cartographie GIS, on obtient une distribution spatiotemporelle de la consommation d'énergie, comme le montre la figure 6. Notez que les bâtiments les plus consommateurs ont été construits entre 1941 et 1990.

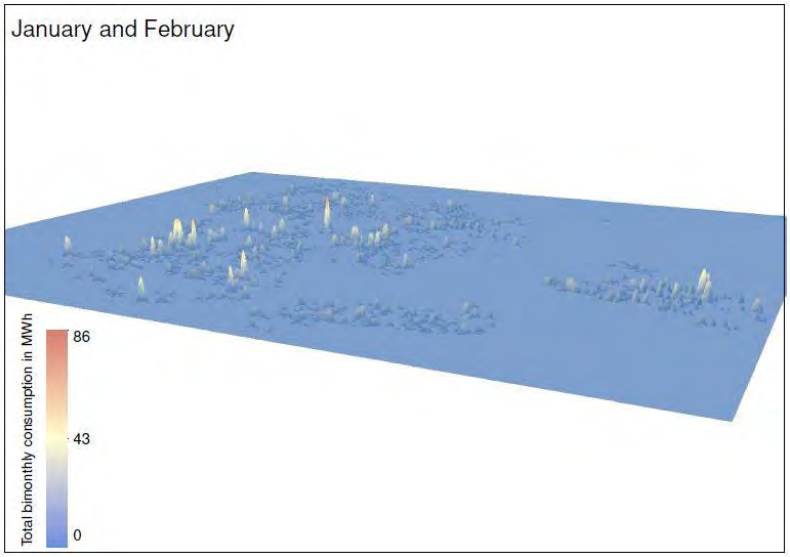

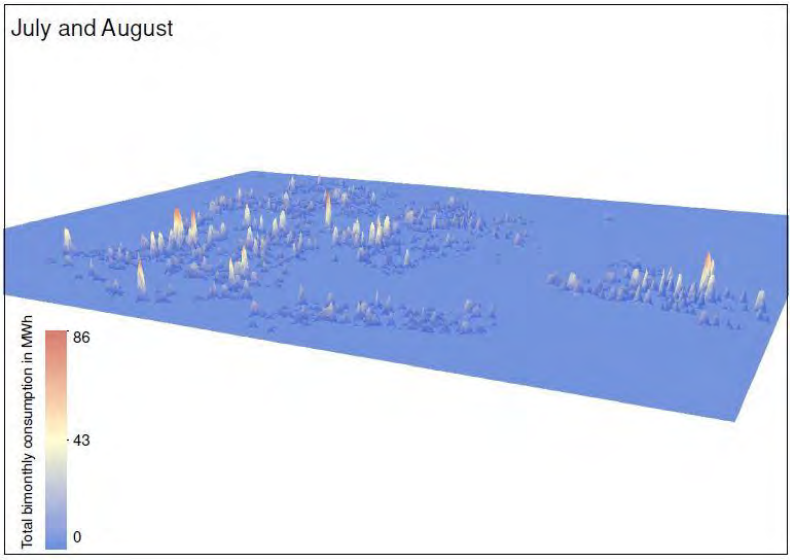

Figure 6: Distribution spatio-temporelle de la consommation d'électricité prédite bimestriellement des bâtiments du district B

2.2 Discussion

Les sections précédentes ont montré comment construire, générer et calibrer un UBEM, capable de de prédire la consommation d'électricité d'une ville en capturant les comportements des bâtiments. Le modèle prend en entrée des données contenant les empreintes, les hauteurs, la surface de plancher, le nombre des étages, des archétypes correspondants ainsi qu'un fichier météo et une carte topographique. Ici, un fichier météo mis à jour, résumant le changement climatique global et l'UHI en Beyrouth est nécessaire pour le modèle énergétique à grande échelle de la ville, en particulier avec la densité des générateurs diesel dispersés dans la ville et entre les bâtiments. De plus, une carte topographique à haute résolution peut réduire la complexité du modèle lors de la génération le profil d'élévation de la ville et la projection des bâtiments sur le plan incliné.

Les propriétés géométriques telles que le WWR et les matériaux de construction ont été obtenues d'études antérieures, tandis que les propriétés non géométriques ont été recueillies auprès de rapports lorsque disponibles et bibliothèques existantes. Des efforts à cet égard

devraient être déployés pour créer pour Beyrouth une base de données appropriée intégrant des matériaux de construction et leurs propriétés thermiques. Les taux de pénétration des systèmes de HVAC et leurs propriétés doivent être plus examinés, en particulier dans les bâtiments construits avant 1945, caractérisés par leur architecture sensible au climat et l'application du concept de durabilité [34]. Ces bâtiments dépendent des conditions environnementales pour assurer le confort thermique intérieur. Cependant, ces bâtiments peuvent avoir perdu leurs caractéristiques prévues avec la construction aléatoire et l'effet du changement climatique. De plus, des audits périodiques approfondis sont nécessaires pour étudier les paramètres liés aux occupants, tels que le statut économique, le confort thermique interne, l'utilisation des appareils, les horaires et les activités d'occupation quotidiens et saisonniers.

Le principal défi rencontré lors de cette étude était la mise en place des calendriers. L'absence de profils d'utilisation et d'occupation de l'énergie a conduit les auteurs à adopter horaires standardisés. Le modèle représentait un lourd fardeau pour le secteur de l'énergie au cas où les citoyens adoptent un style de vie occidental coûteux et confortable. En fait, le Liban est considéré comme un pays économiquement faible. De plus, le rationnement de l'électricité pousse déjà les habitants à modifier leurs schémas comportementaux entraînant à une demande supprimée. Cependant, en présence des données mesurées tous les deux mois (données EDL), il était possible d'inspecter les consommations d'énergie des Libanais et de les relier aux circonstances socio-économiques et politiques du pays. L'énergie prédite a été ajustée par intervention manuelle en fonction d'indices statistiques suivis de graphiques comparatifs. Il était clair qu'une variabilité mensuelle plus faible caractérise la consommation d'électricité des bâtiments résidentiels et mixtes, par rapport à la consommation, principalement attribuable à la demande surestimée de refroidissement.

Ceci a été partiellement corrigé en supposant que les sols des bâtiments sont partiellement refroidis (et chauffé). Les différences restantes s'expliquent par le fait que beaucoup des familles libanaises (jusqu'à 15%) possèdent deux maisons ou plus [35] dans d'autres régions du pays, et quittent la ville pendant les vacances d'été. De plus, un grand nombre d'unités résidentielles sont invendues ou vacantes, appartenant à des expatriés ou des investisseurs. Des statistiques à jour de cet égard sont nécessaires pour estimer correctement la consommation d'énergie par ménage et par habitant. Cependant, des problèmes liés à l'accessibilité des données et à la confidentialité peuvent être soulevés et doivent être résolus et correctement adressés.

L'étalonnage a été utilisé à l'échelle temporelle des données réelles et a donné des résultats satisfaisants de la demande énergétique globale du bâtiment. Cependant, les auteurs ne peuvent prétendre précision au niveau horaire sans données mesurées pour la validation et/ou le calibrage. Des efforts devraient être placés sur l'enregistrement de la consommation d'électricité horaire par EDL ou l'utilisation des techniques de modélisation du comportement des occupants [36]–[38]. La consommation d'électricité calibrée a montré une mise en grappe spatiale similaire à celle des données mesurées d'EDL dans les deux districts. Cela prouve la pertinence de notre processus de calibration.

Le modèle énergétique peut être utilisé pour relier les observations de la consommation d'électricité à un endroit à ceux d'autres endroits. Le principal intérêt à révéler le clustering spatial est son importance dans la création de zones pour la distribution intelligente du réseau. En outre, la ville de Beyrouth représente le centre zone administrative et commerciale du Liban. Mobilité humaine dans et hors de la ville doit être étudié car il pourrait avoir une influence sur la demande énergétique [39], en particulier lorsqu'on étend le champ d'application du modèle à l'ensemble de la ville et qu'il intègre des bâtiments

gouvernementaux. Par conséquent, des recherches supplémentaires sont nécessaires pour améliorer l'étude d'auto-corrélation.

Lors de la génération d'un UBEM, chaque bâtiment est représenté sous la forme d'un modèle thermique 3D individuel. La modélisation en fonction de son contexte urbain, attribue un archétype basé sur un ensemble de paramètres. Les profils de charges temporelles sont ensuite couplés à des techniques de cartographie GIS pour soutenir la prise de décision urbaine. Compte tenu de ces caractéristiques, aucune étude UBEM au sein de la région méditerranéenne était déjà réalisée. Les études ascendantes ont principalement porté sur la définition de bâtiments représentatifs du stock de bâtiments et l'évaluation de leur performance en énergie [40]. L'approche ascendante présentée dans ce papier enrichit la précision du modèle. En outre, son étalonnage se concentre sur l'intégration du poids important des comportements des occupants dans le modèle urbain. Sa capacité à gérer la complexité d'une zone urbaine peut être utilisée pour améliorer les résultats des études précédentes menées dans la région méditerranéenne. Cette méthodologie adoptée peut être reproduite dans n'importe quel autre district ou ville du Liban et de la région. Sa polyvalence est reconnue spatialement, qu'il s'agisse du bâtiment ou de la ville, et temporellement quand allant de résolution horaire à annuelle. Cela permet une analyse des schémas énergétiques spatiotemporels pour allouer les points chauds et les pics d'énergie demandes. À cet égard, les cartes énergétiques urbaines 2D et 3D sont très informatives et permettre l'analyse critique. Application de mesures d'économie d'énergie ou de modernisation à des bâtiments spécifiques à forte consommation d'énergie peuvent ensuite être explorés. De plus, la mise à l'échelle de la consommation d'énergie horaire est cruciale pour la gestion de la distribution d'énergie par « rationnement intelligent » de l'électricité. Dans ce contexte, le modèle peut

fournir un aperçu de la stratégie d'intégration optimale de l'énergie solaire sur les toits des bâtiments, comme sera étudié dans les recherches futures.

2.3 Implications politiques

Pour le Liban, un pays avec des défaillances chroniques du secteur de l'énergie, reflétant le déficit croissant puissance et la qualité, ce travail offre trois liens politiques distincts qui pourraient aider à la résolution de défis réels et existants:

- Tout d'abord, en raison de la facturation non raffinée et bimensuelle de l'électricité ainsi que du marché de l'électricité du pays, EDL, la compagnie nationale d'électricité n'a pas de compte précis des charges de consommation et de leurs variations dans le temps et dans l'espace. Le modèle développé fournit un outil puissant pour comprendre mieux les variations de charge, et ainsi planifier les stratégies et les investissements futurs en conséquence. Par exemple, l'un des principaux défis de la techno-politique résident dans l'estimation de la demande réelle d'électricité des Libanais et son taux de croissance dans le futur en raison des interactions complexes entre EDL et exploitants de groupes électrogènes diesel privés, dont certains sont dotés de compteurs et d'autres largement non réglementés; et l'existence d'une demande supprimée due à l'incapacité des EDL à fournir de l'énergie 24 heures sur 24. Avec l'aide du comptage intelligent que EDL commence à mettre en œuvre, ce modèle peut être utilisé pour calibrer scientifiquement, vérifier et estimer la demande croissante aux niveaux national et sous-national.
- Deuxièmement, jusqu'à ce que EDL puisse fournir de l'électricité sans interruptions, les coupures du courant continueront à se produire. La prédiction des modèles de consommation d'électricité dans l'environnement urbain de Beyrouth, illustrée dans ce travail, pourrait à terme contribuer à informer le rationnement intelligent de l'électricité, ce qui permet d'établir une cartographie efficace entre les charges et la capacité d'approvisionnement disponible.

- Troisièmement, le modèle développé pourrait être utilisé pour tester divers instruments de politique et des idées qui favorisent les économies d'énergie telles que la mise en œuvre des codes d'efficacité énergétique des bâtiments, installation de chauffe-eau, etc. Une application particulièrement utile est de tester le potentiel des systèmes photovoltaïques solaires sur les toits pour répondre à la demande, ou à une partie de celle-ci, pendant certaines périodes.

3 Accès à la lumière du jour

Le bilan radiatif constitue une composante importante du bilan énergétique des bâtiments. Il contribue directement en tant de gains solaires par les surfaces extérieures du bâtiment, et indirectement par les économies d'énergie atteintes par le remplacement de l'éclairage artificiel par la lumière du jour. De nombreuses études ont été réalisées pour mesurer l'accès solaire et la disponibilité de la lumière du jour en contexte urbain [44]–[46] et évaluer son impact sur la consommation d'énergie en milieu urbain [47]. Dans cette étude, le bilan radiatif de deux zones à Beyrouth a été simulé dans DART [48]. Puisque nous cherchons à représenter la lumière du jour, nous utilisons l'illuminant standard D65 défini par la Commission internationale de l'éclairage (CIE) pour convertir l'énergie rayonnante en énergie lumineuse (c'est-à-dire visible). Un illuminant est une représentation mathématique de la source de lumière basée sur un modèle visuel humain, dans ce cas la lumière du jour. La sensibilité spectrale moyenne de la perception visuelle humaine est également présentée, appelée fonction de luminosité. La CIE distribue des tableaux standard avec des valeurs de fonction de luminosité à des intervalles de 5 nm allant de 380 à 780 nm (l'intervalle peut être réduit à 400 nm à 700 nm, car les valeurs de la fonction de luminosité deviennent négligeables aux longueurs d'onde en dehors de cet intervalle).

3.1 Description de l'étude de cas et résultats

Deux zones ont été choisies arbitrairement pour cette étude, ayant une complexité urbaine différente. Le budget radiatif sur les surfaces extérieures de 433 bâtiments de la zone 1 et de 414 bâtiments de la zone B a été simulé. En raison de ressources de calcul limitées, les districts ont été subdivisés en zones (6 zones dans le district A et 3 zones dans le district B). Les limites des zones se chevauchaient pour tenir compte de l'effet des ombres des bâtiments voisins. Les bâtiments avec une fonction manquante étaient considérés comme résidentiels. Lorsque l'année de construction n'est pas disponible, il a été supposé que les bâtiments ont été construits après 1991.

Le profil vertical de la lumière du jour correspond au profil de l'énergie interceptée par une composante urbaine (dans notre cas, les fenêtres) tout au long de la hauteur des bâtiments. L'analyse de cette métrique montre à quel point l'accessibilité à la lumière du jour est en grande partie perdue aux étages inférieurs de chaque zone. Les pertes sont quantifiées entre les étages les plus hauts et les plus bas à des heures et des jours différents de l'année. Les résultats de la zone 1 sont présentées dans la figure 7.

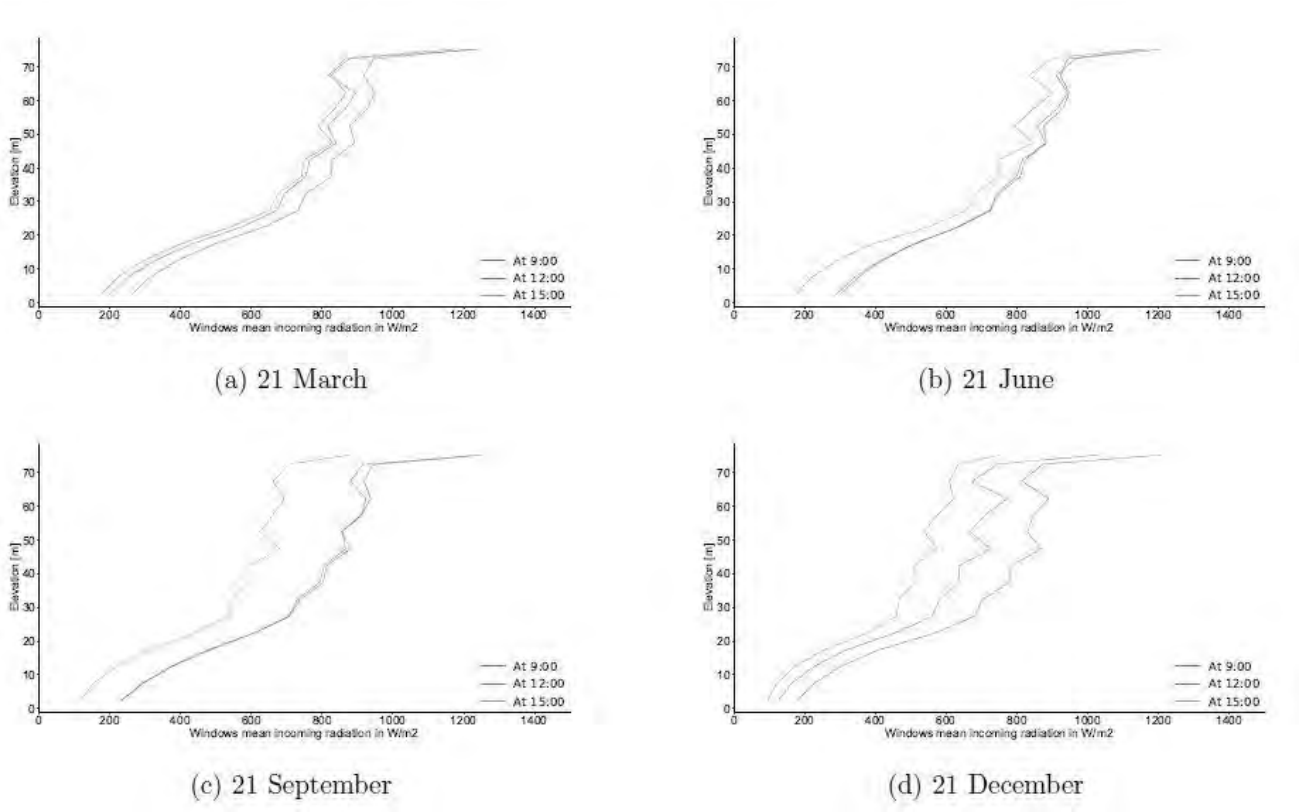

Figure 7: Profil vertical de l'énergie interceptée sur les fenêtres des bâtiments de la zone 1, à différentes heures sur quatre jours de l'année.

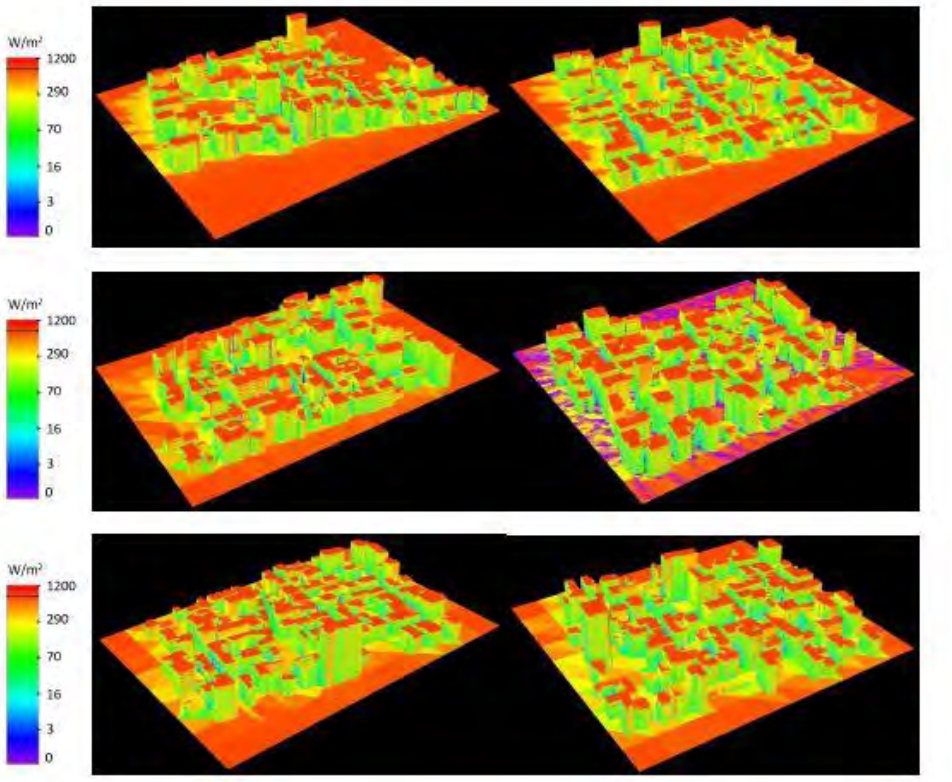

Figure 8: Bilan radiatif 3d de l'énergie interceptée par les surfaces des bâtiments dans les 6 sous-zones de la zone 1, à 9 h le 21 mars (bande [400 nm; 475 nm], grille d'éclairage = 10 cm).

Des aspects urbains tels que la hauteur moyenne et l'orientation des bâtiments environnants, leur niveau déviation, la hauteur du bâtiment et sa position dans l'espace étaient associées à la disponibilité de la lumière du jour sur les façades des bâtiments avec des réseaux de neurones artificiels algorithmes. Avec une erreur MAPE de 17%, l'algorithme formé présente une méthode fiable et cohérente pour évaluer l'accessibilité de la lumière du jour pour les zones urbaines planification, la conception des futurs bâtiments et d'estimer sa variation sur l'année si les caractéristiques d'entrée pourraient être obtenues.

4 Conclusion et perspectives

Le travail présenté dans cette thèse est le premier UBEM à cette échelle au Liban et la région à la connaissance de l'auteur. Bien qu'il se soit avéré présenter plusieurs avancées, des travaux supplémentaires sont encore nécessaires pour promouvoir son utilisation en milieu urbain la planification énergétique et certains développements pertinents peuvent être envisagés.

Gestion de données à grande échelle

La disponibilité des données était un obstacle majeur qui limitait la portée de la thèse à celui représenté dans cette thèse. Par conséquent, un besoin inévitable de bases de données est soulevé. Le référentiel de données devrait inclure:

- Liste actualisée des matériaux utilisés dans la construction des bâtiments, avec leurs propriétés thermiques et optiques, en plus de la construction des méthodes telles que la construction de couches de composants.
- Images satellitaires récentes et anciennes pour les villes d'intérêt utilisables en télédétection, non limitée à la numérisation et à la végétation des bâtiments classification, mais aussi pour l'identification des propriétés urbaines.
- Caractéristiques des utilisations finales de l'énergie, telles que HVAC, appareils électroménagers et l'éclairage, y compris leurs taux de pénétration, leur efficacité et leur modèles d'utilisation.
- Paramètres liés aux occupants, tels que leurs activités, leurs comportements et préférences. Dans ce contexte, la complexité augmente en raison de la stochastique nature des modèles humains.

La gestion et l'organisation des données constituent un facteur clé pour une génération d'UBEM efficace et prenant moins de temps. Des modèles communs d'informations et la possibilité de partage augmenteront l'adoption de ces outils, amélioreront leur fiabilité et faciliteront leur importation aux modèles.

Raffinement des modèles géométriques et non géométriques

De nombreuses améliorations peuvent être envisagées pour améliorer encore la précision du modèle présenté et d'élargir ses applications. Le modèle géomètrique peut être amélioré en considérant les toits inclinés, le zonage des bâtiments en noyau et périmètre, modélisation d'arbres et de parcs, routes et zones piétonnes assez elles, pour en énumérer quelques-uns. Ces améliorations sont importantes à la fois pour le modèle énergétique et le modèle radiatif. La classification archétypale peut être améliorée en ajoutant d'autres paramètres clés que le type et l'année de construction du bâtiment. Cependant, l'identification des paramètres clés doit être basée sur une analyse de sensibilité pour éviter la génération d'archétypes inutiles.

Fonctionnalité de modèle

Le modèle BEEM présenté aux chapitres 3 et 5 est un algorithme automatisé permettant de générer les modèles 3D et les fichiers prêts à être utilisés pour les simulations énergétiques. Cependant, les entrées et les sorties du modèle nécessitent des efforts considérables pour les utiliser et procéder. En d'autres termes, BEEM peut encore être développé pour les fonctionnalités de gestion des données et devenir une plate-forme efficace et réalisable pour des utilisateurs de différents horizons. Il devrait être adapté pour être compatible avec d'autres formats, tels que CityGML afin qu'il puisse être utilisé dans d'autres études. Un de plus La barrière est le coût de calcul des simulations.

Un autre obstacle est le coût de calcul des simulations. Cette étude a été réalisée avec un service de cloud computing. Les simulations d'énergie prennent du temps, à moins que des ordinateurs puissants ne soient utilisés. Par conséquent, une attention devrait être prise à cet égard.

Amélioration de l'évaluation du bilan énergétique

- Le budget radiatif contribue au budget énergétique grâce au gain solaire des surfaces et aux économies d'énergie résultant de la lumière du jour. Le module radiatif dans EnergyPlus est simple, tandis que celui dans DART est plus avancé et plus précis. Il serait utile de coupler les sorties de DART à EnergyPlus ou à n'importe quel logiciel de modélisation énergétique dynamique.
- Des paramètres climatiques tels que UHI, les conditions de vent locales, l'évaporation près de la mer et la chaleur dégagée par les transports doivent être prises en compte, compte tenu de leur influence sur les bilans énergétique et radiatif des bâtiments et donc sur la demande en électricité. Par conséquent, l'étude pourrait être étendue pour prendre en compte les effets des conditions microclimatiques en en le reliant à une analyse CFD de la dynamique des fluides numérique, ou en utilisant des générateurs de temps urbains pour simuler l'effet UHI.

Autres études

Le modèle présenté permet d'évaluer la demande en énergie dans un cadre spatio-temporel. Il évalue la consommation d'énergie actuelle et estime les schémas énergétiques futurs dans le cadre de certaines interventions technologiques, telles que la mise en œuvre de mesures d'économie d'énergie. De plus, il permet d'estimer la contribution des formes urbaines et de l'énergie utilisations finales de la demande

d'énergie à l'échelle du bâtiment et de la ville. Les résultats du modèle énergétique, du modèle de lumière du jour et leur relation avec les métriques urbaines peuvent être combinés pour une analyse plus holistique de différents modèles, énergie et stratégies à faibles émissions de carbone et planification urbaine. Nous avons commencé à explorer ces relations cette étude, prouvant que le modèle convient à une tel analyse. Un autre aspect important de BEEM est sa capacité à gérer l'approvisionnement en énergie. Les cartes d'énergie spatio-temporelles peuvent être couplées à l'irradiation solaire et aux cartes solaires pour estimer les économies potentielles réalisées par les systèmes photovoltaïques sur les toits, la répartition optimale de l'énergie produite et la gestion du réseau pour répondre à la demande énergétique. Il peut également être utilisé pour des simulations de réseau telles que le chauffage urbain. Ces capacités aident à informer les urbanistes et les décideurs politiques sur des scénarios possibles pour réduire la demande en énergie, répondre aux besoins urbains et réduire les émissions de GES. Évaluer les impacts économiques et sociaux de ces interventions doivent être complémentaires su modèle pour fournir un plan complet adaptable pour l'énergie urbaine la gestion.

5 Références

[1] United Nations Department of Economic and Social Affairs Population Division, *The World's Cities in 2016*. Population and Vital Statistics Report, UN, New York: United Nations, 2016.

[2] UN-Habitat, "Urbanization and Development: Emerging Challenges," Nairobi, 2016.

[3] M. Santamouris, "On the energy impact of urban heat island and global warming on buildings," *Energy Build.*, vol. 82, pp. 100–113, 2014.

[4] R. Madlener and Y. Sunak, "Impacts of urbanization on urban structures and energy demand: What can we learn for urban energy planning and urbanization management?," *Sustain. Cities Soc.*, vol. 1, no. 1, pp. 45–53, 2011.

[5] B. B. Osorio, N. Mccullen, I. Walker, and D. Coley, "Understanding the relationship between energy consumption and urban form," *Athens J. Sci.*, vol. 4, no. 2, pp. 115–142, 2016.

[6] L. Suganthi and A. A. Samuel, "Energy models for demand forecasting - A review," *Renew. Sustain. Energy Rev.*, vol. 16, no. 2, pp. 1223–1240, Feb. 2012.

[7] Y. Chen, T. Hong, and M. A. Piette, "Automatic generation and simulation of urban building energy models based on city datasets for city-scale building retrofit analysis," *Appl. Energy*, vol. 205, no. July, pp. 323–335, 2017.

[8] C. C. Davila and C. Reinhart, "Urban energy lifecycle : An analyitical framework to evaluate the embodied energy use of urban developments," in *Proceedings of BS2013: 13th Conference of International Building Performance Simulation*

Association, Chambéry, France, August 26-28, 2013, pp. 1280–1287.

[9] M. Hajj-Hassan and H. Khoury, "Energy Modelling and Sustainability : A Review on Current Theories , Practices , and Challenges," *4th Int. Conf. Build. Energy, Environ.*, pp. 781–786, 2018.

[10] V. Masson, "A physically-based scheme for the urban energy budget in atmospheric models," *Boundary-Layer Meteorol.*, vol. 94, no. 3, pp. 357–397, 2000.

[11] A. Lemonsu, "Simulation of a summer urban breeze over paris," *Boundary-Layer Meteorol.*, vol. 104, no. 3, pp. 463–490, 2002.

[12] H. C. Ward, S. Kotthaus, L. Järvi, and C. S. B. Grimmond, "Surface Urban Energy and Water Balance Scheme (SUEWS): Development and evaluation at two UK sites," *Urban Clim.*, vol. 18, pp. 1–32, 2016.

[13] C. Cerezo Davila, C. F. Reinhart, and J. L. Bemis, "Modeling Boston: A workflow for the efficient generation and maintenance of urban building energy models from existing geospatial datasets," *Energy*, vol. 117, pp. 237–250, Dec. 2016.

[14] J. Bemis, "Urban Building Energy Modeling as a Dynamic Tool for Suatainability Planning," Massachusetts Institute of Technology, 2016.

[15] T. Hong, Y. Chen, S. H. Lee, and M. A. Piette, "CityBES : A Web-based Platform to Support City-Scale Building Energy Efficiency," in *Urban Computing*, 2016, no. August, p. 9.

[16] S. Evans, R. Liddiard, and P. Steadman, "3DStock: A new kind of three-dimensional model of the building stock of England and Wales, for use in energy

analysis," *Environ. Plan. B Urban Anal. City Sci.*, vol. 44, no. 2, pp. 227–255, 2017.

[17] C. F. Reinhart and C. Cerezo Davila, "Urban building energy modeling – A review of a nascent field," *Build. Environ.*, vol. 97, pp. 196–202, Feb. 2016.

[18] C. C. Davila, C. Reinhart, and J. Bemis, "Modeling Boston: A workflow for the generation of complete urban building energy demand models from existing urban geospatial datasets," *Energy*, 2016.

[19] Robert McNeel & Associates, "Rhinoceros 3D V5." 2015.

[20] D. Coakley, P. Raftery, and M. Keane, "A review of methods to match building energy simulation models to measured data," *Renewable and Sustainable Energy Reviews*, vol. 37. pp. 123–141, 2014.

[21] H. Lim and Z. J. Zhai, "Review on stochastic modeling methods for building stock energy prediction," *Build. Simul.*, vol. 10, no. 5, pp. 607–624, 2017.

[22] R. T. Muehleisen and J. Bergerson, "Bayesian Calibration - What , Why And How," in *International High Performance Buildings Conference*, 2016, p. 167.

[23] R. W. Da Fonseca, E. L. Didoné, and F. O. R. Pereira, "Using artificial neural networks to predict the impact of daylighting on building final electric energy requirements," *Energy Build.*, vol. 61, pp. 31–38, 2013.

[24] C. Chatzipoulka, "An Image-Based Method to Evaluate Solar and Daylight Potential in Urban Areas An image-based method to evaluate solar and daylight potential in urban areas," no. June, 2018.

[25] C. F. Reinhart, T. Dogan, J. A. Jakubiec, T. Rakha, and A. Sang, "Umi - an Urban

Simulation Environment for Building Energy Use , Daylighting and Walkability," *Proc. BS2013 13th Conf. Int. Build. Perform. Simul. Assoc.*, pp. 476–483, 2013.

[26] N. Mohajeri *et al.*, "A solar-based sustainable urban design: The effects of city-scale street-canyon geometry on solar access in Geneva, Switzerland," *Appl. Energy*, vol. 240, no. February, pp. 173–190, 2019.

[27] V. MEYRAND, G. B. Tabet, and O. Kassamani, "Lebanon Municipality of Beirut Sustainable energy action plan (SEAP)," Lebanon, 2012.

[28] IEA - International Energy Agency, "Lebanon: Indicators for 2014," 2016. [Online]. Available: http://www.iea.org/statistics/.

[29] MoE/UNDP/GEF, "Lebanon's Third National Comuunication to the UNFCCC," Beirut, Lebanon, 2016.

[30] World Bank, "Energy Efficiency Study in Lebanon," Beirut, Lebanon, 2009.

[31] F. Fardoun, O. Ibrahim, R. Younes, and H. Louahlia-Gualous, "Electricity of Lebanon: Problems and recommendations," *Energy Procedia*, vol. 19, pp. 310–320, 2012.

[32] S. Najem, "Beirut Solar Map." [Online]. Available: http://rredc.nrel.gov/solar/old_data/nsrdb/1961-1990/redbook/atlas/serve.cgi.

[33] UNDP/GEF and MPWT/DGU, "Groundwork for a Technical Guide for the application of the Thermal Standard for Buildings in Lebanon," Beirut, Lebanon, 2005.

[34] A. Yeretzian, "Beirut a sustainable dimension of the city and its buildings," *Al Mohandes*, Beirut, Lebanon, Mar-2010.

[35] S. Mortada, “The First Energy Indicators Report of the Republic of Lebanon,” 2018.

[36] D. Yan *et al.*, “Occupant behavior modeling for building performance simulation: Current state and future challenges,” *Energy Build.*, vol. 107, pp. 264–278, 2015.

[37] U. Wilke, F. Haldi, J. L. Scartezzini, and D. Robinson, “A bottom-up stochastic model to predict building occupants’ time-dependent activities,” *Build. Environ.*, vol. 60, pp. 254–264, 2013.

[38] F. Haldi and D. Robinson, “The impact of occupants’ behaviour on building energy demand,” *J. Build. Perform. Simul.*, vol. 4, no. 4, pp. 323–338, 2011.

[39] N. Mohammadi and J. E. Taylor, “Urban Energy Flux : Human Mobility as a Predictor for Spatial Changes,” *arXiv*, 2016.

[40] S. Yathreb, “Analysis of a Residential Building Energy Consumption as Base Model in Tripoli, Lebanon,” *Energy Prod. Mgmt*, vol. 1, no. 4, pp. 359–370, 2016.

[41] M. Braulio-gonzalo, M. D. Bovea, M. J. Ruá, and P. Juan, “A Methodology for Predicting the Energy Performance and Indoor Thermal Comfort of Residential Stocks on the Neighbourhood and City Scales. A Case Study in Spain,” *J. Clean. Prod.*, pp. 646–665, 2016.

[42] A. Salvati, P. Monti, H. Coch, and C. Cecere, “Climatic performance of urban textures : Analysis tools for a Mediterranean urban context,” *Energy Build.*, vol. 185, pp. 162–179, 2019.

[43] N. Kaloustian and Y. Diab, “Effects of urbanization on the urban heat island in Beirut,” *Urban Clim.*, vol. 14, pp. 154–165, 2015.

[44] M. Morganti, O. Le Corre, I. A. Agnese, A. Pina, P. Ferrão, and J. Coch, “Effects of urban compactness on the building energy performance in Mediterranean climate,” in *Energy Procedia*, 2017, vol. 122, pp. 499–504.

[45] T. Dogan and M. Knutins, “CitySeek: Towards Urban Daylight Models Based on GIS Data and Semi-Automated Image Processing,” no. June, 2018.

[46] F. De Luca, “Facade-Floor-Cluster . Methodology for Determining Optimal Building Clusters for Solar Access and Floor Plan Layout in Urban Environments Facade-Floor-Cluster,” no. June, 2018.

[47] J. Strømann-andersen and P. A. Sattrup, “The urban canyon and building energy use : Urban density versus daylight and passive solar gains,” vol. 43, pp. 2011–2020, 2011.

[48] J. P. Gastellu-Etchegorry *et al.*, “Discrete anisotropic radiative transfer (DART 5) for modeling airborne and satellite spectroradiometer and LIDAR acquisitions of natural and urban landscapes,” *Remote Sens.*, vol. 7, no. 2, pp. 1667–1701, 2015.